PROBING THE PRESSURE DENATURED STATE OF STAPHYLOCOCCAL NUCLEASE

by

Kelly J. Frye

A dissertation submitted in partial fulfillment of the

requirements for the degree of

Doctor of Philosophy

(Pharmaceutical Sciences)

at the

UNIVERSITY OF WISCONSIN-MADISON

1997

PROBING THE PRESSURE DENATURED STATE OF STAPHYLOCOCCAL NUCLEASE

Kelly J. Frye

Under the supervision of Associate Professor Catherine A. Royer

At the University of Wisconsin-Madison

The application of hydrostatic pressure to aqueous protein solutions results in unfolding of the protein structure because the protein-solvent system volume is smaller for the unfolded state. Contributions to this decrease in volume upon unfolding (ΔV_u) derive from altered interactions of the protein with solvent and are presumed to include electrostriction of charged residues, hydration of hydrophobic surfaces upon unfolding, and elimination of packing defects. This work addresses the contributions of hydrophobic hydration and cavities to the volume change by monitoring the intrinsic tryptophan fluorescence for the pressure induced denaturation of WT staphylococcal nuclease (nuclease). Two mutants of nuclease with altered cooperativity values and three mutants with modified cavity sizes were used to examine the contribution of hydrophobic hydration and imperfect packing, respectively. The results indicate that hydration of exposed surface area does not contribute significantly to ΔV_u in nuclease while cavities appear to provide a

significant contribution to the volume change. To further explore the role of solvation in protein stability and in the folding process, the effects of water activity on the stability and on the rates of folding/unfolding for nuclease were investigated. By carrying out pressure-jump relaxation experiments in the presence of the colligative agent xylose, the underlying kinetic basis for the stabilization of nuclease by sugars was determined in this thesis to arise primarily from an increase in the folding rate. This result implicates the release of a large number of water molecules for the transition from the unfolded to the transition state. Furthermore, this result implies that the transition state exposes a similar amount of surface area as compared to the native state and thus lies closer to the native than the denatured state on the reaction coordinate.

ACKNOWLEDGEMENTS

I would like to thank my advisor Dr. Catherine Royer for her guidance and mentorship throughout my graduate career. It has been a great experience working with someone who has such vast scientific insight and enthusiasm. Her support and encouragement in sending me to numerous scientific meetings has proven to be very valuable in my development as a scientist. She has been an admirable role model as a scientist as well as a woman in science. I hope one day to be as insightful as she is in my own research.

Next, I would like to thank my entire defense committee for their support and input during my tenure as a graduate student. Specifically, Dr. Tim Heath has offered support. Dr. Dexter Northrop has been an inspiration with his excitement about high pressure work and assisted with the nonlinear analysis of the kinetic data. Dr. John Markley has been helpful with his support and career advice as well as for the gift of the plasmids which overexpressed WT nuclease. Finally, Dr. George Zografi has been invaluable for his undying support of me and my research which has meant a great deal to me. He has been like a second advisor.

Dr. David Shortle was generous in supplying the plasmids which overexpressed the mutants. Dr. John Carra was a great asset with his assistance with the calorimetry and CD thermal melt experiments. He also provided helpful

discussions regarding m-value mutants. Dagmar Truckses was kind enough to help me with making protein structures.

Past and present Royer lab members have been instrumental in providing helpful discussions and making the workplace more enjoyable. An undergraduate in the laboratory, Chris Perman, helped with some of the cooperativity mutant experiments. I would like to single out the post doctoral fellows in the laboratory who have taught me a great deal. Dr. John Hill offered advice about protein preparations. Dr. Gediminas Vidugiris assisted with the initial kinetic data analysis. He was also a great help with the high pressure instrument. Finally, Dr. Martha Brown has offered priceless advice both professional and personal. She has also taught me a great deal about fluorescence. I would like to give her a big thanks for helping to proof read this thesis as well.

I would like to thank my best friend, Jon Eichman. He has been there for me throughout my graduate career and has always been very supportive helping me though all the rough spots such as the qualifying exam, traumatic protein prep failures, my prelims, and finally the thesis.

Finally, I would like to thank my parents without whom I would not be where I am today. They have always told me that I could do and be whatever I set my mind to. Their never ending encouragement and advice have helped me to fulfill all of my dreams and goals. Thanks mom and dad, I love you and could not have done it without you!!

TABLE OF CONTENTS

TITLE PAGE..... i

ABSTRACT..... ii

ACKNOWLEDGEMENTS..... iii

TABLE OF CONTENTS..... v

LIST OF FIGURES..... vii

LIST OF TABLES..... x

CHAPTER 1: INTRODUCTION..... 1

Thermodynamics of protein folding..... 5

Effect of chemical denaturants and stabilizers on protein stability..... 9

Protein folding models..... 19

Pressure effects on protein stability..... 22

Staphylococcal nuclease..... 34

CHAPTER 2: AIM OF THESIS..... 37

CHAPTER 3: MATERIALS AND METHODS..... 40

Protein preparation..... 41

Wild type..... 41

Mutants..... 43

Pressure experiments..... 45

ANS binding experiments..... 47

Cooperativity mutants..... 47

Pressure-jump relaxation kinetics..... 49

Cavity mutants..... 49

Circular dichroism..... 50

Osmolarity..... 51

Data analysis of pressure experiments..... 51
Cooperativity mutants..... 51
Pressure-jump relaxation kinetics..... 55
Cavity mutants..... 58
CHAPTER 4: THE PRESSURE DENATURED STATE OF WT STAPHYLOCOCCAL NUCLEASE..... 59
Results..... 61
Discussion..... 67
CHAPTER 5: THE CONTRIBUTION OF THE EXPOSURE OF BURIED SURFACE AREA TO ΔV_u..... 77
Results..... 81
Discussion..... 94
CHAPTER 6: THE ROLE OF CAVITIES IN THE PRESSURE DENATURATION OF STAPHYLOCOCCAL NUCLEASE..... 102
Results..... 106
Discussion..... 110
CHAPTER 7: THE KINETIC BASIS FOR THE STABILIZATION OF STAPHYLOCOCCAL NUCLEASE BY XYLOSE..... 118
Results..... 121
Discussion..... 135
CHAPTER 8: FINAL CONCLUSIONS..... 141
REFERENCES..... 145
APPENDIX I..... 155
APPENDIX II..... 158
APPENDIX III..... 170

LIST OF FIGURES

	Page
Figure 1-1. Gibbs free energy as a function of temperature	8
Figure 1-2. Idealized folding funnel	23
Figure 1-3. Contours of pH in the pressure-temperature plane	27
Figure 1-4. Structure of Staphylococcal nuclease	35
Figure 3-1. Pressure instrument lay out	46
Figure 3-2. Chemical structure of bis-tris	48
Figure 3-3. Chemical structure of xylose	48
Figure 4-1. Chemical structure of ANS	61
Figure 4-2. Fluorescence emission spectrum of WT	62
Figure 4-3. Fluorescence intensity of ANS vs. pressure	64
Figure 4-4. Fluorescence intensity of ANS + WT	65
Figure 4-5. Unlinked unfolding profiles for WT vs. xylose	66
Figure 4-6. Average volume change for WT vs. xylose	68
Figure 4-7. Global unfolding profiles for WT vs. xylose	69
Figure 5-1. Structure of nuclease with cooperativity mutants	80
Figure 5-2. Global unfolding profiles of H121P vs. xylose	82
Figure 5-3. Global unfolding profiles of A69T+A90S vs. xylose	83
Figure 5-4. Unfolding profile for M98I	85
Figure 5-5. Free energy of unfolding vs. xylose concentration	86

Figure 5-6. CD thermal melt data for WT 90

Figure 5-7. CD thermal melt data for H121P 91

Figure 5-8. CD thermal melt data for A69T+A90S 92

Figure 5-9. CD spectra for H121P and A69T+A90S 93

Figure 5-10. ΔV_u vs. xylose for H121P and A69T+A90S 95

Figure 5-11. Diagram of the position of *m*-value mutants 99

Figure 6-1. Structure of nuclease with cavity mutant 105

Figure 6-2. Unfolding profile of V66G 107

Figure 6-3. Unfolding profile of V66A 108

Figure 6-4. Unfolding profile of V66L 109

Figure 6-5. Structure of V66G superimposed on the WT 113

Figure 7-1. Equilibrium unfolding profiles for WT 122

Figure 7-2. Pressure-jump relaxation profiles for WT 124

Figure 7-3. Close up of a relaxation profile 125

Figure 7-4. Linear plot ln τ as a function of pressure 127

Figure 7-5. Nonlinear plot of ln τ as a function of pressure 128

Figure 7-6. ln rate constant as a function of xylose 132

Figure 7-7. ln rate constant as a function of osmolarity 133

Figure 7-8. Free energy diagram 136

Figure 7-9. Schematic of the volume change 139

Figure I-1. Unfolding profile for WT vs. xylose 156

Figure I-2. Unfolding profile for WT vs. xylose 157

Figure II-1. Unfolding profile for H121P vs. xylose 159

Figure II-2. Unfolding profile for H121P vs. xylose 160

Figure II-3. Unfolding profile for H121P vs. xylose 161

Figure II-4. Unfolding profile for H121P vs. xylose 162

Figure II-5. Unfolding profile for A69T+A90S vs. xylose 163

Figure II-6. Unfolding profile for A69T+A90S vs. xylose 164

Figure II-7. Unfolding profile for A69T+A90S vs. xylose 165

Figure II-8. Unfolding profile for A69T+A90S vs. xylose 166

Figure II-9. CD spectra of WT vs. temperature 167

Figure II-10. CD spectra of H121P vs. temperature 168

Figure II-11. CD spectra of A69T+A90S vs. temperature 169

Figure III-1. Unfolding profiles for V66G 171

Figure III-2. Unfolding profiles for V66A 172

Figure III-3. Unfolding profiles for V66L 173

LIST OF TABLES

	Page
Table 4-1. Average volume change upon unfolding for WT	70
Table 5-1. *m*-values and ΔV_u for cooperativity mutants	88
Table 6-1. ΔV_u for cavity mutants	111
Table 6-2. Side chain and predicted volumes for cavity mutants	114
Table 7-1. Equilibrium and kinetic ΔG_u and ΔV_u for WT	123
Table 7-2. Rate constants and activation volumes for WT	129

CHAPTER 1: INTRODUCTION

Proteins are essential biomolecules whose functions are dictated by their specific three-dimensional structure. Under the appropriate conditions, these biomolecules are known to spontaneously fold into their proper, unique, native structure. However, it is still not well established how a protein, composed of a particular sequence of amino acids, adopts a specific three-dimensional structure which renders it biologically active.

The specific structure of all proteins can be divided into four classes: primary, secondary, tertiary, and quaternary structures. The primary structure is the amino acid sequence. There are 20 amino acids that combine in a specific order to create a protein. The peptide bond connects the basic unit of all amino acids which when put together becomes the peptide backbone. Just as words are made up of various letters in the alphabet and words differ only by the number and order in which the letters are placed together, proteins signify uniqueness by the number of amino acids and the sequence in which the amino acids occur.

The amino acids can be separated into categories based on their chemical structure. The charged amino acids are aspartic acid, glutamic acid, lysine, and arginine. Amino acids which are polar but not charged are serine, threonine, asparagine, and glutamine. Cysteine and methionine contain sulfur in their chemical structure, while aromatic residues consist of histidine, tryptophan, tyrosine, phenylalanine, and proline. The remainder of the amino acids are considered to be hydrophobic which includes alanine, valine, isoleucine, and

leucine. Globular proteins contain a nearly constant ratio of hydrophilic to hydrophobic groups (Bigelow, 1967).

The secondary structure is made up of alpha helices, beta sheets, turns, and loops. These are structures common to all proteins and are stabilized primarily through hydrogen bonding between the polypeptide backbone along with favorable van der Waals interactions. The tertiary structure provides a means for secondary structures to pack together while the quaternary structure enables two or more polypeptide monomers to interact and form a polymer.

From numerous available x-ray crystal structures, it is known that in the native state the majority of hydrophobic residues are buried in the interior of the protein. In fact, it was demonstrated that proteins bury a constant fraction of their available surface area (Janin, 1976, Teller, 1976). On average, carbon or sulfur are 86% buried, neutral oxygen or nitrogen are 40% buried, and charged oxygen or nitrogen are 32% buried (Lesser & Rose, 1990). Another interesting piece of the puzzle is that mutations alter packing slightly but are accommodated locally without changing the overall fold. In other words, there is local or microscopic rearrangement around the site of the mutation which helps the residue to fit into place, but this microscopic change does not modify the global structure, although mutations can be stabilizing or destabilizing. However, packing faults perturb the equilibrium in the direction of the unfolded state, not toward a new conformation (Rose & Wolfenden, 1993).

Thermodynamically, the conformation of many small globular proteins can be described by a simple two-state reversible transition between folded and unfolded forms. The transition is highly cooperative which means that partially folded intermediates are not significantly populated because they are too close in energy to either the folded or unfolded states. That is, the protein is always either in the native or denatured state without any intermediates. Due to the high degree of cooperativity, the transition can be thought of as similar to a phase transition.

The stability of native proteins is only marginal, 5-10 kcals/mol, as a result of the compensating effects of enthalpy and entropy. The Gibbs free energy (ΔG) is a measure of the stability of the protein and is defined as:

$$\Delta G = \Delta H - T\Delta S \qquad (1)$$

where ΔH is the change in enthalpy upon folding, ΔS is the change in entropy upon folding, and T is temperature in degrees Kelvin. When a protein is unfolded, the random structure is stabilized by a large conformational entropy (ΔS_{conf}) which increases as the number of possible conformations for each residue increases. As the protein folds, the number of possible conformations decreases which makes the conformational entropy of a folded protein energetically unfavorable. Therefore, in order for the protein folding reaction to favor the native state, the protein must overcome this loss of conformational

entropy. The protein accomplishes this with a compensating enthalpic term which is a result of stabilizing interactions within the native protein along with a favorable entropic contribution due to the release of water into the bulk upon folding.

The types of interactions involved in stabilizing a folded polypeptide include electrostatic, hydrogen bonding, van der Waals interactions, and hydrophobic interactions. The importance of hydrogen bonds can be seen most directly by the crucial role they play in stabilizing the secondary structure. In addition to intramolecular hydrogen bonding, there can also be hydrogen bonding to the aqueous solvent surrounding the protein which competes with intramolecular hydrogen bonds. All of these interactions can be influenced by changes in temperature, pressure, and pH which means that the folding reaction can also be perturbed by temperature, pressure, and pH.

Thermodynamics of protein folding

Although all of the interactions play a critical role, Kauzmann was the first to recognize that hydrophobic interactions are the driving force in protein folding (Kauzmann, 1959). From experiments performed by Christensen (Christensen, 1952), it can be seen that the stability of a protein decreases at low as well as high temperatures. This temperature dependence parallels nonpolar solvation where nonpolar solutes have increased solubility in water at lower temperatures.

Subsequently, evidence emerged from spectroscopic and high-resolution differential scanning calorimetry experiments that demonstrated the similarity between the free energy of folding and the transfer of nonpolar molecules from an aqueous to a nonpolar environment (Pace, 1975, Privalov, 1979, Privalov & Gill, 1988), in that both result in large decreases in the heat capacity. The heat capacity (C_p) describes the amount of heat added to the system (dq) producing a rise in temperature (dT).

$$C_P = \left(\frac{dq}{dT}\right)_P \qquad (2)$$

At constant pressure the amount of heat added to the system is equal to the enthalpy such that:

$$\Delta C_P(unfolding) = \left(\frac{\partial \Delta H}{\partial T}\right)_P \qquad (3)$$

The change in entropy can also be defined in terms of the heat capacity:

$$d\Delta S = \Delta C_P \ln\left(\frac{T_f}{T_i}\right) \qquad (4)$$

where T_f is the final temperature and T_i is the initial temperature. A large heat capacity change implies that both the enthalpy and entropy of folding are strongly dependent on temperature. The enthalpy and entropy combine to make the free energy a complex function of temperature. Figure 1-1 shows the free energy, enthalpy, and entropy of unfolding for myoglobin as a function of temperature (Privalov & Khechinashvili, 1974). From the graph, it is apparent that the temperature at which the protein is most stable is the temperature at which the change in entropy is zero. Therefore, the protein structure at this temperature of maximum stability is stabilized only by the change in enthalpy between the native and denatured states. The change in enthalpy upon denaturation is determined by intramolecular versus intermolecular hydrogen bonds, van der Waals interactions, and solvation of nonpolar groups. The change in entropy upon denaturation is due to the freedom of the polypeptide chain also referred to as dissipative forces and the solvent structure due to hydration of nonpolar groups. The native protein structure is stabilized at a temperature where nonpolar hydration and dissipative forces are small compared to intramolecular hydrogen bonds and van der Waals interactions. At high temperatures, denaturation is driven by the positive entropy term due to the increase in dissipative forces. At low temperatures, denaturation is driven by the

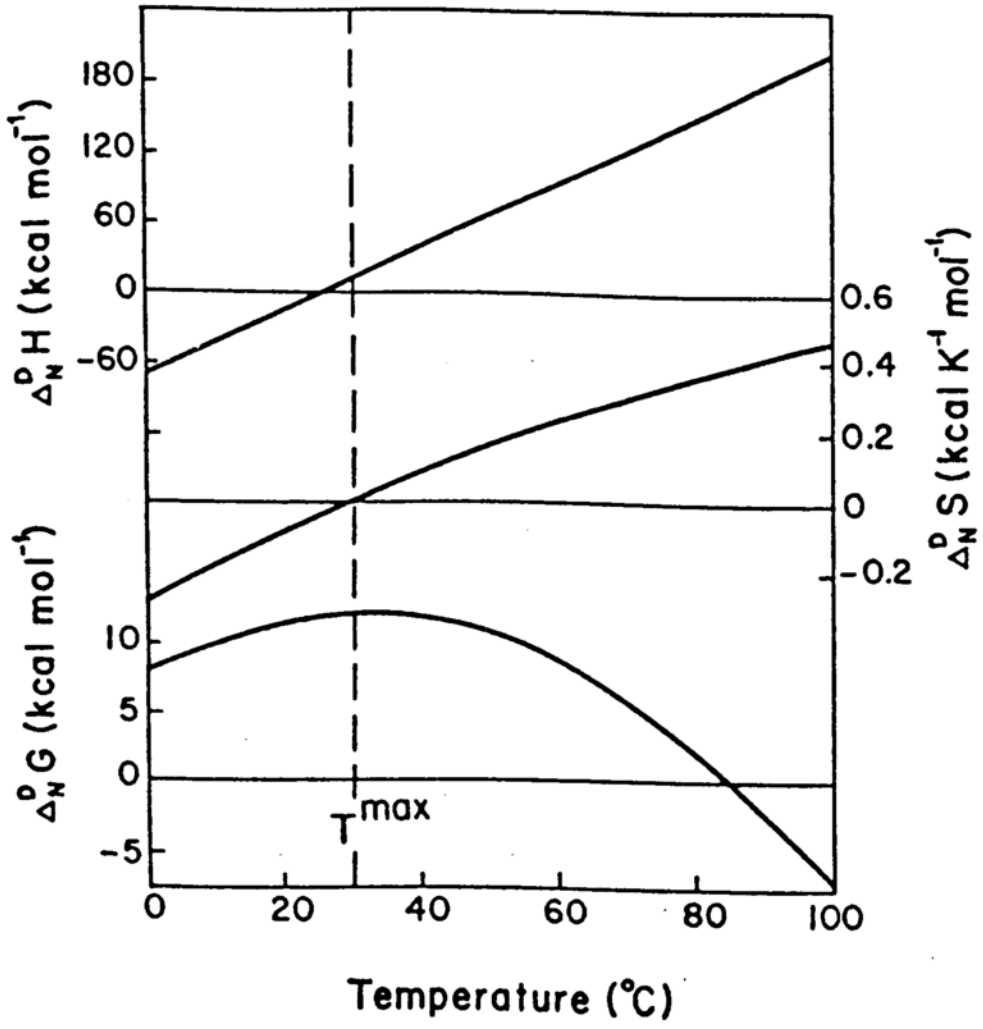

Figure 1-1. The enthalpy, entropy, and Gibbs free energy as a function of temperature for the unfolding of myoglobin according to (Privalov & Khechinashvili, 1974).

negative enthalpy term since the negative entropy term in this temperature range favors folding over unfolding. The negative entropy is the consequence of the increase in hydrophobic hydration due to the decrease in the hydrophobic effect at low temperatures which causes the solvent molecules to become more ordered (Privalov, 1979).

Effect of chemical denaturants and stabilizers on protein stability

In addition to temperature, the stability of a protein can be altered by chemical denaturants such as guanidine or urea. When guanidine or urea are used to denature small, globular, single domain proteins, a sharp two-state transition results due to the cooperativity of the unfolding transition. From this transition, the change in free energy between the native and denatured states can be determined by defining an equilibrium constant, K_u, as the fraction of the protein present in the denatured state divided by the fraction in the native state. The change in free energy at zero concentration of denaturant ($\Delta G°$), or the conformational stability, may then be estimated. There are different models that may be utilized to obtain $\Delta G°$ estimations including Tanford's Model, the Denaturant Binding Model and the Linear Extrapolation Model (Pace, 1986, Tanford, 1970). The most common and simplest method is the Linear Extrapolation Model. This model assumes that the linearity of ΔG with respect to

denaturant concentration, which is seen in the transition region, continues to zero concentration so that the data fits to the linear equation

$$\Delta G_i = \Delta G^\circ - m[denaturant]_i \qquad (5)$$

where ΔG_i is the free energy of unfolding at denaturant concentration i and m is the cooperativity coefficient. Although the original consideration for using this model was good empirical agreement between estimates of ΔG° from urea and guanidine denaturation, it became the model of choice because neither of the more complicated models provide a more reliable estimate of ΔG° (Pace, 1986). Schellman has since shown that theoretically this is a sound model (Schellman, 1987). He considered a protein with a binding site in solution with solvent 1 (water) and solvent 3 (denaturant). The free energy of the solution can be written as the sum of five components: components 1 and 3, protein with vacant sites (PO), protein with site occupied by component 1 (P1) and protein with site occupied by component 3 (P3). Thus, the free energy of the system can be expressed as follows:

$$G = n_1\mu_1 + n_3\mu_3 + n_{P0}\mu_{P0} + n_{P1}\mu_{P1} + n_{P3}\mu_{P3} \qquad (6)$$

where n_i is the amount of species i and μ_i is the chemical potential of species i. Free and bound ligands are in equilibrium:

$$\mu_{P1} = \mu_1 + \mu_{P0} \tag{7a}$$

$$\mu_{P3} = \mu_3 + \mu_{P0} \tag{7b}$$

Equations (7a & b) can be used to eliminate μ_{P1} and μ_{P3} from equation (6).

$$G = (n_1 + n_{P1})\mu_1 + (n_3 + n_{P3})\mu_3 + (n_{P0} + n_{P1} + n_{P3})\mu_{P0} \tag{8}$$

For the ideal solution being considered, $\mu_{P0} = \mu_{P0}^{\circ} + RT\ln[P0]$. This is done, even though the species P0 does not exist, for the sake of completeness. From elementary binding theory we know that:

$$[P0] = \frac{[P]}{(1 + K_1\alpha_1 + K_3\alpha_3)} \tag{9}$$

where [P] = [P0] + [P1] + [P3] is the total protein concentration and α_1 and α_3 are the activities of solvents 1 and 3 on the mole fraction scale. So the total free energy can now be written as:

$$G = (n_1 + n_{P1})\mu_1 + (n_3 + n_{P3})\mu_3 + (n_{P0} + n_{P1} + n_{P3})(n^{\circ}_{P0} + RT\ln[P]) - (n_{P0} + n_{P1} + n_{P3})RT\ln(1 + K_1\alpha_1 + K_3\alpha_3) \quad (10)$$

As mentioned previously, the probability of a vacant site is negligible. Therefore, the first term of the binding polynomial can be eliminated. The free energy of interaction, $\Delta\beta$ (the remaining portion of the binding polynomial), can then be separated into $-RT\ln K_1$ (the free energy of hydration in pure solvent 1) and $-RT\ln(\alpha_1 + K\alpha_3)$ where $K = K_3/K_1$. When summed over the sites of the folded (N) and unfolded (D) protein, the binding polynomial becomes:

$$-\Delta\beta = \Sigma_D \ln(\alpha_1 + K\alpha_3) - \Sigma_N \ln(\alpha_1 + K\alpha_3) \quad (11)$$

Thus, in the presence of two solvents, with K as the equilibrium constant for the interchange of molecule 3 for molecule 1, the free energy of unfolding with this model becomes $\Delta G = \Delta G^{\circ} + RT\Delta\beta$. At this point Schellman replaced the more accurate activity with the mole fraction (X). In the limit of extreme dilution, $X_1 = 1 - X_3$, and by eliminating X_1, $\Delta\beta$ becomes:

$$-RT\ln[1 + (K-1)X_3] \quad (12)$$

From equation (12) the following can be seen: (1) If K=1, there is no intrinsic free energy for the interchange of 1 and 3 on the site and the free energy of solvation also goes to zero. (2) If $K >> 1$, then $K - 1 \approx K$ and the formula is reduced to the ordinary binding polynomial for single binding at the site. (3) If $K < 1$, the interaction of 3 is repulsive and negative binding is seen resulting in component 1 binding to the site. If $K' = (K-1)/W$, and W is 55.5 moles per kilogram for water as the primary solvent, then the logarithmic term becomes $-\ln(1 + K'X)$. Two points can be made about the equilibrium constants. First, the constants in this binding polynomial are not typical equilibrium constants because they contain a subtractive term for selectivity relative to the primary solvent and thus can be negative or zero. The second point is that these constants will be small because of the W factor. This makes K'X small even for concentrated solutions. Therefore, the logarithmic term can be approximated by its linear expansion. This is proposed as the basis for the linear relationship between free energy and denaturant concentration (Schellman, 1987).

Using this linear expansion, a straight line is observed with the slope typically referred to as the *m*-value of the protein. Since the *m*-value is the change in free energy as a function of denaturant concentration, it is a measure of the cooperativity of folding for the protein. Thus, the more narrow the range of guanidine concentrations over which unfolding occurs, the steeper the slope of the line, the larger the *m*-value, and the more cooperative the unfolding. The *m*-value is generally known to correlate to the amount of surface area exposed

upon unfolding, ΔA_u, since K' is a pseudo-binding constant and is affected by the number of binding sites exposed and hence the amount of surface area exposed upon unfolding (Schellman, 1978, Shortle & Meeker, 1986, Shortle et al., 1988).

Shortle and Meeker (Shortle & Meeker, 1986) determined that there are three classes of *m*-value mutants for staphylococcal nuclease. The first class has an *m*-value that is less than that of the wild type for which denaturation occurs over a broader range of guanidine concentrations (the m^- mutant). The second class has an *m*-value that is greater than that of the wild type for which denaturation occurs over a narrower range of guanidine concentrations (the m^+ mutant). The third class has an *m*-value that is similar to the wild type ($0.9 \leq m \leq 1.1$) and is the m° mutant.

In addition to chemicals being used to decrease the stability of proteins, there are also chemicals which can increase protein stability. Organisms protect themselves from osmotic shock by compounds known as osmolytes which help maintain a constant osmotic pressure across cellular membranes. Sugars are examples of osmolytes which have been used to stabilize protein structure for the better part of a century. It was initially thought that the stabilization occurred by the sugar forming a protective coat or shell around the protein, although there was no experimental evidence (Timasheff, 1993). Timasheff discredited this theory by demonstrating that sugars are actually excluded from the surface of the protein which then becomes surrounded by water (Lee & Timasheff, 1981). Both stabilization and denaturation occur through weak interactions since they

are neither strong nor specific. Denaturants are preferentially bound to the protein and stabilizers are preferentially excluded from the protein with respect to water (Timasheff, 1993). The thermodynamics of this behavior can be described through three parameters. The first parameter is the transfer free energy, $\Delta\mu_{2,tr}$. This indicates how the protein interactions change when the protein is transferred from pure solvent (water) to a cosolvent system:

$$\Delta \mu_{2,tr} = \mu_2(\text{cosolvent}) - \mu_2(water) \qquad (13)$$

where μ is the chemical potential of the protein (component 2). The preferential interaction term, $\left(\partial \mu_2/\partial m_3\right)_{T,P,m_2} = \left(\partial \mu_3/\partial m_2\right)_{T,P,m_3}$ is the second parameter. It is the gradient of the transfer free energy with respect to cosolvent concentration. Thus,

$$\Delta \mu_{2,tr} = \int_0^{m_3} \left(\frac{\partial \mu_2}{\partial m_3}\right)_{T,P,m_2,m_3} \qquad (14)$$

The final parameter is the preferential binding term, $\left(\partial m_3/\partial m_2\right)_{T,P,\mu_3}$. This is how much cosolvent would have to be added to (or removed from) the solvent system to restore thermodynamic equilibrium when the protein is added:

$$\left(\frac{\partial m_3}{\partial m_2}\right) = \frac{\left(\partial \mu_2/\partial m_3\right)_{T,P,m_2}}{\left(\partial \mu_3/\partial m_3\right)_{T,P,m_2}} \qquad (15)$$

where the denominator is the nonideality of the cosolvent. The preferential binding term is equal to the binding measured by dialysis, ν_3 (moles ligand/mole protein) with the approximation that $\left(\partial m_3/\partial m_2\right)_{T,P,\mu_3} \approx \left(\partial m_3/\partial m_2\right)_{T,\mu_1,\mu_3}$. The cosolvent effect can best be described by the Wyman linkage relation (Wyman, 1964), which is the change of the equilibrium constant with respect to solvent composition and its dependence on the change in the preferential interaction parameter throughout the reaction:

$$\left(\frac{\partial \ln K}{\partial \ln a_3}\right)_{T,P,m_2} = \frac{\left(\partial \mu_3/\partial m_2\right)_{T,P,m_3}(product) - \left(\partial \mu_3/\partial m_2\right)_{T,P,m_3}(reactant)}{\left(\partial \mu_3/\partial m_3\right)_{T,P,m_2}} \qquad (16)$$

Combining this equation with the equation for the preferential binding parameter shows that the slope of the plot of lnK vs. $\ln a_3$ is a function of the change in preferential binding parameter:

$$\left(\partial \ln K/\partial \ln a_3\right) = \nu_3(product) - \nu_3(reactant) = \Delta\left(\partial m_3/\partial m_2\right)_{T,P,\mu_3} \qquad (17)$$

The slope determines the direction of cosolvent displacement from equilibrium and can be either positive, negative, or zero depending on whether $\Delta\nu_3$ enhances, inhibits, or has no effect on binding, respectively (Timasheff, 1993). The preferential interaction term can also be positive, negative, or zero depending on whether the interaction of the protein with the cosolvent system is unfavorable, favorable, or neutral. What this means is that the thermodynamically measured preferential binding term can also be negative. Negative binding is defined as the concentration of water being higher around the protein relative to the bulk and for that reason the protein becomes preferentially hydrated and the cosolvent is preferentially excluded. From the derivation by Schellman presented above, it is seen that cosolvents compete with water for binding to the protein. If water binds with higher affinity, the cosolvent is preferentially excluded. In order to minimize the amount of surface area exposed to the unfavorable cosolvent upon unfolding, the protein native state is stabilized. If, on the other hand, the surface of the protein prefers to bind the cosolvent instead of water, then the cosolvent is considered a denaturant.

Preferential exclusion can be divided into two categories: (1) the exclusion is independent of the chemical nature of the protein surface *i.e.*, the protein is a surface with no attraction or repulsion of the cosolvent, and (2) the chemical nature of the protein surface does play a part, so the cosolvent is either attracted to or repelled from a particular portion of the protein surface. Sugars belong to the first category which consists of two main mechanisms. The first is

steric exclusion due to the difference in size between the cosolvent and water molecules. Since water molecules are small, they are able to penetrate into crevices on the exterior of the protein resulting in a hydration shell around the protein which large cosolvent molecules cannot penetrate. An example of this mechanism is polyethylene glycol since it is larger than water molecules and is excluded from the protein surface based on its size (Timasheff, 1993). The result of steric exclusion is preferential hydration of the protein.

The second mechanism is perturbation of surface tension which results in a change of cosolvent concentration at the protein surface. The Gibbs adsorption isotherm for this system becomes:

$$\left(\partial m_3/\partial m_2\right)_{T,P,\mu_3} = \left(S_2/RT\right)\left(\partial\sigma/\partial \ln a_3\right)_{T,P,m_2} \qquad (18)$$

where S_2 is the molar surface area of the protein, and σ is the surface tension (Timasheff, 1993). From this equation it is clear that a cosolvent that increases the surface tension will be excluded from the protein surface. Sugars, nonhydrophobic amino acids, and most salts increase the surface tension of water. Thus, they will be preferentially excluded from the protein surface and the protein will be preferentially hydrated (Timasheff, 1993). Cioci (Cioci, 1996) has verified experimentally that an increase in surface tension is the mechanism of protein stabilization for sugars by showing the linearity of melting temperature

and surface tension for various proteins as a function of cosolvent. Timasheff and coworkers (Kita et al., 1994, Lin & Timasheff, 1996) have also demonstrated experimentally the importance of surface tension in the mechanism for protein stabilization by sugars. For cosolvents such as guanidine and urea which increase the surface tension but destabilize the protein, the surface tension is not the only mechanism involved. Timasheff and coworkers (Lin & Timasheff, 1996) have proposed that the preferential interaction parameter (equation 15) measured experimentally consists of contributions from surface tension and weak binding as follows:

$$\left(\frac{\partial m_3}{\partial m_2}\right)_{T,\mu_1,\mu_3}^{EXP} = \left(\frac{\partial m_3}{\partial m_2}\right)_{T,\mu_1,\mu_3}^{bind} + \left(\frac{\partial m_3}{\partial m_2}\right)_{T,\mu_1,\mu_3}^{\sigma} \qquad (19)$$

In this way, the preferential hydration of the protein surface due to the increase in surface tension by guanidine and urea is overcome by their affinity to the protein surface which causes the cosolvents to preferentially bind to the protein surface thereby denaturing the protein.

Protein folding models

While experiments can be carried out to examine the effects of temperature, pH, pressure, or chemical stability of proteins, the question as to

how proteins find their specific three-dimensional structure is not so easily answered. Levinthal's paradox (Dill, 1985, Levinthal, 1968, Zwanzig et al., 1992) concludes that there are too many possible chain conformations for a protein to test each one for the biologically active, native state on a practical time scale. For example, it would take 10^{77} years for a polypeptide chain of 100 residues with 10^{100} possible conformations to convert from one conformation to the next in the shortest amount of time possible. Consequently, a specific folding pathway must exist. Proteins must reach a global free energy minimum (thermodynamic control) and do so rapidly (kinetic control). Thermodynamic control was considered to be pathway independent and therefore the protein must take a long time to reach the global free energy minimum. Kinetic control was pathway dependent so the protein was able to reach its free energy minimum quickly instead of spending time searching blindly for the pathway, but it may only be the local not global free energy minimum. Therefore, protein folding is governed by thermodynamic control.

Scientists began searching for folding intermediates along the folding pathway to help determine the specific sequence of events which a protein was thought to follow in reaching the native state. Intermediates were found that were considered to be either on-pathway (Tsong et al., 1971) or off-pathway (Ikai & Tanford, 1971). Off-pathway intermediates were thought to be dead ends that did not give any information about the pathway. Proteins were thought to either follow an on-pathway, off-pathway, or sequential (the protein passed

through more than one intermediate along the way to the native state) pathway. Studies have now been conducted showing that proteins can fold without going through any detectable kinetic intermediates (Fersht, 1995, Huang & Oas, 1995, Jackson & Fersht, 1991, Schindler et al., 1995, Sosnick et al., 1996, Sosnick et al., 1994).

Several different models have been proposed to describe what happens first in the specific sequence of folding events. Among those are the framework model which suggests that the protein first develops secondary structures that are isolated from one another before proceeding through the remaining events for folding (Kim & Baldwin, 1982). The diffusion-collision model describes the association of isolated secondary structures (Karplus & Weaver, 1976). The molten globule model, also referred to as the hydrophobic collapse model, has been another favorite among protein folding scientists. This model suggests that there is an initial collapse of hydrophobic portions of the protein (Ptitsyn, 1987) followed by the formation of secondary structure. The funnel theory concludes that for a two-state transition, the initial collapse and the formation of secondary structure coincide in a single exponential process.

The new view of protein folding is one of folding funnels (Dill et al., 1995, Socci et al., 1996). The funnel concept describes parallel events in folding not sequential events along a pathway. It is irrelevant what the denatured state looks like or where it begins. The protein flows down through the funnel to reach the global free energy minimum, or native state, from wherever it begins. There

is not a specific pathway which depends on the structure of the denatured state. A smooth funnel landscape (Figure 1-2) leads to a simple two-state transition, while a bumpy landscape leads to multi-state kinetics where intermediates may accumulate in small crevices or valleys along the funnel before finally reaching the bottom of the funnel or native state.

Pressure effects on protein stability

The denatured state is a result of differences in solvation between the native and denatured states under a particular set of conditions such as pH, concentration of denaturants or stabilizers, temperature, or pressure. Pressure denaturation perturbs the equilibrium without addition of heat or change in the chemical potential and depends only on the volume change for the reactions. Therefore, pressure denaturation can give information about the volume change upon unfolding which cannot be determined by conventional methods of denaturation. The underlying contributions to the volume change upon unfolding are due to differential solvation between the native and denatured states. If the volume change upon unfolding could be understood, it may offer insight into the contribution of protein-solvent interactions in protein folding. Pressure represents the other thermodynamic variable and as such offers a complimentary way of denaturing proteins.

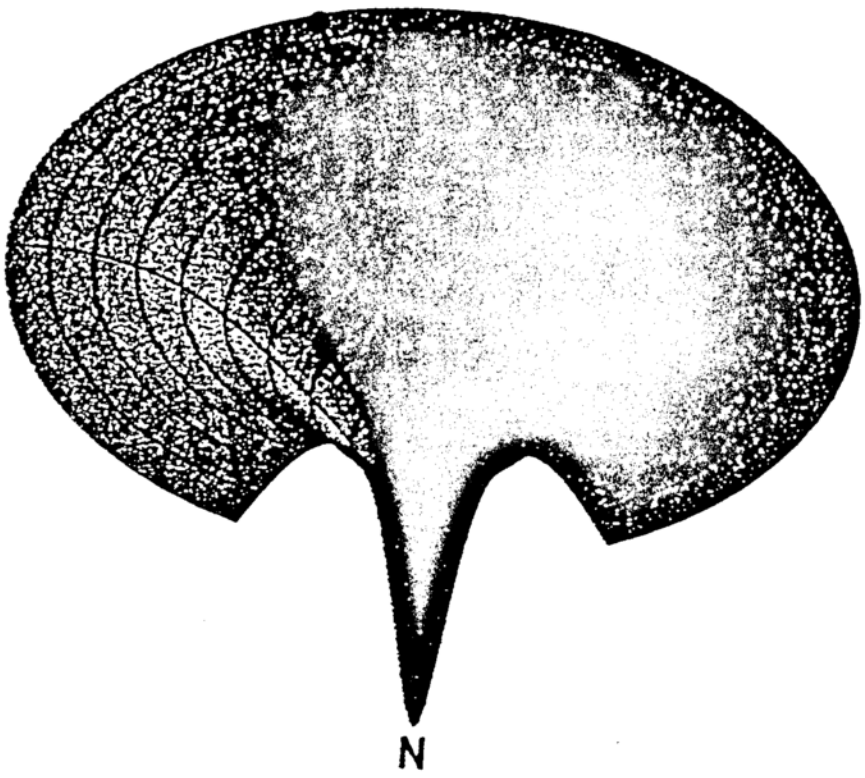

Figure 1-2. An idealize folding funnel (Dill & Chan, 1997).

Pressure denaturation was first demonstrated by Brandts with ribonuclease (Brandts et al., 1970) and again by Zipp and Kauzmann on metmyoglobin (Zipp & Kauzmann, 1973). High pressure absorbance spectroscopy was used to monitor the pressure denaturation of the above proteins as well as chymotrypsinogen (Hawley, 1971). High pressure fluorescence studies were carried by Weber and coworkers on lysozyme, chymotrypsinogen, egg-white riboflavin-binding protein, and several flavodoxins (Li et al., 1976a, Li et al., 1976b, Visser et al., 1977). In general the midpoints for the transitions of the above proteins were between 4-8 kbar. However, Royer and coworkers reported the denaturation of a relatively unstable protein, Staphylococcal nuclease, at pressures below 2 kbar at a slightly acidic pH (Royer et al., 1993).

The thermodynamics of this process can be seen by deriving the free energy of unfolding in terms of pressure-volume work. The equation for a closed system of constant composition defines the internal free energy (U) as:

$$dU = TdS - PdV \qquad (20)$$

where S is the entropy, and T, P, and V are the temperature, pressure, and volume, respectively. The second law of thermodynamics states that the entropy always increases for all spontaneous reactions,

$$dS - \frac{dq}{T} \geq 0 \qquad (21)$$

where dq is the heat exchanged. If the heat exchanged is then defined to be the internal energy and the pressure-volume work, the equation becomes:

$$d(U + PV - TS) \leq 0 \qquad (22)$$

This is the Gibbs free energy (G), which decreases for all spontaneous processes. The Gibbs free energy can then be defined by:

$$G = U + PV - TS = H - TS \qquad (23)$$

where H is the enthalpy. Substituting for the previous definition of U,

$$dG = VdP - SdT \qquad (24)$$

results in a definition of the Gibbs free energy in terms of pressure. At constant temperature, the second term drops out and the pressure dependence of the Gibbs free energy for a reaction, ΔG, can be written as:

$$\left(\frac{d(\Delta G)}{dP}\right)_T = (\Delta V)_T \qquad (25)$$

If pressure is applied to a system, the equilibrium will shift to the side occupying the smallest volume.

The work by Zipp and Kauzmann (Zipp & Kauzmann, 1973) on metmyoglobin was fundamental in characterizing pressure effects on protein stability. In Figure 1-3, Zipp and Kauzmann (Zipp & Kauzmann, 1973) characterize the delicate balance between temperature, pressure, and pH for metmyoglobin. The figure shows the temperature-pressure plane with contours at constant pH where $\Delta G = 0$ for the denaturation of metmyoglobin. It is evident from the graph that at any pH, there exists a pressure where the protein goes from denatured to native and back to denatured when the protein is heated from 0 to 80°C. The temperature at which the protein is most stable is dependent upon the pH and, as seen in Figure 1-3, can be quite high. The results in the figure can be interpreted qualitatively using the Clapeyron equation, similar to what Hawley showed for chymotrypsinogen (Hawley, 1971). The Clapeyron equation states that

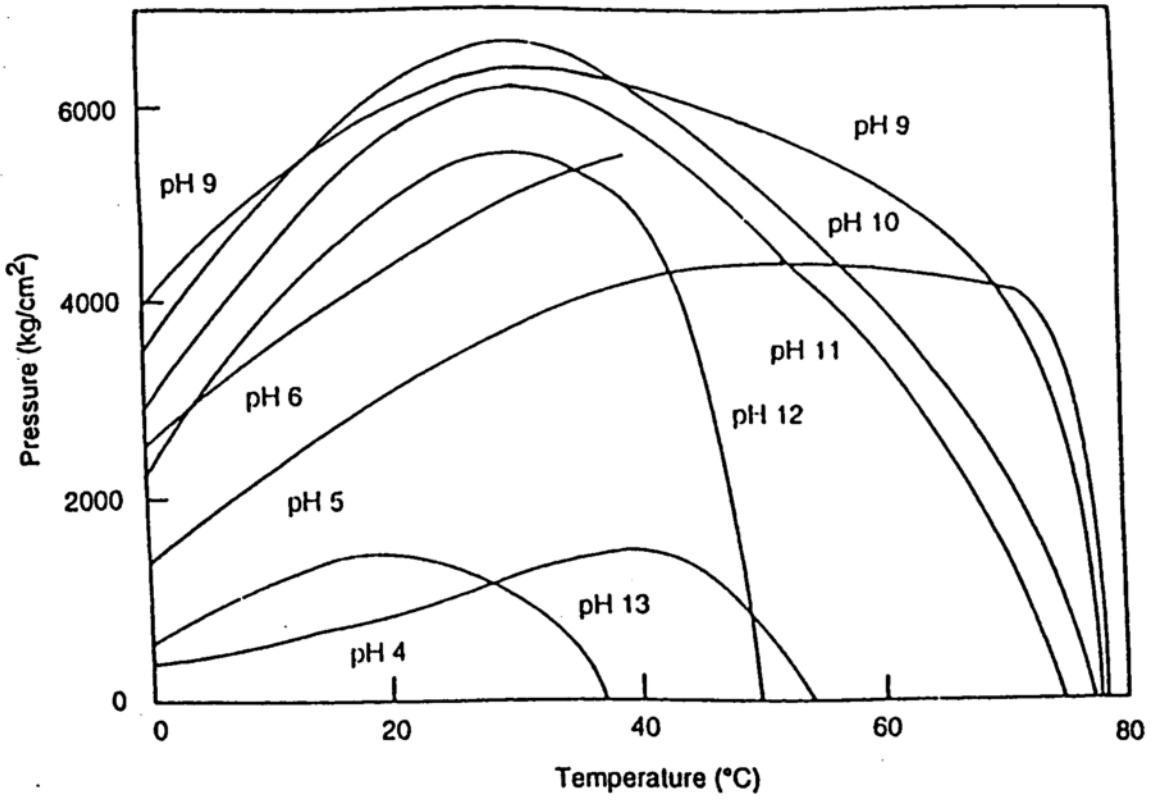

Figure 1-3. Contours of constant pH in the pressure-temperature plane where $\Delta G=0$ for the denaturation of metmyoglobin. The native state is more stable than the denatured state inside each contour (Zipp & Kauzmann, 1973).

$$\frac{dP_{1/2}}{dT} = \frac{(S_D - S_N)}{(V_D - V_N)} = \frac{\Delta S}{\Delta V} \qquad (26)$$

where P is pressure, T is temperature, S_D and S_N are the entropy of denatured and native states, respectively. V_D and V_N are the volume of denatured and native states. For a given pH, the free energy, ΔG, decreases as temperature increases (Hermans & Acampora, 1967) giving a positive entropy change, ΔS, at 1 atm. Since the high-temperature side of each pH contour arises from the axis with a negative slope, $(dP/dT)_{\Delta G=0}$ is negative requiring ΔV to be negative for the transition from native to denatured at 1 atm for the entire pH range. At high temperatures, $(dP/dT)_{\Delta G=0}$ becomes increasingly negative meaning that ΔS becomes more positive and/or ΔV becomes more negative.

At high pressures for each pH, $(dP/dT)_{\Delta G=0}$ becomes zero indicating that ΔS must also become zero. As the temperature is lowered, $(dP/dT)_{\Delta G=0}$ becomes positive, so ΔS must become negative since in order for ΔV to change sign, $(dP/dT)_{\Delta G=0}$ must go to infinity which is not observed. For this reason, Zipp and Kauzmann concluded that ΔV must remain negative at all values of pH, temperature, and pressure studied. If this trend continues (ΔS negative and ΔV negative) as the temperature is lowered, then the curve will intersect the atmospheric pressure axis again, somewhere below 0°C giving rise to "cold denaturation" as predicted by Brandts (Brandts, 1969).

As Weber and Drickamer (Weber & Drickamer, 1983) pointed out, the most important issue involved in applying pressure to a system is the difference in intermolecular forces due to solvation of products and reactants. This is evident because of Born repulsion, which dominates at shorter interatomic distances and predicts that at high pressures the compressibility of all materials will converge to similar, small values. That is, as pressure increases, the compressibility, {-(1/V)dV/dP}, decreases. For all practical purposes, since covalent bonds and bond angles are already dictated through Born repulsion they can be thought of as incompressible in liquid water up to a pressure of 12 kbar (Benson & Drickamer, 1957). As a result, solvation is the most significant cause of the pressure induced shift in equilibrium.

The volume change that is observed upon protein denaturation is negative. This volume change is thought to result from an overall contribution of changes in electrostriction, packing defects, and exposure of more of the polypeptide chain to solvent (Weber & Drickamer, 1983). When a charged side chain is exposed to the solvent either by a buried charge being exposed or by an ion pair dissociating, the aqueous solvent packs more tightly around that charge. This results in electrostriction, causing a decrease in system volume. The significance of the electrostriction contribution to the overall volume change is thought to be minimal because most charged side chains are already exposed, and thus, solvated (Weber & Drickamer, 1983). In addition, Royer and coworkers (Royer et al., 1993) showed that for Staphylococcal nuclease, the

electrostriction of buried charges does not contribute significantly since there is no change in the volume between pH 3.5 and 7.

The protein system volume should decrease due to the elimination of packing defects upon unfolding. If the protein in the native state contains solvent inaccessible cavities, as the protein unfolds, those cavities become exposed to the solvent which is able to permeate the cavities resulting in decreased system ,volume. It is unclear, however, how significant the packing defects are to the volume change. For Staphylococcal nuclease, the change in partial molar volume of the protein upon unfolding at 21°C is about 0.5% of the total hydrated volume of the folded protein (Royer et al., 1993). The volume sizes of internal cavities of various proteins, studied by Honig and coworkers (Rashin et al., 1986), ranged from 0 to 2% of the total volume, and are therefore, large enough to contribute to the total volume change of unfolding.

There is much controversy over the volume change due to the so called hydrophobic effect. If the classic view is used to describe the hydrophobic effect, then the predicted volume change would be considered to be positive based on the ordering of water molecules around the hydrophobic residues into a clatharate structure. This would give rise to the large negative entropy term observed for the transfer of nonpolar molecules to a hydrophilic environment (Frank & Evans, 1945). If the scaled particle theory, also known as the solvophobic effect, is used, the large negative entropy term originates from the creation of a cavity in the solvent for the solute to be placed (Mirejovsky & Arnett,

1983, Sjoberg et al., 1993). This view of hydrophobic hydration accounts for the decreased system volume by assuming that solvent molecules are hard spheres which become more densely packed as a cavity is created for the insertion of a solute (Klapper, 1973).

Kauzmann concludes that there is a decrease in volume with the transfer of a nonpolar group to an aqueous environment upon unfolding. However, the decrease in volume is not as large as would be expected from the oil drop model used in hydrophobic transfer studies (Kauzmann, 1959). This is generally accounted for by the fact that the interior of the protein is much more tightly packed than liquid hydrocarbons resulting in a smaller decrease in volume than expected. Taniguchi and coworkers (Sawamura et al., 1989) also found the volume change due to hydrophobic hydration to be negative based on solubility studies of benzene and alkylbenzenes in water. Boje and Hvidt (Boje & Hvidt, 1972) pointed out that small molecules were not accurate models for the observation of hydrophobic residues within a protein and decided to use a hydrophobic polymer chain as a model protein. According to their experimental results, the volume change due to the transfer of nonpolar groups from the interior of the protein to the aqueous environment upon unfolding results in a small positive volume change, which is primarily due to the volume change of the solvent.

More recently Chalikian and Breslauer (Chalikian et al., 1996) have also come to the conclusion that small molecules are not accurate models for how

amino acid residues behave within a protein. In fact, they showed that for nonpolar groups, the ability of small molecular weight molecules to model the effect of nonpolar residues within a protein is dependent upon the temperature. At low temperatures, hydrophobic protein groups appear to be hydrated independently, while at high temperatures, the surrounding polar groups influence the solvating water molecules.

Placing specific contributions to the negative volume change aside, we know that upon unfolding proteins exhibit a decrease in volume anywhere from -30 to -100 ml/mol (Weber & Drickamer, 1983). Therefore, there must be some compensating effect in the positive direction. Chothia and coworkers (Harpaz et al., 1994) along with Prehoda and Markley (Prehoda & Markley, 1996) conclude that this positive contribution probably comes from a positive volume change due to the hydration of hydrophobic residues. In any case, the fact that large proteins have similar volume changes to that of smaller ones does raise suspicion as to how the three contributions (electrostriction, packing defects, and hydrophobic hydration) could lead to such a relatively small change in volume without there being some type of compensating term. Chalikian and Breslauer (Chalikian & Breslauer, 1996) propose that the positive compensating term comes from a previously ignored term, the thermal volume, which is a result of the formation of the cavity mentioned in the scaled particle theory. Protein denaturation from the standpoint of volume changes can be described in a three step process where the tightly packed interior of the protein is disrupted, a cavity

is created in the solvent large enough to accommodate the unfolded protein followed by placement of the protein into the cavity, and solvation of exposed surfaces upon unfolding. Each of these steps has a distinct volume change associated with it. The disruption of the protein interior is analogous to packing defects which brings about a negative volume, ΔV_v, contribution due to the exposure of cavities within the protein interior. The thermal volume, ΔV_T, comprises the cavity creation from the solvophobic effect and causes a positive change in volume due to an increase in the accessible surface area of the protein. The solvation of exposed surfaces upon unfolding corresponds to the hydration effects of previously buried groups, which consists of electrostriction and hydration of polar groups and gives a negative volume change, ΔV_I. The volume change upon unfolding can then be expressed as follows:

$$\Delta V^\circ = \Delta V_V + \Delta V_T + \Delta V_I \qquad (27)$$

As can be gleaned from the preceding discussion, the contributions to the negative volume change are not well understood to date. The primary objective of the work described in the present thesis is to attempt to determine the magnitude and sign of the various classes of contributions to the volume change accompanied by protein denaturation.

Staphylococcal Nuclease

In order to complete this objective, a model protein was used. Staphylococcal nuclease (nuclease) is a commonly studied protein which was chosen as the model protein in this study because it is a small (only 149 amino acids), monomeric, single domain protein which contains no sulfhydryl residues or disulfide linkages. Nuclease also undergoes reversible denaturation by temperature, pH, chemical denaturants, and pressure. The protein structure was crystallized to the best resolution by Hynes and Fox (Hynes & Fox, 1991) and is shown in Figure 1-4 with the tryptophan labeled by use of the MOLSCRIPT software package (Kraulis, 1991). The protein contains one tryptophan residue at position 140 which makes it an excellent candidate for monitoring the unfolding by intrinsic tryptophan fluorescence. It has been shown that upon unfolding by pH, temperature, guanidine, and pressure, the intrinsic tryptophan fluorescence decreases dramatically (Eftink et al., 1991b, Royer et al., 1993, Shortle & Meeker, 1986) and that these changes coincide with changes in CD, NMR, and biological activity. The reason for the decrease in intrinsic tryptophan fluorescence is not clearly understood, but is thought to be a consequence of protein quenching groups in the unfolded state. Also, the unfolding of WT nuclease by monitoring tryptophan intensity gives the same results as CD, i.e. it is a two-state transition (Eftink, 1995, Shortle & Meeker, 1986). There are several mutants with site-specific amino acid substitutions

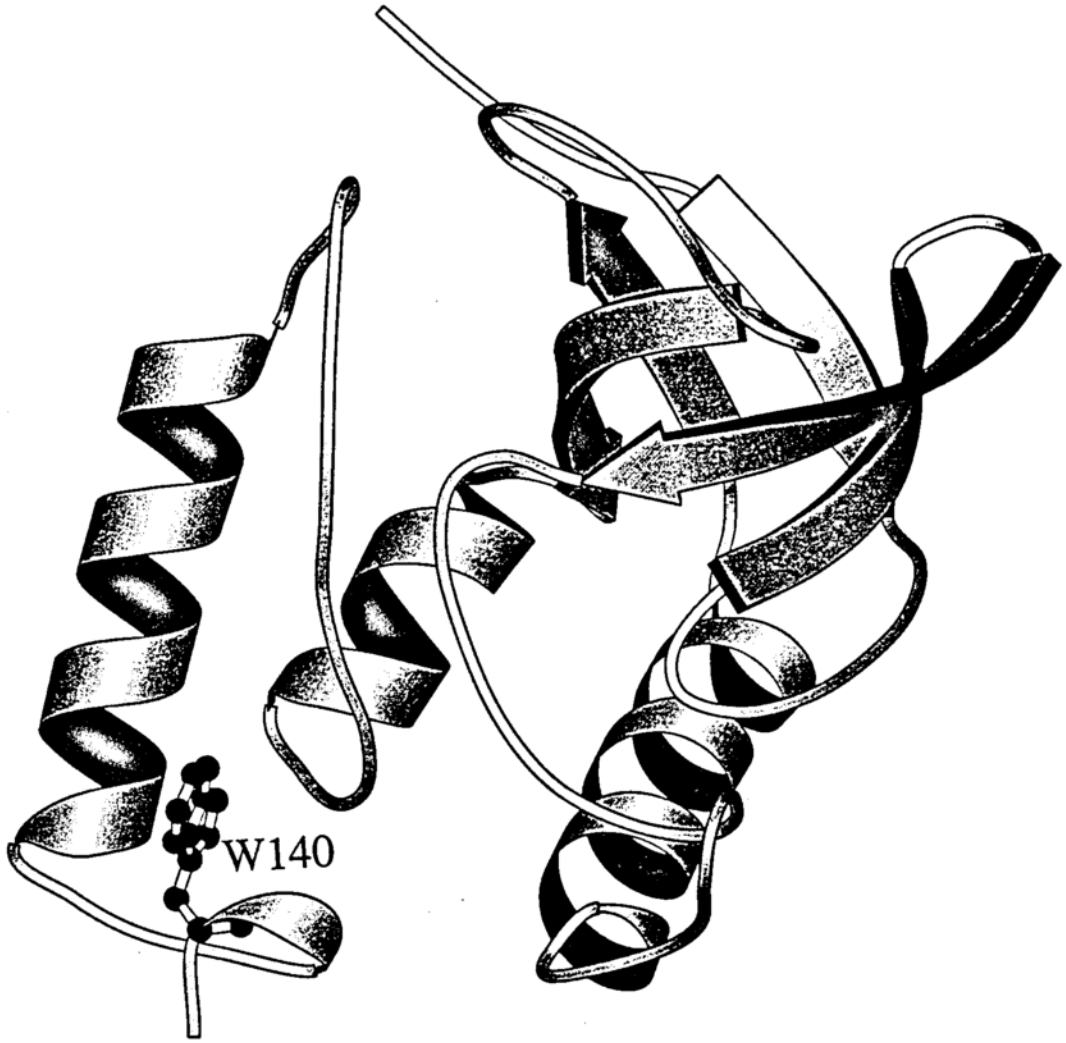

Figure 1-4. The structure of Staphylococcal nuclease crystallized by Hynes and Fox (Hynes & Fox, 1991) with the tryptophan residue denoted by MOLSCRIPT (Kraulis, 1991).

available. Many of the mutants cause large perturbations in the stability of the protein against denaturation with respect to the cooperativity of the unfolding transition while others result in changes within the packing of the protein interior (Alexandrescu et al., 1990, Alexandrescu et al., 1989, Fox et al., 1986, Shortle et al., 1988).

Privalov and coworkers (Carra et al., 1994, Carra & Privalov, 1995) have concluded that for Staphylococcal nuclease, m^+ behavior is a result of either mutational destabilization or stabilization of the hydrophobic core or the β-barrel. The m^- behavior is much more complex and is a result of either an increased intrinsic stability of the β-barrel subdomain, a decreased intrinsic stability of the α-helical subdomain, loss of interactions maintaining cooperativity between subdomains, or differential destabilization of the native versus intermediate states at positions integral to the hydrophobic core.

Shortle also discovered that when the hydrophobic side chains were shortened to an alanine or glycine, an increase in m_{GuCl} was seen instead of the expected decrease based on the amount of surface area. Those mutations were located in the β-barrel of the protein while mutations that did result in the expected decrease in m_{GuCl} were located outside of this hydrophobic core region (Shortle et al., 1990).

CHAPTER 2: AIM OF THESIS

The primary aim of this thesis was to characterize the underlying contributions to the negative volume change observed upon protein unfolding, ΔV_u, in our model protein, staphylococcal nuclease. The secondary aim was to elucidate the kinetic basis for the stabilization of nuclease by xylose, thereby further addressing the role of solvation in protein folding.

The first objective in the characterization of the underlying contributions to ΔV_u was to evaluate the contribution of hydrophobic hydration to ΔV_u. This was done by investigating the pressure-induced unfolding of three mutants of nuclease that exhibit chemically induced unfolding cooperativity higher than, lower than, and similar to wild type. As discussed in Chapter 1, this cooperativity, termed *m*-value, correlates with differences in exposed surface area (ΔA_u) upon unfolding. To test the correlation between ΔA_u and ΔV_u, high pressure denaturation studies were carried out as a function of xylose, an osmolyte known to stabilize proteins through preferential hydration.

The second contribution to ΔV_u which was evaluated was the role of excluded volume. Imperfect packing of the folded protein results in cavities, or solvent excluded volume, in the folded state, which become solvated upon unfolding. The degree to which such effects contribute to ΔV_u was investigated by determining the values for ΔV_u in a series of nuclease mutants. The mutants either introduced cavities into the interior of the protein by replacing a large hydrophobic residue with smaller side chains or decreased cavity size by replacing a residue with a large more hydrophobic residue. If the ΔV_u for the

cavity mutants is larger in absolute value than for the wild type, $\Delta\Delta V_u$ may be correlated to the size of the cavity.

The final objective was to determine the kinetic basis for the stabilization of nuclease by xylose, a colligative agent that changes the activity of water. This study addresses the role of solvation in protein folding. The stabilization of proteins by sugars must come from changes in either the rate of folding, unfolding, or both. Pressure-jump relaxation experiments were carried out as a function of increasing xylose to determine the rates of folding and unfolding. From these rates, as well as the activation volumes, the basis for the kinetic stabilization was determined. In addition, these studies provided information about where the transition state lies along the reaction coordinate with respect to the amount of surface area exposed relative to the native and unfolded states, and about the number of water molecules involved in the folding transition.

CHAPTER 3: MATERIALS AND METHODS

Protein Preparation

Wild type (WT)

WT nuclease was produced using the T7 expression system from the *E. coli* strain BL21(DE3) as described by Alexandrescu *et al.* (Alexandrescu et al., 1989) and Royer *et al.* (Royer et al., 1993). Both the growth procedure and the protein purification procedure were carried out according to Wang *et al.* (Wang et al., 1990) and Royer *et al.* (Royer et al., 1993) with the exception that the protein was stored in solution instead of lyophilized. A 5 ml starter culture of LB media containing 50 μg/ml of ampicillin and 34 μg/ml chloramphenicol (to select for the ampicillin and chloramphenicol resistant plasmids which overproduce the protein) was inoculated and grown in a shaker at 37°C overnight (8-12 hours). This 5 ml culture was used to inoculate 1 L of LB media with ampicillin and chloramphenicol which was incubated in the shaker at 37°C. The growth of the culture was monitored by measuring the visible absorbance at 600 nm in a Hitachi U-3000 spectrophotometer every 30 minutes. When the absorbance at 600 nm reached approximately 1.3, the growth was induced with 100 mg of IPTG (Isopropyl-b-D-thiogalactopyranoside) per liter. The cells were then grown an additional 3 hours at 37°C in the shaker. The cells were harvested by centrifuging in 500 ml centrifuge bottles (all centrifugation was carried out in a Sorvall R-5B centrifuge with a GSA rotor at 4° C and 10 rpm) for 20 minutes. The harvested cell pellets were resuspended in 50 ml of cold 0.1 M Tris base,

2.5 mM Na_2EDTA. The cell suspensions were then combined and frozen at -20°C. The cells were then thawed in 37°C water bath a procedure which results in an increase in the viscosity of the solution indicative of cell lysing. Next, 1 ml of 1.0 M $CaCl_2$ was added which causes an abrupt decrease in viscosity due to activation of nuclease by Ca^{++}. The pH of the suspension was then lowered to 9.2 with glycine and incubated at room temperature for one hour. The precipitate was then spun out by centrifuging for 20 minutes. The supernatant was poured off and saved as the crude extract, which was then loaded onto a preequilibrated DEAE Sephadex A-50 anion exchange column (1 inch by 5 inch) connected in series with a CM Sephadex C-25 cation exchange column (1 inch by 10 inch) at a rate of 2.5 ml/min. Both columns were washed with 500 ml of 0.1 M Tris-Gly pH 8.8. The anion exchange column was detached and the cation exchange column was then washed with 500 ml of 0.2 M Tris-HCl pH 7.6. The protein was then eluted with 250 ml of 0.2 M Tris-HCl, 0.6 M NaCl pH 7.6 and the eluant was collected with a Gilson Microfractionator fraction collector. Those fractions containing protein were pooled and dialyzed with 6000-8000 MW cutoff dialysis tubing at 4°C in 10 mM bis-Tris, 1 M NaCl pH 5.5 for 5 hours. Dialysis continued in 10 mM bis-Tris, pH 5.5 at 4°C for 5 hours with 3 changes of buffer. Purity was determined with a 15% SDS polyacrylamide gel. An activity assay was carried out as described by Cuatrecasas and coworkers (Cuatrecasas et al., 1967) where the increase in absorbance at 260 nm due to the hydrolysis of nucleic acids by the protein was monitored.

Mutants

Staphylococcal nuclease mutants were produced using the λ expression system in the *E. coli* strain Arλ9 as described by Shortle and Lin (Shortle & Lin, 1985). The cells were grown according to the procedure described by Shortle and coworkers (Shortle et al., 1989) with the exception that SB media was used instead of MOPS media. The protein purification followed the method used in Shortle and Meeker (Shortle & Meeker, 1989) except an additional extraction step was added without any salt and a Pharmacia Fast Flow S-Sepharose column was used alone without any further column. A 5 ml starter culture of SB media with 100 μg/ml ampicillin was inoculated and grown at 37°C in a shaker for 8-12 hours. This starter culture was used to inoculate 1 L of SB media containing 100 μg/ml ampicillin and grown at 37°C in a shaker overnight (12-15 hours). The absorbance at 600 nm after 12-15 hours was between 1.5-3.0. The cells were then harvested by centrifugation for 20 minutes. The supernatant was discarded and the cells were drained briefly. Each cell pellet was then resuspended in 50 ml of ice cold extraction buffer #1 (6 M urea, 25 mM Tris, 2.5 mM EDTA, pH 8.0). Once the cells were fully resuspended they were swirled gently on ice for 20 minutes. The cell extract was then centrifuged at 4°C and 10 rpm for 20 minutes and the supernatant was discarded. The cell pellets were then gently resuspended in ice cold extraction buffer #2 (6 M urea, 25 mM Tris, 2.5 mM EDTA. 0.2 M NaCl, pH 8.0). Once the cell pellets were fully resuspended, they were swirled gently on ice for 20 minutes. The cell extract

was then centrifuged for 30 minutes after which the cleared extract was transferred to new centrifuge bottles to which an equal volume of ice cold 200 proof ethanol was added. The mixture was then incubated at -20°C for 3-5 hours. The large precipitate that formed was removed by centrifugation for 30 minutes. The supernatant was saved and an equal volume of ice cold 200 proof ethanol was added to the cleared supernatant. The solution was then incubated at -20°C for 60 minutes. The precipitate was recovered by centrifugation for 20 minutes. The supernatant was discarded and the pellets were drained briefly. The pellets were then resuspended in about 10 mls of extraction buffer #1. The extract was loaded over a preequilibrated S-Sepharose Fast Flow Econo column 0.75 inches by 2 inches (10-15 mls of resin). The column was rinsed with 10 bed volumes of extraction buffer #1. Elution of the protein was accomplished by adding 3 bed volumes of extraction buffer #1 with 0.4 M NaCl and the eluant was collected with Gilson Microfractionator fraction collector. The eluate containing protein was pooled together and 1/20th of this volume of 1 M Tris-HCl pH 7.0 was added. The protein was precipitated with 4 volumes of ice cold 200 proof ethanol and incubating at -20°C for 60 minutes. The precipitate was collected by centrifugation for 20 minutes. The supernatant was discarded and the pellets were drained briefly. The pellet was then resuspended in 6 M urea, 10 mM bis-Tris pH 7.0 and dialyzed in 6000- 8000 MW cutoff dialysis tubing in 4 L of 1 M NaCl, 10 mM bis-Tris pH 7.0 for about 5 hours at 4°C. The protein was dialyzed 3 more times in 4 L of 10 mM bis-Tris pH 7.0 at 4°C for 5 hours each. The

sample was then centrifuged to remove particulates. The protein was stored in solution in small aliquots at -20°C. The protein was checked for purity with a 15% SDS-Polyacrylamide gel and the activity was tested as described previously.

Pressure Experiments

High pressure experiments were carried out in a Vascomax high pressure cell using a high pressure generating system similar to that described by Paladini and Weber (Paladini & Weber, 1981) (Figure 3-1). The pressure generator (High Pressure Equipment Co.) is connected to a high pressure gauge and the pressure cell through a series of metal tubing and high pressure valves. The steady state fluorescence unfolding profiles were measured using an ISS spectrofluorometer (ISS, Urbana, IL). Exciting light from a xenon arc lamp was brought to the pressure cell from the monochromator via a UV multifiberoptic bundle (Oriel Corp., Stratford, CT). The excitation wavelength was fixed at 295 nm to spectroscopically select the intrinsic tryptophan residue and minimize fluorescence contributions from tyrosine for all experiments except those involving ANS (8-Anilino-1-naphthalene-sulfonate) (see Chapter 4 for the chemical structure). The tryptophan emission (or ANS emission) was monitored at a 90° angle through a Corion 340 nm high pass filter for all experiments except ANS binding. The signal was then sent through a photomultiplier tube

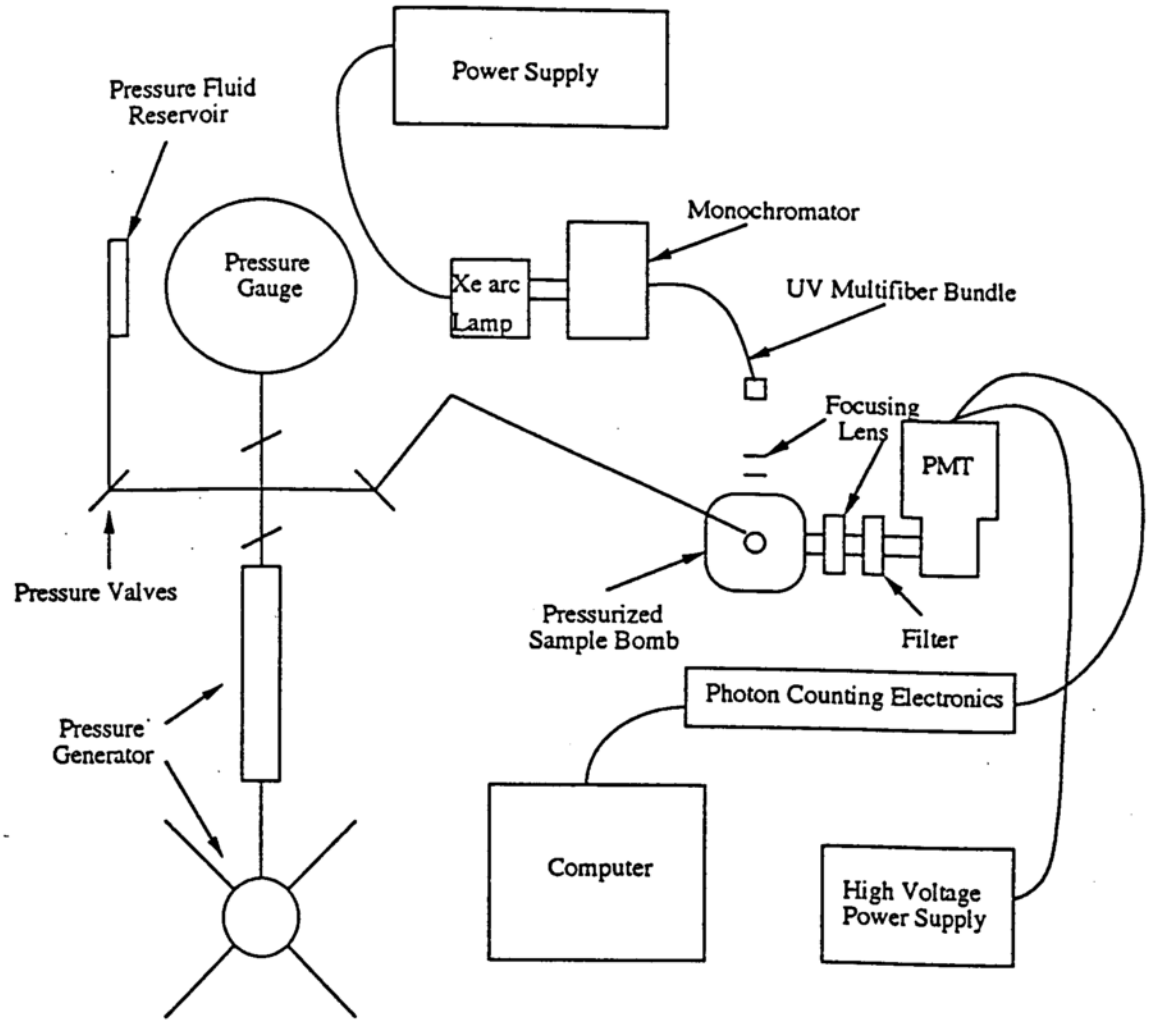

Figure 3-1. The lay out of the high pressure instrument.

which was connected to the detection electronics (also from ISS). The detection electronics were also connected to the computer. ISS software was used to translate the signal into the relative intensity.

ANS Binding Experiments

The ANS was excited at 340 nm and fluorescence emission was detected at 90° from the excitation beam through a 500 nm high pass filter. The WT experiments were carried out in 10 mM bis-Tris (shown in Figure 3-2) pH 5.5 with approximately 20 μM protein and 20 μM ANS. Pressure jumps of 100 bar to 2200 bar were made and the intensity was measured in the photon counting mode.

Cooperativity Mutants

Pressure jumps of 100-200 bar were made and the fluorescence intensity was measured with a 20 second integration time. Equilibrium was reached after 20-25 minutes for all pressures and those intensity values were used for the equilibrium unfolding profiles. The experiments were carried out at concentrations less than 10 μM (as determined by UV absorption at 280 nm) to avoid any aggregation which can occur in unfolding experiments at high concentrations. The buffer was 10 mM bis-Tris at pH 4.5 and 7 for the WT and the cooperativity mutants respectively due to the instability of the mutants at lower pH. The bis-Tris was used because the pKa is pressure insensitive and

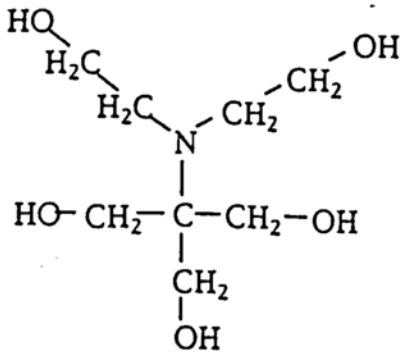

Figure 3-2. Chemical structure of bis-Tris.

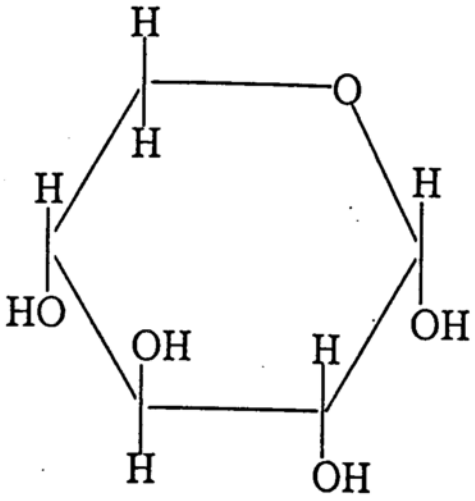

Figure 3-3. Chemical structure of xylose.

therefore no volume change due to electrostriction is observed. The experiments were carried out in triplicate at 7-8 different xylose (structure shown in Figure 3-3) concentrations for each mutant and for WT. All pressure runs were greater than 95% reversible.

Pressure-jump Relaxation Kinetics

Pressure jumps of 75-150 bar were made by closing the valve to the sample compartment, pumping to the desired new pressure, and then rapidly reopening the valve. Fluorescence intensity data were acquired with 5 second integration times, which are fast relative to the relaxation time scales. The pressure jumps were small enough that the adiabatic heating of the sample amounted to no more than 0.3°C, which, at the sample temperature of 21°C, would not perturb the folding equilibrium of nuclease significantly. In addition, the extent of the perturbation of the equilibrium due to the pressure jump itself was less than 10%, such that the linearized rate expression holds (Eigen & deMaeyer, 1963). All pressure runs were greater than 95% reversible.

Cavity Mutants

Experiments involving cavity mutants were carried out as described above for pressure-jump relaxation kinetics with the values of the intensities 25 minutes after the jump taken as the equilibrium intensities. The V66L mutant was very stable at a pH of 5.5 in 10 mM bis-Tris. Therefore, 0.5 M guanidine was added

to the buffer to destabilize the protein just enough so that it was poised on the edge of the unfolding transition and the pressure was enough to completely unfold the protein by 2200 bar. A pH of 7.0 in 10 mM bis-Tris in the absence of destabilizers or stabilizers was sufficient to allow observation of the entire unfolding transition for the V66A mutant. For the V66G mutant, a pH of 7.0 in 10 mM bis-Tris with 15% w/v xylose was needed in order to observe the entire unfolding profile.

Circular Dichroism (CD)

CD experiments were performed with a Jasco J-710 spectropolarimeter (Japan Spectroscopic Co.). The temperature was controlled with a jacketed 0.05 cm circular cell connected to a programmable water bath. The buffer conditions were the same as the pressure experiments for the cooperativity mutants with a protein concentration of approximately 0.4 mg/ml. The temperature was increased at 0.5 K/min for the melting curves. A molar ellipticity [θ] of 112.5 was calculated by taking the average molecular weight per amino acid residue. The Jasco J-710 software was used to smooth out noise in the data.

Osmolarity

The osmolarity of xylose solutions for the xylose kinetic experiments was measured on a Wescor 5500 vapor pressure osmometer.

Data Analysis of Pressure Experiments

Cooperativity Mutants

The equilibrium data were analyzed using the BIOEQS analysis program to determine the free energy and volume change of unfolding at constant temperature (Royer, 1993, Royer et al., 1990) according to the relation

$$\Delta G = P\Delta V \qquad (1)$$

and ΔG is defined as

$$\Delta G = -RT\ln K_{eq} = -RT\ln\left[\frac{(I_f - I_p)}{(I_p - I_u)}\right] \qquad (2)$$

where I_f and I_u are the relative fluorescence intensities of the folded and unfolded states and I_p is the intensity at a pressure p. This program is a nonlinear least-squares data analysis program which uses a numerical solver (EQS) developed

by Smith and Missen (Smith & Missen, 1982). This solver uses Lagrange multipliers to solve for the various species concentrations given the free energy and volume change of unfolding values. However, when analyzing data that follows a simple two-state folding model, the numerical solver (EQS) is replaced by the closed-form analytical equation for the monomer unfolding equilibrium. It works by first inputting an estimate for the free energies, volume changes, and starting and ending values. The solver then takes the estimated ΔG value and solves for the equilibrium constant K by the following equation:

$$K = \exp(-\Delta G / RT) \tag{3}$$

Next, the species fractions are solved for by using the equilibrium constant because

$$\text{K=[unfolded]/[folded]} \tag{4}$$

$$X_{un} = \frac{CK}{(1+K)} \tag{5}$$

$$X_f = C - X_{un} \tag{6a}$$

$$X_{un} = \frac{X_{un}}{C} \qquad (6b)$$

$$X_f = \frac{X_f}{C} \qquad (6c)$$

(where X_{un} and X_f are the unfolded and folded species, respectively and C is the protein concentration). The BIOEQS program calculates data points at each pressure from the current parameters, ΔV, ΔG and the asymptotic values of the folded and unfolded state intensities, I_f and I_u, using the equilibrium constant K_{eq}, which is calculated from the intensities measured at each pressure, I_p:

$$\Delta G = -RT \ln K_{eq} = -RT \ln \frac{(I_f - I_p)}{(I_p - I_u)} \qquad (7)$$

The nonlinear least squares program then goes through an iterative process to yield a fit for the data. The least squares program compares the values obtained from the solver to the real data. If the values are not similar, the least squares algorithm changes the ΔG and ΔV values and sends them back to the solver. The program continues to iterate until the calculated data obtained from the solver are similar to the real data. Confidence limits of 67% on the reported values of ΔV were calculated by performing complete minimizations at each

tested value of the parameter and by recording the χ^2 value obtained. In these confidence limit tests, all of the other parameters (ΔG and asymptotic intensities) were allowed to vary. The confidence limits were calculated using the numerical methods F-statistic program given the degrees of freedom and global χ^2 of the fit. The data can be analyzed in a linked manner in which the program is told to solve a series of data sets for the same value of ΔV or ΔG.

The data were first analyzed in the unlinked, or single curve, mode to verify that there was no systematic difference in the volume change with increasing xylose concentrations. Next, each set of raw intensity data consisting of 7-8 xylose concentrations was globally analyzed by linking the ΔV_u across the set allowing its value, the ΔG_u, and asymptotic intensity values for each individual curve to vary. An identical analysis was performed for each replicate set of xylose concentrations for both mutants. The volume and free energy changes recovered from the fits of each replicate set were averaged and standard deviations calculated. For purposes of visual comparison the raw data from the unfolding profiles were then normalized to a scale from 0 to 100% native protein by calculating the percentage decrease in intensity at each pressure relative to the asymptotic intensity values recovered from the fits.

Since the WT is significantly more stable than the mutants, reasonable fits could not be obtained when the asymptotic intensity values were allowed to float. Therefore, the WT data were analyzed globally by linking the ΔV_u across each data set allowing ΔG_u to vary for each xylose concentration. The asymptotic

values were obtained from the averaged total intensity decrease observed for the pressure profiles at 0% xylose since these were the only profiles of WT that exhibited complete unfolding. The three experiments on WT protein completed without xylose yielded an average decrease in intensity upon unfolding of 57.7%. For experiments in the presence of xylose, the value of the intensity of the denatured state in each profile was fixed at a value 57.7% lower than the intensity observed at atmospheric pressure. The ΔV_u and ΔG_u for each data set were averaged and standard deviations calculated. Like the mutants, the raw data were also normalized for purposes of presentation.

Pressure-Jump Relaxation Kinetics

The pressure-jump fluorescence intensity relaxation profiles were fit to a single-exponential decay using the time-domain fluorescence global analysis program described by Beechem and coworkers (Beechem et al., 1991). The intensity of fluorescence at time t after the pressure jump, I(t), was taken to be an exponentially decaying function

$$I(t) = I_o e^{-t/\tau} \qquad (8)$$

where I_o is the intensity prior to the jump and τ is the relaxation time.

The effect of pressure on the Gibbs free energy of unfolding necessarily arises from pressure effects on the rates of unfolding, refolding, or both. A

reaction rate k_p at a given pressure p can be expressed in terms of the rate at atmospheric pressure k° and the activation volume $\Delta V^{\ddagger}$ for the formation of the transition state (Gladstone et al., 1941):

$$k_p = k^\circ e^{\left[-P(\Delta V^{\ddagger})/RT\right]} \tag{9}$$

For a simple, two-state system undergoing small perturbations near equilibrium, the observed relaxation time τ at a given pressure is represented by the inverse of the sum of the two individual rate constants for the forward and backward reactions, unfolding and folding,

$$\tau = \frac{1}{\left(k_f + k_u\right)} \tag{10}$$

and as such should be independent of the sign of the perturbation (Eigen & deMaeyer, 1963). The values of ln τ across the pressure range above and below the midpoint (the point where $\Delta G_p = 0$) respectively for the values of unfolding and folding rate constants at atmospheric pressure $(k^\circ)_f$ and $(k^\circ)_u$, and their individual activation volumes $\Delta V_f^{\ddagger}$ and $\Delta V_u^{\ddagger}$, were fit using linear analysis. At pressures below the midpoint the rate of folding dominates in the sum, while above the midpoint, the unfolding rate predominates (Vidugiris et al., 1995). It is evident from looking at a plot of ln τ vs. pressure (see Chapter 7) that above the

midpoint the slope of the line is much smaller than below the midpoint. Linear regression analysis below the midpoint was completed according to the equation

$$\ln \tau = -\ln k_f^\circ + \left(\frac{\Delta V_f^\ddagger}{RT}\right) P \qquad (11)$$

while above the midpoint the linear regression analysis was completed according to the equation

$$\ln \tau = -\ln k_u^\circ + \left(\frac{\Delta V_u^\ddagger}{RT}\right) P \qquad (12)$$

The data were also fit in a continuous manner without the assumption that the folding rate dominated at low pressures and the unfolding rate at high pressures to the equations

$$\ln 1/\tau = \ln\left[k_f^\circ \exp\left[-P\left(\frac{\Delta V_f^\ddagger}{RT}\right)\right] + k_f^\circ K_{eq} \exp\left[-P\left(\frac{\Delta V_{eq}}{RT}\right)\right]\right] \qquad (13)$$

$$k_u^\circ = \left(k_f^\circ\right)\left(K_{eq}\right) \qquad (14)$$

$$\Delta V_u^\ddagger = \Delta V_f^\ddagger + \Delta V_{eq} \qquad (15)$$

with the help of Dr. Dexter Northrop using a computer program by Duggleby (Duggleby, 1984). The data were first fit allowing the values of k°_{f}, K_{eq}, $\Delta V^{\ddagger}_{f}$, and ΔV_{eq} all to float. Since there was reasonable agreement between the recovered K_{eq} and the K_{eq} from the equilibrium data, the data were analyzed fixing K_{eq} as the constant value determined from the equilibrium analysis.

The values of the intensities 25 minutes after the jump were taken as the equilibrium intensities, and these equilibrium profiles were fit using the BIOEQS analysis program for the equilibrium free energy ΔG and volume change ΔV of the unfolding (Royer, 1993, Royer & Beechem, 1992, Royer et al., 1990) as described above.

Estimates of the experimental error of the equilibrium volume changes and free energies were obtained from rigorous confidence limit testing of these two recovered parameters as described above and previously by Beechem (Beechem, 1992). Error estimates on the rate constants and activation volumes were obtained from linear error analysis.

Cavity Mutants

The data were fit as described in the Pressure-Jump Relaxation Kinetics section. The experiments were performed 5-6 times for each mutant. The single curve analysis was done first. Then data sets for each mutant were analyzed globally linking both the ΔG and ΔV. As mentioned above, the 67% confidence limits on these values were determined as described earlier.

CHAPTER 4: THE PRESSURE DENATURED STATE OF WT STAPHYLOCOCCAL NUCLEASE

As discussed earlier, the denaturation of Staphylococcal nuclease (nuclease) by temperature, pH, and chemical denaturants has been previously studied (Eftink et al., 1991b, Royer et al., 1993, Shortle & Meeker, 1986). The equilibrium unfolding transition has been shown to fit well to a simple two-state transition where there are no intermediate states only either the native or denatured states (Carra et al., 1994, Eftink et al., 1991a, Schechter et al., 1970, Shortle & Meeker, 1986, Shortle et al., 1988, Shortle et al., 1990). When pressure is used to denature nuclease however, it cannot be assumed that the transition will also be a simple two-state transition. In fact Weber and coworkers showed that for lysozyme and chymotrypsinogen that the pressure denatured state represented a plurality of states (Li et al., 1976b). The pressure denatured state must be characterized in order to compare results from pressure denaturation to those obtained by other perturbation methods. In order to determine whether or not the pressure denatured state could be described as a molten globule, the pressure denaturation of nuclease was carried out in the presence of ANS (8-Anilino-1-naphthalene-sulfonate). ANS (Figure 4-1) is a fluorescent probe that is known to bind to hydrophobic regions and the molten globule (Semisotnov et al., 1991). The unfolding transition was also studied in the presence of xylose, an osmolyte known to stabilize native proteins, to see how the unfolding transition was affected. By studying the equilibrium pressure denaturation as a function of xylose, information regarding the change in the amount of surface area exposed in the unfolded state relative to the folded state

can be acquired as well as information relating to the hydration of exposed surfaces.

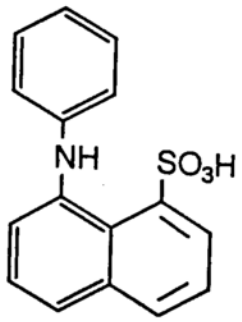

Figure 4-1. Chemical structure of ANS.

RESULTS

Figure 4-2 shows the fluorescence emission spectra of the intrinsic tryptophan residue of nuclease excited at 295 nm at atmospheric pressure and 2500 bar. There is a red shift in the emission maximum from approximately 335 nm to 355 nm which is typical for the denaturation of tryptophan containing proteins. This red shift is a result of the increase in solvation around the tryptophan residue as the protein unfolds (Lakowicz, 1983). In addition to the red shift, there is a fluorescence quench. The quench is not completely understood but is possibly due to the interaction of the tryptophan with a charged side chain in the unfolded state (Eftink et al., 1991a). Based on this modification for the intrinsic tryptophan fluorescence of nuclease, the pressure studies of

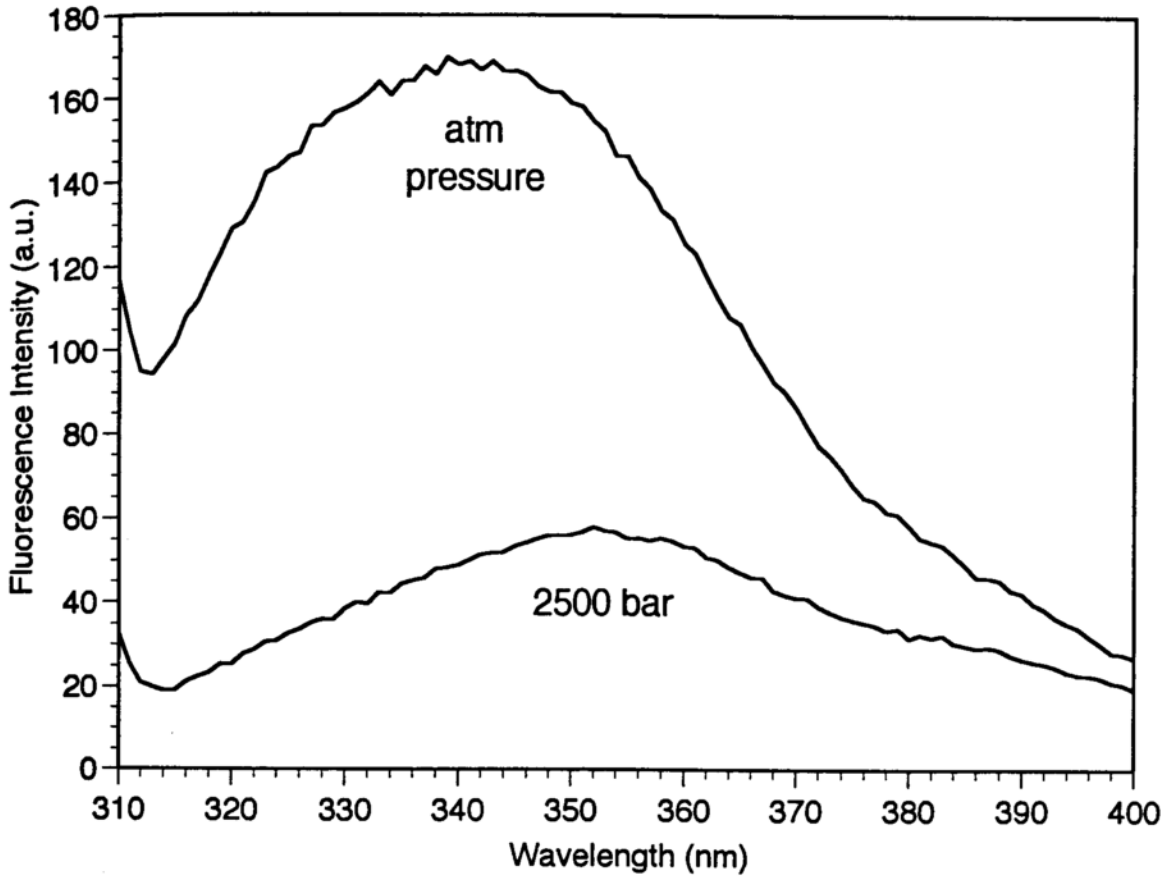

Figure 4-2. The fluorescence emission spectrum of intrinsic tryptophan excited at 295 nm for WT nuclease at pH 5.5 and 21°C for atmospheric pressure and 2500 bar.

nuclease presented in this thesis were carried out by exciting the protein at 295 nm and monitoring the fluorescence intensity of the intrinsic tryptophan through a 340 nm cuton filter.

Before determining whether ANS binds to nuclease, the behavior of ANS alone under pressure was determined. Figure 4-3 shows the fluorescence intensity of ANS as a function of pressure excited at 340 nm and monitored through a 500 nm cuton filter. There is a decrease in intensity as the pressure is increased. When ANS binds to a protein, there is a large increase in ANS intensity up to 100 times the original value in some cases (Li et al., 1976b). Figure 4-4 shows the fluorescence intensity of ANS with WT nuclease. The figure looks analogous to that of ANS alone. Since there was no increase in fluorescence intensity, this seemingly negative result suggests that ANS does not bind to nuclease. This further implies that the pressure denaturation of nuclease occurs without populating the molten globule state since ANS binds the molten globule state (Semisotnov et al., 1991). Therefore, these results lend support to pressure denaturation reaching a final unfolded state similar to other methods of denaturation without populating the molten globule state.

The addition of an osmolyte, such as xylose, stabilizes the native protein, and, as shown in Figure 4-5, shifts the pressure unfolding profile to higher pressures. The extent of stabilization of the native state depends on the amount of surface area exposed. Therefore, it can be determined if a mutant exposes the same amount of surface area as the WT protein. The figure shows a

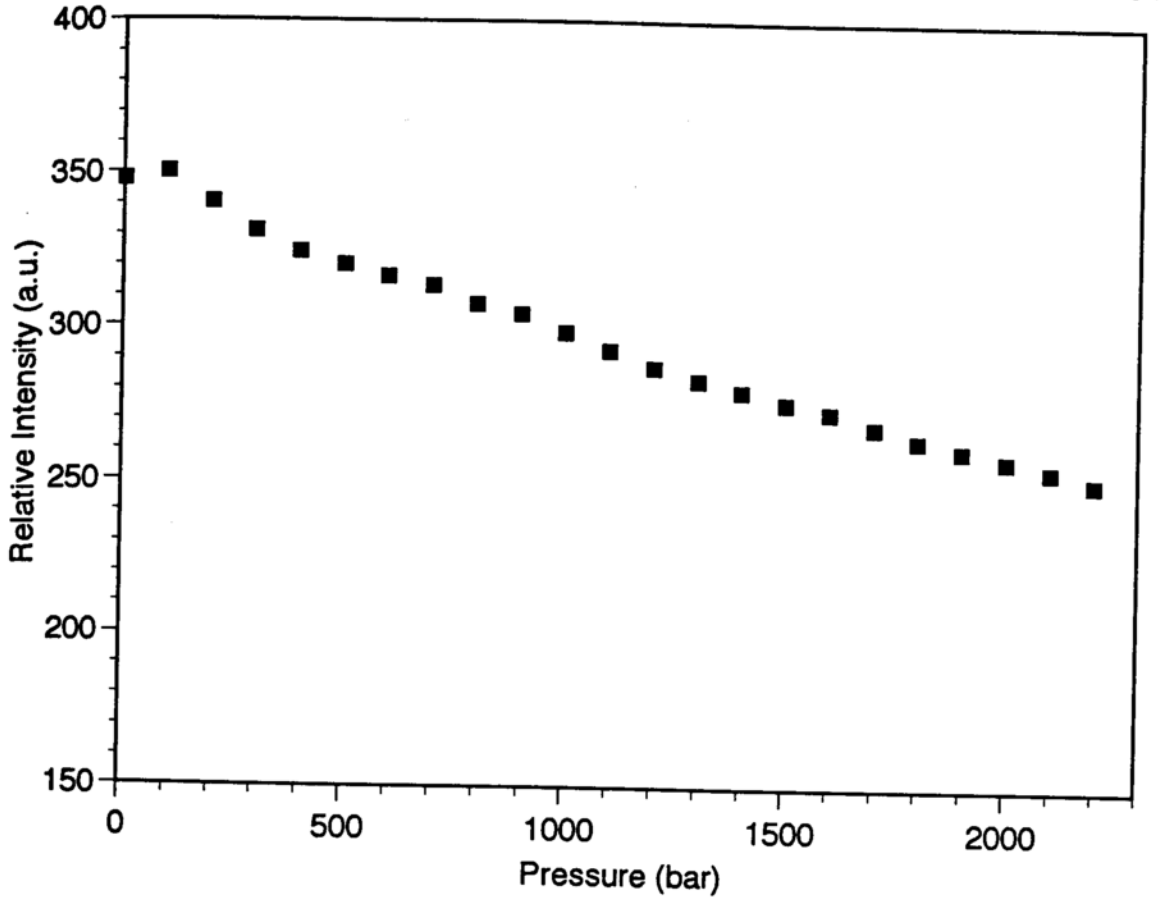

Figure 4-3. Fluorescence intensity of ANS as a function of pressure at pH 5.5 and 21°C.

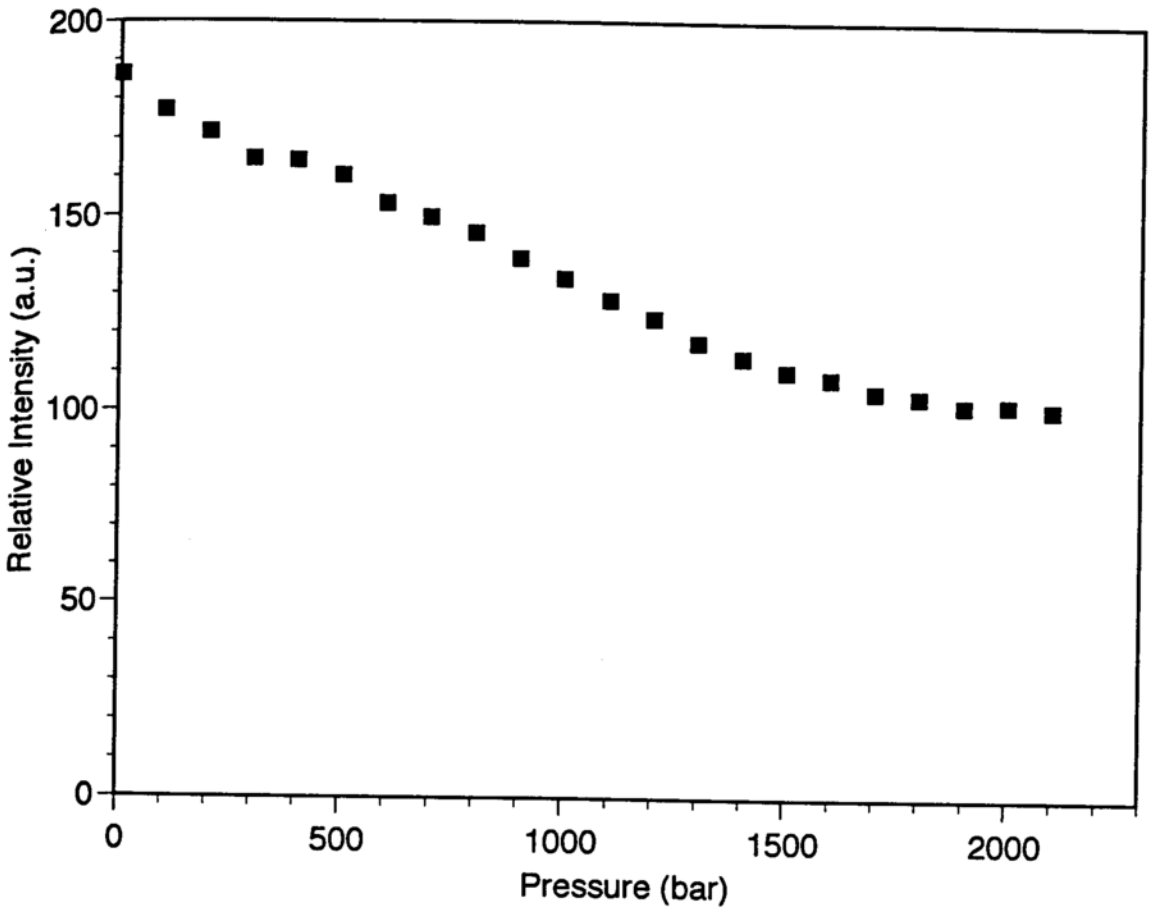

Figure 4-4. Fluorescence intensity of ANS (19 μM) with WT nuclease (19 μM) as a function of pressure at pH 5.5 and 21°C.

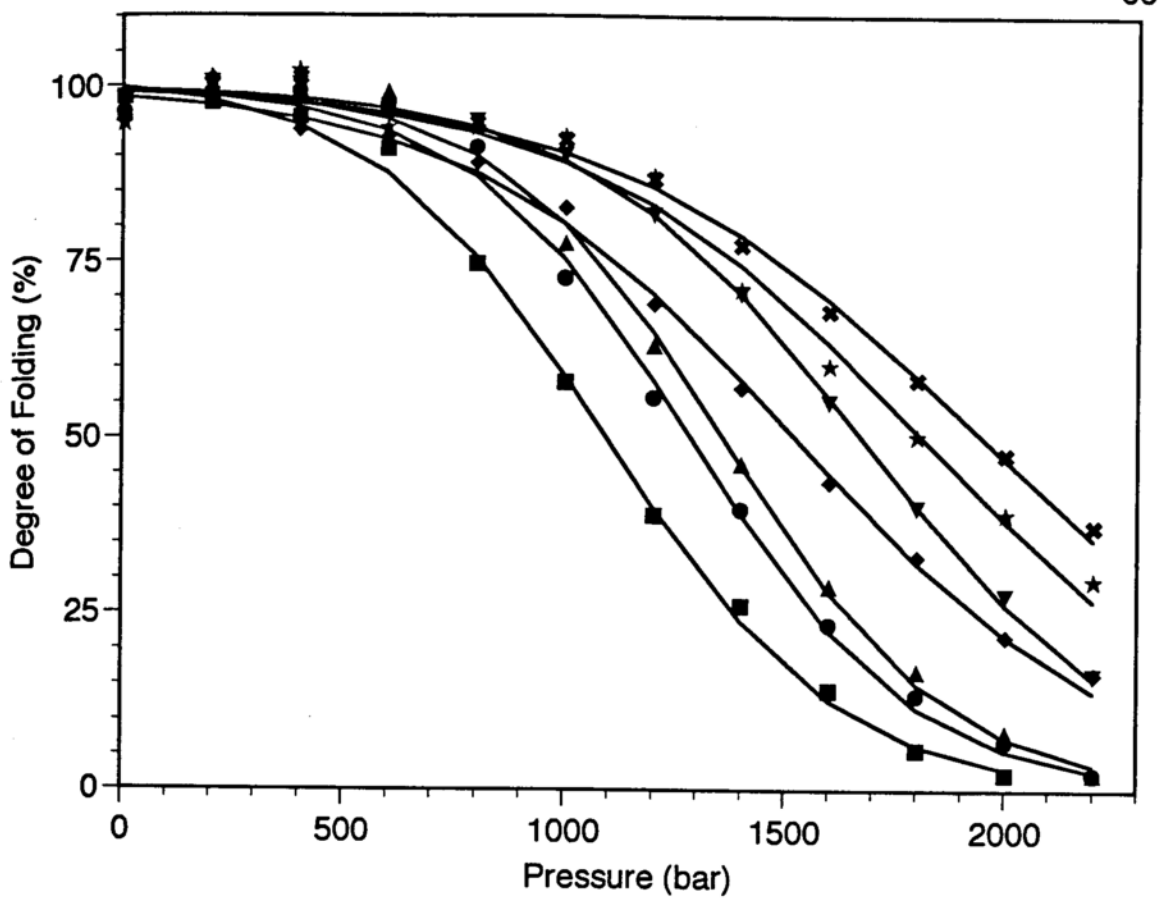

Figure 4-5. Unfolding profiles for WT nuclease as a function of pressure and millimole fraction xylose at pH 4.5 and 21°C. The symbols are data from a representative set of experiments and the solid lines represent the unlinked curve analysis fits to the data. (■) 0 mole fraction xylose, (●) 3 millimole fraction xylose, (▲) 6.2 millimole fraction xylose, (◆) 9.4 millimole fraction xylose, (▼) 12.7 millimole fraction xylose, (✖) 16.1 millimole fraction xylose, (★) 19.6 millimole fraction xylose.

representative set of normalized data for the pressure denaturation of WT nuclease in the presence of increasing amounts of xylose (see Appendix I for other representative sets of data). The average of the observed volume change, determined as described in Chapter 3, as a function of xylose with the standard deviations can be seen in Figure 4-6 for all WT unfolding experiments. As is evident from the figure, there is no trend for the volume change as a function of xylose concentration. The volume changes are all within experimental error of one another, therefore, the data can be analyzed by linking the volume change across each data set as shown in Figure 4-7 (additional data sets can be seen in Appendix I). Table 4-1 shows the comparison of the average ΔV_u with standard deviation for the unlinked analysis and the ΔV_u with rigorous confidence limits for the linked analysis. The overall average of ΔV_u with standard deviations for all representative data sets in the linked and unlinked mode are 75.3 ± 1.3 and 77.3 ± 5.3 ml/mol, respectively. As demonstrated by Figure 4-6, the volume change upon unfolding for the two analyses is within experimental error and does not change. Therefore, the volume change is not a function of xylose concentration and thus not a function of surface tension or surface area.

DISCUSSION

The molten globule state is described as a state with substantial secondary structure, little or no tertiary structure, with highly mobile side chains,

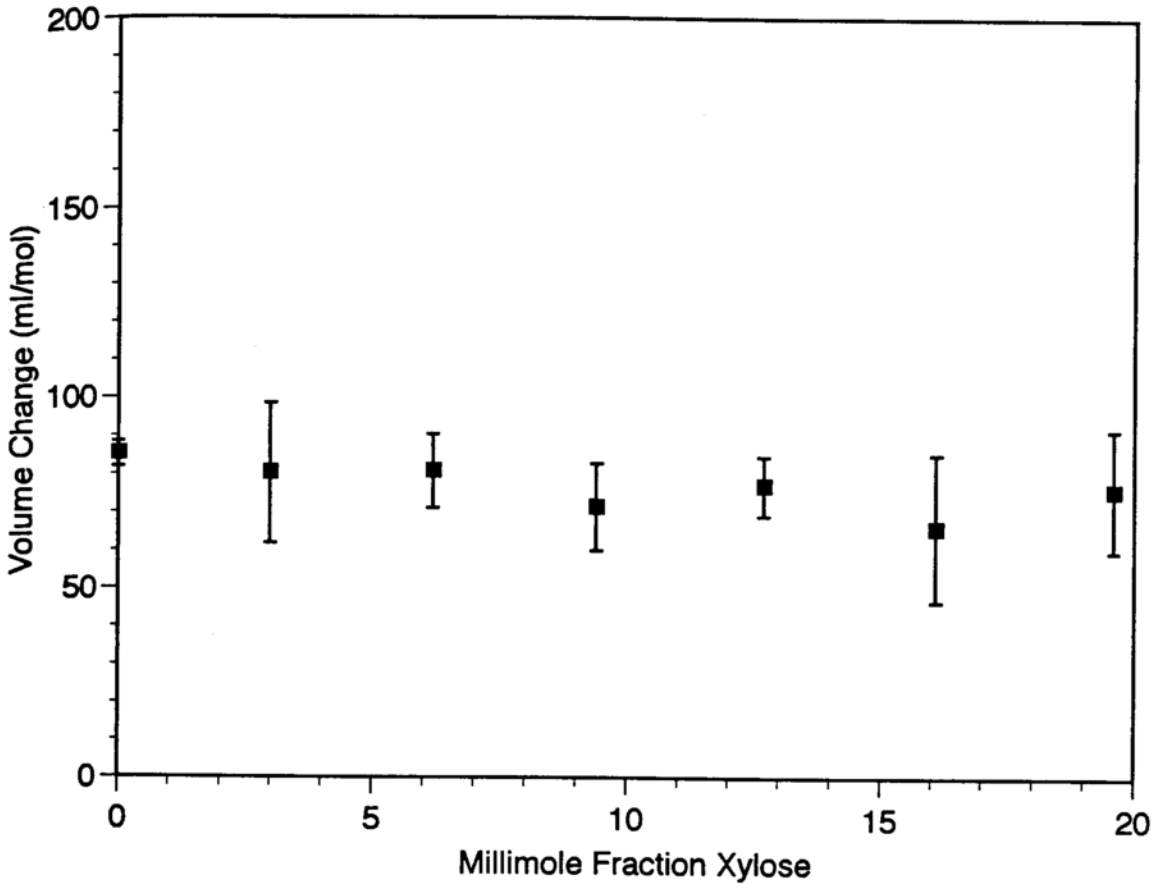

Figure 4-6. Average volume change with standard deviations as a function of millimole fraction xylose for each WT nuclease experiment at pH 4.5 and 21°C.

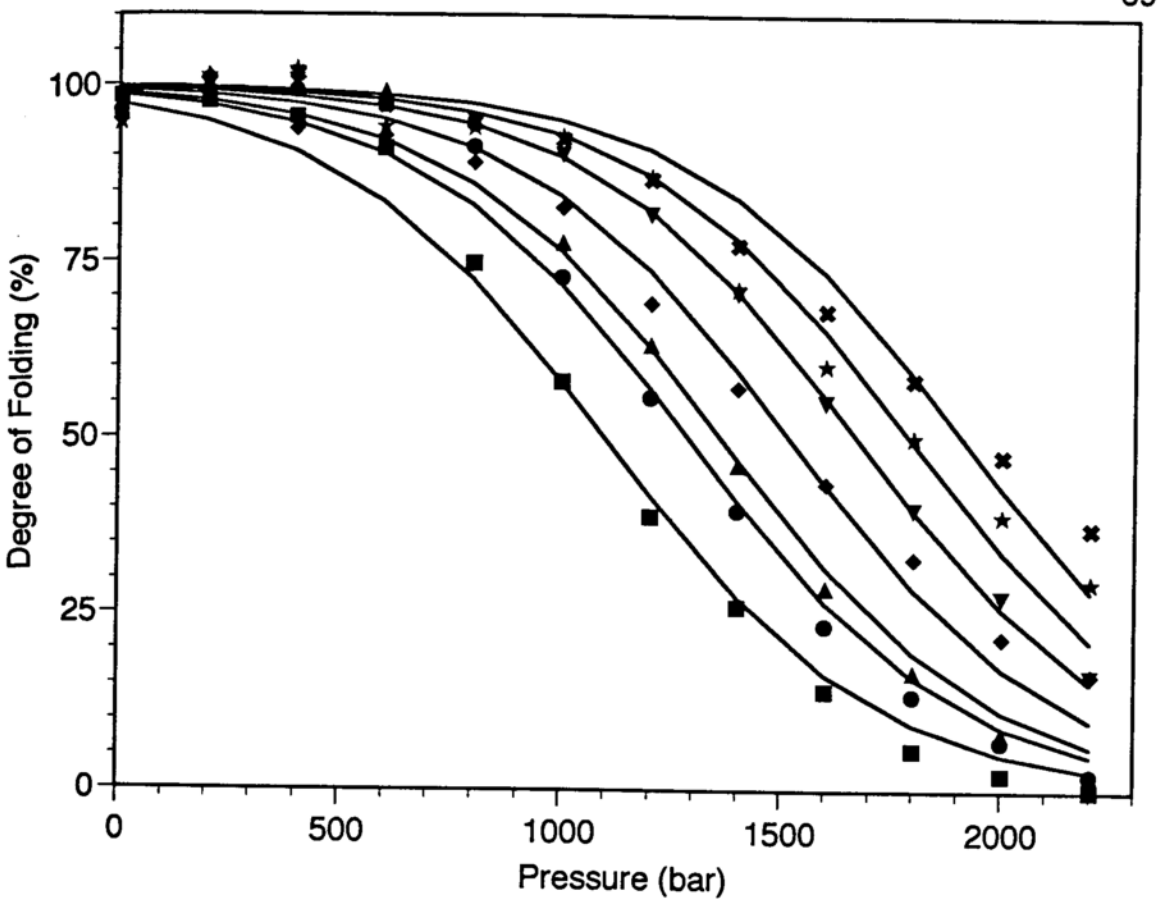

Figure 4-7. Unfolding profiles for WT nuclease as a function of pressure and millimole fraction xylose at pH 4.5 and 21°C. The symbols are data from a representative set of experiments and the solid lines represent the global curve analysis fits to the data. (■) 0 mole fraction xylose, (●) 3 millimole fraction xylose, (▲) 6.2 millimole fraction xylose, (◆) 9.4 millimole fraction xylose, (▼) 12.7 millimole fraction xylose, (✖) 16.1 millimole fraction xylose, (★) 19.6 millimole fraction xylose.

WT nuclease data sets	ΔV_u ml/mol	
	unlinked	linked
1	71.8 ± 16.3	73.8 ± 6.2
2	77.6 ± 10.2	75.7 ± 8.1
3	82.4 ± 6.3	76.3 ± 6.4
overall average	77.3 ± 5.3	75.3 ± 1.3

Table 4-1. The average volume change upon unfolding for the unlinked analysis with standard deviation and the volume change upon unfolding for the global curve analysis with confidence limits for each data set.

compact size, and more exposed hydrophobic surface than in the native state (Ptitsyn, 1987). Since pressure stabilizes the state with the smallest system volume, the compact state of a molten globule would be expected to be stabilized over the native state. In fact pressure denaturation of chymotrypsinogen, lysozyme, and cholinesterase does result in the presence of a molten globule (Clery et al., 1995, Li et al., 1976b). The molten globule was detected by the binding of ANS to an intermediate state designated by a large increase in ANS intensity. The results in Figure 4-4 show that ANS does not bind to the pressure denatured state of nuclease, thereby providing evidence that the pressure denatured state of this protein is not a molten globule since ANS does bind the molten globule state (Semisotnov et al., 1991). In addition to this Fink and coworkers (Fink et al., 1993) showed that the acid denatured and the guanidine denatured states of nuclease do not bind ANS either. Since neither pressure, pH, nor guanidine denaturation bind ANS, the unfolding transition for all three methods of denaturation follow a two-state transition without population of any molten globule intermediates.

Further evidence of a two-state transition comes from Royer and coworkers (Royer et al., 1993). They showed that the loss of the fluorescence intensity seen upon unfolding by decreasing the pH from 5.5 to 2.6 was similar in magnitude to that seen by pressure denaturation (increasing the pressure from 1 atm to 2.5 kbar). In addition, they determined through the pH studies that although the free energy of denaturation is dependent upon pH (there is a shift in

the pressure denaturation curves to lower pressures upon decreasing pH), there was virtually no pH dependence upon the volume change of unfolding for WT and the mutants studied. By NMR they further showed that the NMR signals of the histidine $H^{\varepsilon 1}$ protons of WT nuclease seen at high pressure is similar to that seen with temperature denaturation (Alexandrescu et al., 1990) indicating that the protein becomes fully unfolded at high pressures. The unfolding profiles observed by NMR and fluorescence in this paper were in good agreement and consistent with the theory that the high pressure induced denaturation of nuclease is a global two-state transition. The one difference Royer and coworkers did show between the pressure induced denaturation and the pH, temperature, and chemical denaturation is that the mechanism of tryptophan fluorescence quenching is predominately dynamic in origin for the latter cases, whereas the pressure denatured state has a large static component. The differences in the mechanism of tryptophan quenching are possibly due to less mobility of the tryptophan molecule (Trp 140) and to the formation of a ground-state complex with a quenching moiety (possibly Lys 133) in the pressure denatured state (Royer et al., 1993).

More recently, high pressure synchrotron small-angle X-ray scattering (SAXS) and fourier-transform infrared spectroscopy (FTIR) experiments have been completed by Panick and coworkers (Panick et al., 1997). They found that the radius of gyration (R_g) for native nuclease is 17 Å. The pressure denatured state of nuclease has an R_g of 33 Å while urea denatured nuclease has an R_g of

35 Å (Flanagan et al., 1992, Kataoka et al., 1994). If nuclease were to unfold to a complete random coil structure the R_g would be 45 Å (Miller & Goebel, 1968) which suggests that the pressure and urea denatured states do not reach a random coil, but have some residual structure. In fact they showed that the pair-distance-distribution function for the pressure denatured state has an R_{max} of 100 Å at 2800 bar characteristic of an elongated ellipsoidal shape or an extended coil. The temperature denatured state on the other hand has an R_g of 43 Å and shows a bimodal pair-distance-distribution function indicative of a dumbbell shape with little secondary structure remaining which suggests that the temperature denatured state unfolds to a random coil structure.

By FTIR Panick and coworkers (Panick et al., 1997) also showed that the bands associated with β-sheets and α-helices both decrease as a function of pressure. Although the band for α-helices nears zero for the pressure denatured state, the band for the β-sheet is not completely disrupted indicating that a portion of the β-sheet is still present. This is consistent with the urea denatured state where there is evidence of a three-stranded, antiparallel β-sheet stabilized by hydrophobic interactions (Wang et al., 1995, Wang & Shortle, 1996). In agreement with the SAXS data, the temperature denatured state as monitored by FTIR does loose all of the β-sheet indicating that the temperature denatured state is more like a random coil. The volume change and free energy change upon unfolding obtained from the FTIR data is also in accord with previous data (Frye et al., 1996, Frye & Royer, 1997, Vidugiris et al., 1995, Vidugiris et al.,

1996). For that reason, both high pressure SAXS and FTIR reveal that the pressure denatured state is similar to that of urea induced denaturation and that in both cases the unfolded state does not unfold to a random coil, but has some residual β-sheet. These results support earlier work by Brand and coworkers which suggests that the guanidine denatured state is unlikely to be a random coil based on time-resolved nonradiative energy transfer experiments (James et al., 1992). On the other hand according to both SAXS and FTIR, the temperature state does appear to unfold to a random coil state. Despite this, Eftink and coworkers (Eftink & Ramsay, 1997) conclude that the temperature denatured state does not unfold to a random coil but their evidence is based on the results of one mutant which appears to have a more compact denatured state as measured by size exclusion chromatography. In any case, the manifold of pressure denatured states appears similar in many respects to that obtained by pH and chemical denaturant. Although some residual structure remains, the pressure denatured state does not appear to conform to the idea one has of a molten globule. In fact, the ΔG_u values obtained by pressure and guanidine are found to be within experimental error (Vidugiris et al., 1996). All evidence supports a global two-state transition for the pressure denaturation of WT nuclease.

Now that it has been established that the equilibrium pressure denaturation of WT nuclease is in fact a simple two-state transition, the consequence of chemical stabilizers, chemical denaturants, and pH on the

pressure unfolding transition can be observed. The results in Figure 4-5 showed how the unfolding transition shifts as a function of xylose. The xylose simply acts to stabilize the native protein structure by shifting the transition to higher pressures. It is evident from Figure 4-6 and Table 4-1 that the volume change for unfolding does not change as a function of xylose no matter how the data are analyzed. In addition, Vidugiris and coworkers (Vidugiris et al., 1996) similarly established that guanidine has no effect on the volume change for unfolding. The effect of guanidine is simply to destabilize the protein native state by shifting the transition to lower pressures. Similarly, it was illustrated by Royer and coworkers (Royer et al., 1993) that the volume change is also independent of pH and that the effect of decreasing pH is to shift the transition to lower pressures. Therefore, chemical stabilizers or chemical denaturants can be added to the protein solution, along with changing the pH, to alter the stability of the unfolding transition without changing the volume. This is particularly useful for mutants that are either more or less stable than WT resulting in the incomplete unfolding profile from 1 to 2500 bar at room temperature. For example, if a mutant does not begin to unfold until 1500 bar, a small amount of guanidine can be added to destabilize the protein just enough so that pressure will force the denaturation and the entire unfolding profile can be observed from 1 to 2500 bar. This technique can also be adapted for the opposite case where the mutant is less stable and xylose is required to stabilize the protein allowing for observation of the entire pressure denaturation profile. Since most proteins do not unfold until

7-11 kbar and 2.5 kbar is the pressure limit for our instrument, this technique can be applied to other proteins which are more stable to pressure denaturation than nuclease.

CHAPTER 5: THE CONTRIBUTION OF THE EXPOSURE OF BURIED SURFACE AREA TO ΔV_u

Thermodynamically, the conformation of many small globular proteins exhibit a high degree of cooperativity of folding and can be described by a simple two-state, reversible transition between folded and unfolded forms. The application of hydrostatic pressure to aqueous protein solutions results in the reversible unfolding of such proteins because the protein-solvent system volume is smaller for the unfolded state. As mentioned in Chapter 1, the microscopic contributions to this decrease in system volume, ΔV_u, upon unfolding are not well defined. They arise from differences in protein-solvent interactions and are thought to involve hydrophobic hydration, electrostriction and excluded volume (Weber & Drickamer, 1983). The work in this chapter addresses the role of exposed surface area and hydrophobic hydration to the ΔV_u observed for Staphylococcal nuclease (nuclease).

It has been demonstrated that a relationship exists between the change in heat capacity (ΔC_p) and the change in available surface area (ΔA) by:

$$\Delta C_P = (0.32)(\Delta ASA_{np}) - (0.14)(\Delta ASA_{pol}) \qquad (1)$$

where ΔASA_{np} and ΔASA_{pol} are the change in available nonpolar and polar surface area, respectively (Livingstone et al., 1991). It has also been demonstrated that there is a correlation between the change in surface area upon unfolding and the cooperativity of unfolding by denaturant, known as the

m-value (Schellman, 1978, Shortle & Meeker, 1986, Shortle et al., 1988). Based on this relationship, it would seem plausible that there may also be a correlation between ΔV_u and ΔA_u. To determine whether a relationship does in fact exist between ΔV_u and ΔA_u, and from that if the exposure of buried surface area is a determining factor in ΔV_u, the pressure denaturation for three nuclease mutants as a function of xylose was investigated. Two of the mutants, H121P and A69T + A90S (Figure 5-1), exhibit strongly altered cooperativity values for unfolding by denaturant, 28% smaller and larger, respectively, relative to WT. The third, M98I, has a comparable cooperativity to WT (Shortle et al., 1989). In order to verify that the changes in *m*-values for these mutants arise from differences in ΔA_u, the effect of the osmolyte xylose on the stability of these proteins over a range of pressures was examined. As noted in Chapter 1, xylose is a colligative agent and as such stabilizes proteins through surface tension perturbation, *i.e.*, since the unfolded state exposes more surface area than the folded state, these additives favor the folded state (Lee & Timasheff, 1981). A xylose *m*-value (m_{xy}) can be defined as the extent of increase in free energy of unfolding, ΔG_u, as a function of xylose concentration. If the guanidine *m*-values correlate with ΔA_u, then m^+ and m^- mutants should have m_{xy} values greater (m_{xy}^+) and smaller (m_{xy}^-), respectively, than wild type (WT) while the m° mutant should be similar to WT. The values of ΔV_u for these mutants were precisely determined to evaluate the contribution of hydrophobic hydration to the volume change of unfolding.

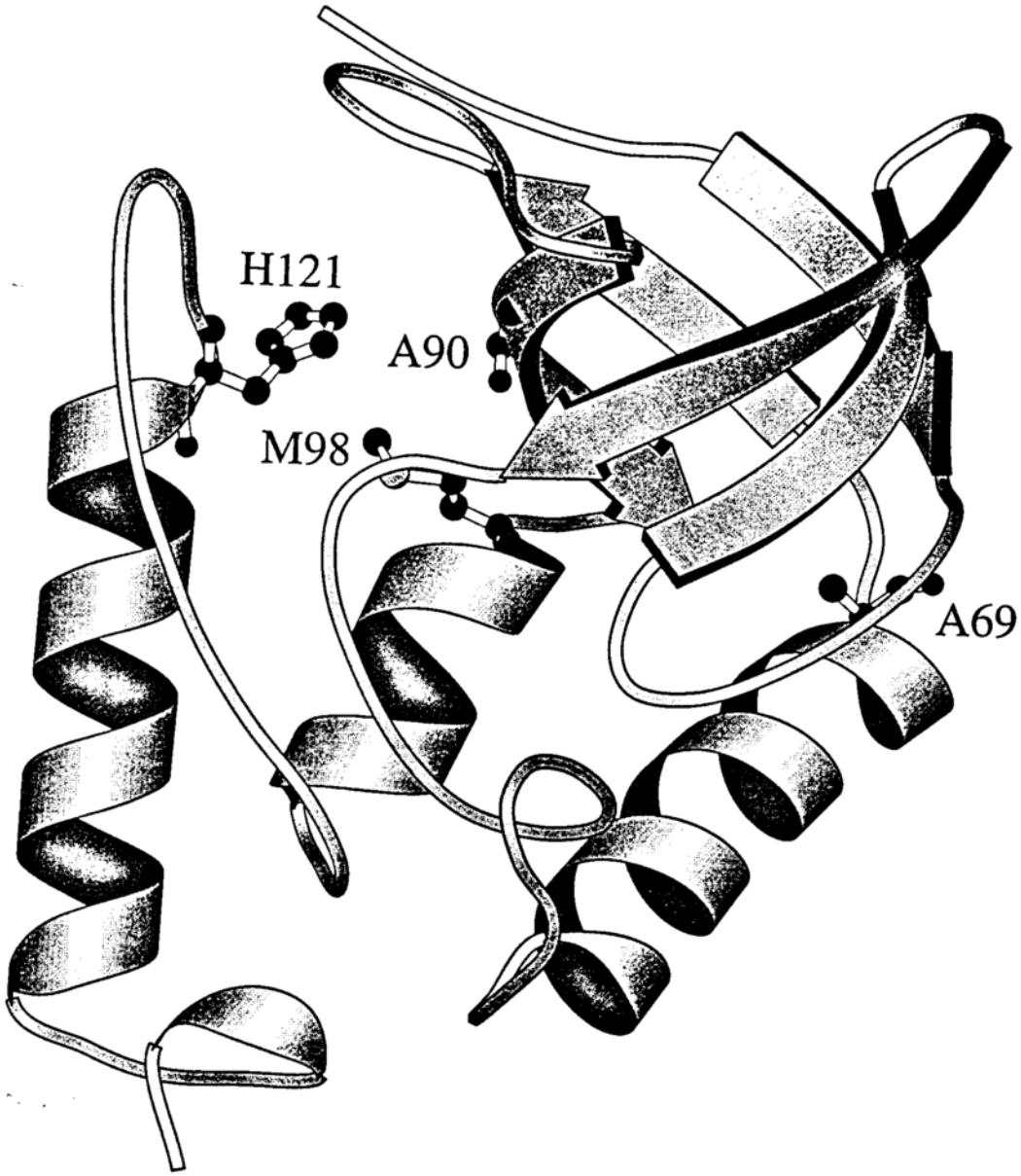

Figure 5-1. The three dimensional structure of Staphylococcal Nuclease determined from x-ray crystallographic data (Hynes & Fox, 1991). The figure was drawn using the program Molscript (Kraulis, 1991). Histidine 121, alanine 69, alanine 90 and methionine 98 are shown in ball-and-stick presentation.

RESULTS

Prior to examining the correlation between ΔV_u and ΔA_u, the hypothesis that there is a correlation between *m*-values and the amount of surface area exposed upon unfolding (Shortle & Meeker, 1986, Shortle et al., 1988) was tested for the three mutants used in the study. The pressure-induced denaturation of WT nuclease, the m^- mutant (H121P), the m^+ mutant (A69T + A90S), and the m° mutant (M98I) was conducted as a function of xylose. The decrease in intensity of the intrinsic fluorescence of the sole tryptophan residue in nuclease, tryptophan 140 (see Figure 5-1), upon unfolding was monitored in order to observe pressure denaturation (Shortle & Lin, 1985).

Figures 5-2 and 5-3 show representative, normalized denaturation curves with fits to the data for H121P and A69T + A90S, respectively, as a function of xylose concentration analyzed in the linked mode as done in Chapter 3 (Appendix II shows additional data sets analyzed in the linked mode as well as analysis for all data sets in the unlinked mode). Due to the previously mentioned surface area perturbation by this agent, as the xylose concentration is increased, the curves shift to higher pressures because the free energy of unfolding increases as a function of xylose concentration. Furthermore, since the mutants are partially unfolded at atmospheric pressure, addition of xylose causes the fluorescence intensity to increase at atmospheric pressure upon xylose induced-folding of the proteins.

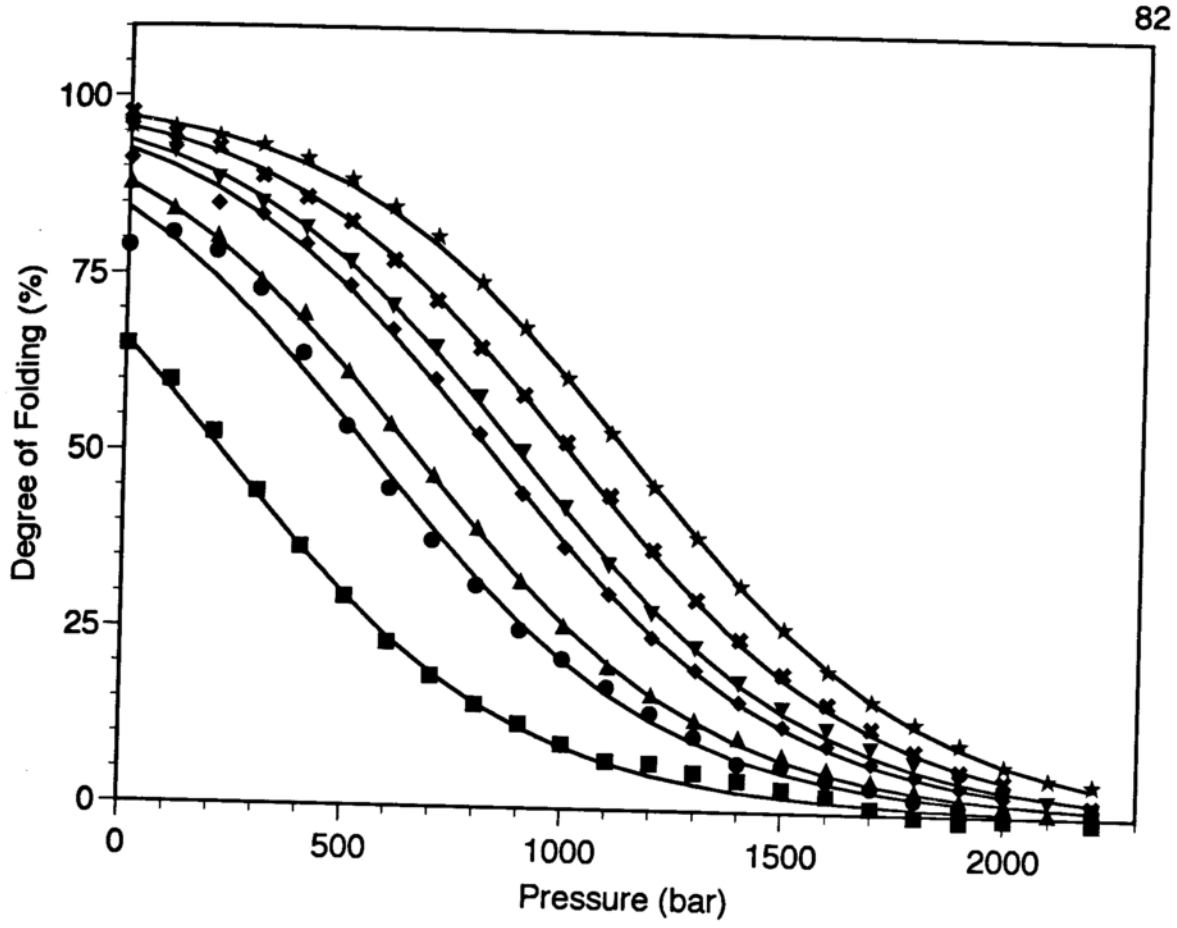

Figure 5-2. Unfolding profiles for H121P as a function of pressure and millimole fraction xylose at pH 7.0 and 21°C. The symbols are the data from a representative set of experiments and the solid lines represent the global curve analysis fits to the data. (■) 0 mole fraction xylose, (●) 6.2 millimole fraction xylose, (▲) 10.5 millimole fraction xylose, (◆) 12.7 millimole fraction xylose, (▼) 15.0 millimole fraction xylose, (✖) 17.2 millimole fraction xylose, (★) 19.6 millimole fraction xylose.

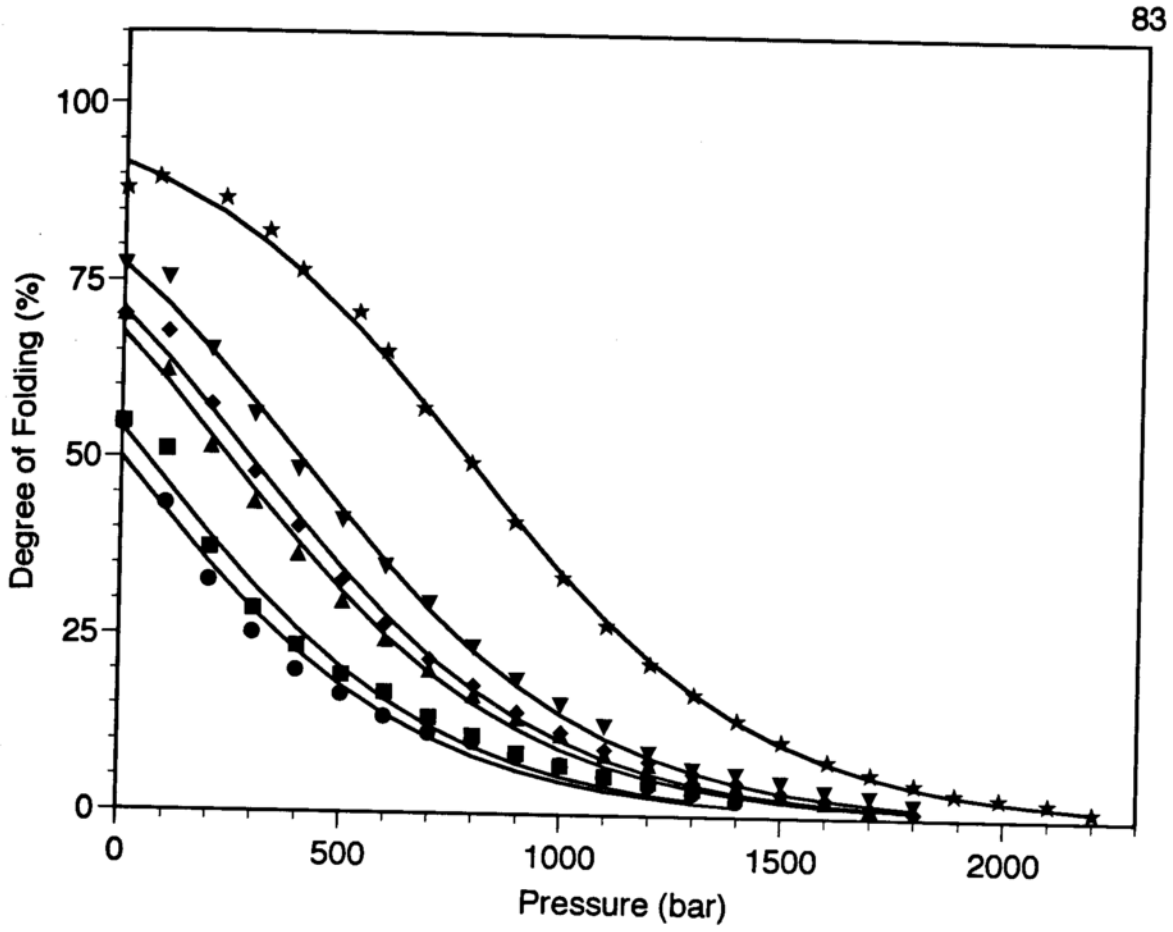

Figure 5-3. Unfolding profiles for A69T + A90S as a function of pressure and millimole fraction xylose at pH 7.0 and 21°C. The symbols are the data from a representative set of experiments and the solid lines represent the global curve analysis fits to the data. (■) 0 mole fraction xylose, (●) 3.0 millimole fraction xylose, (▲) 6.2 millimole fraction xylose, (◆) 9.4 millimole fraction xylose, (▼) 12.7 millimole fraction xylose, (★) 19.6 millimole fraction xylose.

Figure 5-4 shows results for one xylose concentration for M98I. The curve does not represent a smooth transition as seen in previous plots; there is a break in the curve at approximately 600 bar. At all xylose concentrations a break in the curve persisted which is indicative of an intermediate state. The experiments were repeated a second time and again showed an identical break in the curve. The analysis became complicated because the mutant could not be analyzed via a simple two-state transition. This mutant could not be included in the remainder of this study since it did not fit the two-state model.

Plotted in Figures 5-5 a and b are the free energies of unfolding as a function of mole fraction xylose for WT (from chapter 3), H121P, and A69T + A90S from analysis of the pressure denaturation data and the intensity values at atmospheric pressure, respectively. The ΔG_u at atmospheric pressure was calculated by using equation 2 in Chapter 3 where I_p was taken as the intensity at atmospheric pressure and I_f was calculated based on the data at higher sugar concentrations where the entire unfolding profile was observed. No evidence for non-two-state behavior was observed, such that the unfolding profiles for these mutants, like that of WT nuclease, were analyzed according to a two-state equilibrium unfolding model. If a correlation exists between *m*-values and exposed surface area, the m^+ mutant should exhibit a larger slope than that of the WT and the m^- mutant should exhibit a smaller slope than that of the WT since stabilization by xylose is a function of surface area. The slopes of the ΔG_u vs. [xylose] plots obtained from analysis of the pressure profiles and the stability

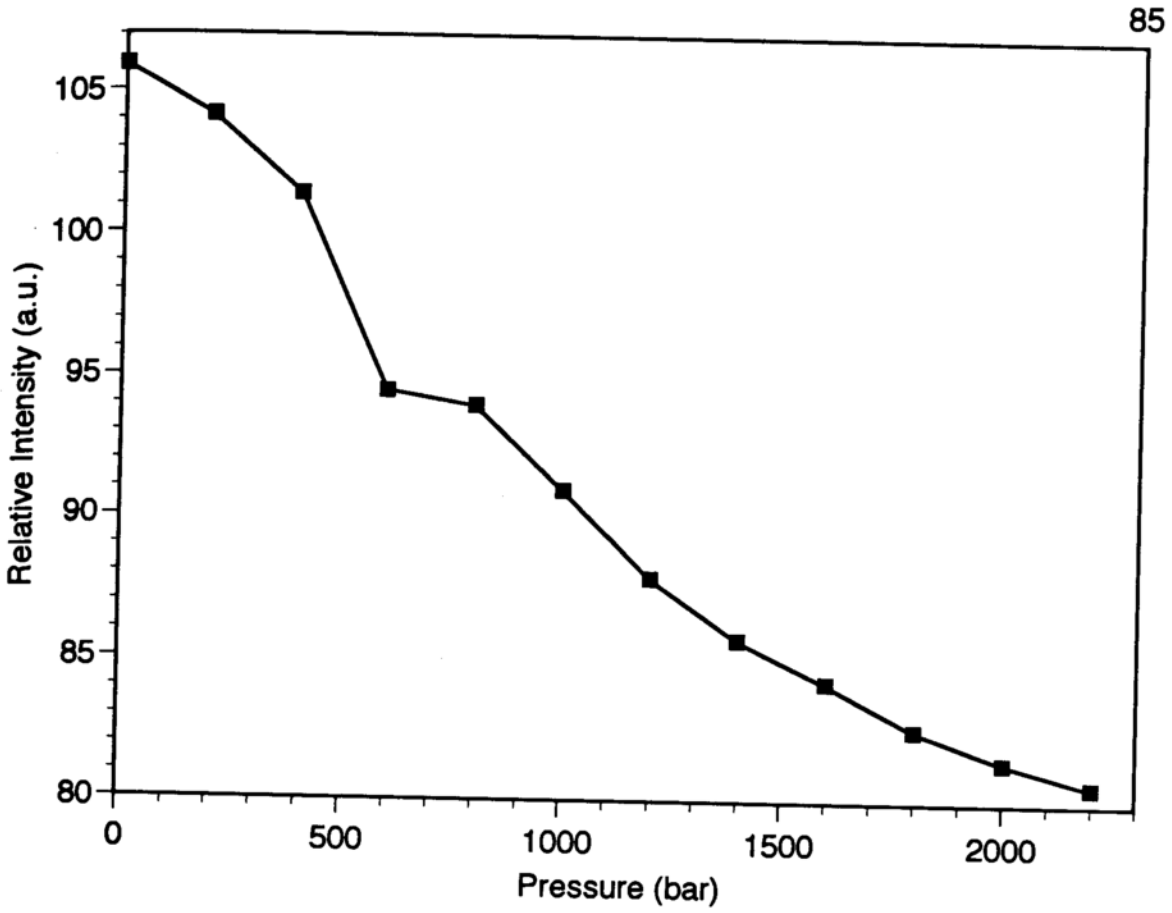

Figure 5-4. Unfolding profile for M98I as a function of pressure at 15 millimole fraction xylose at pH 7.0 and 21°C. The symbols are the data from a representative set and the solid line is included to guide the eye.

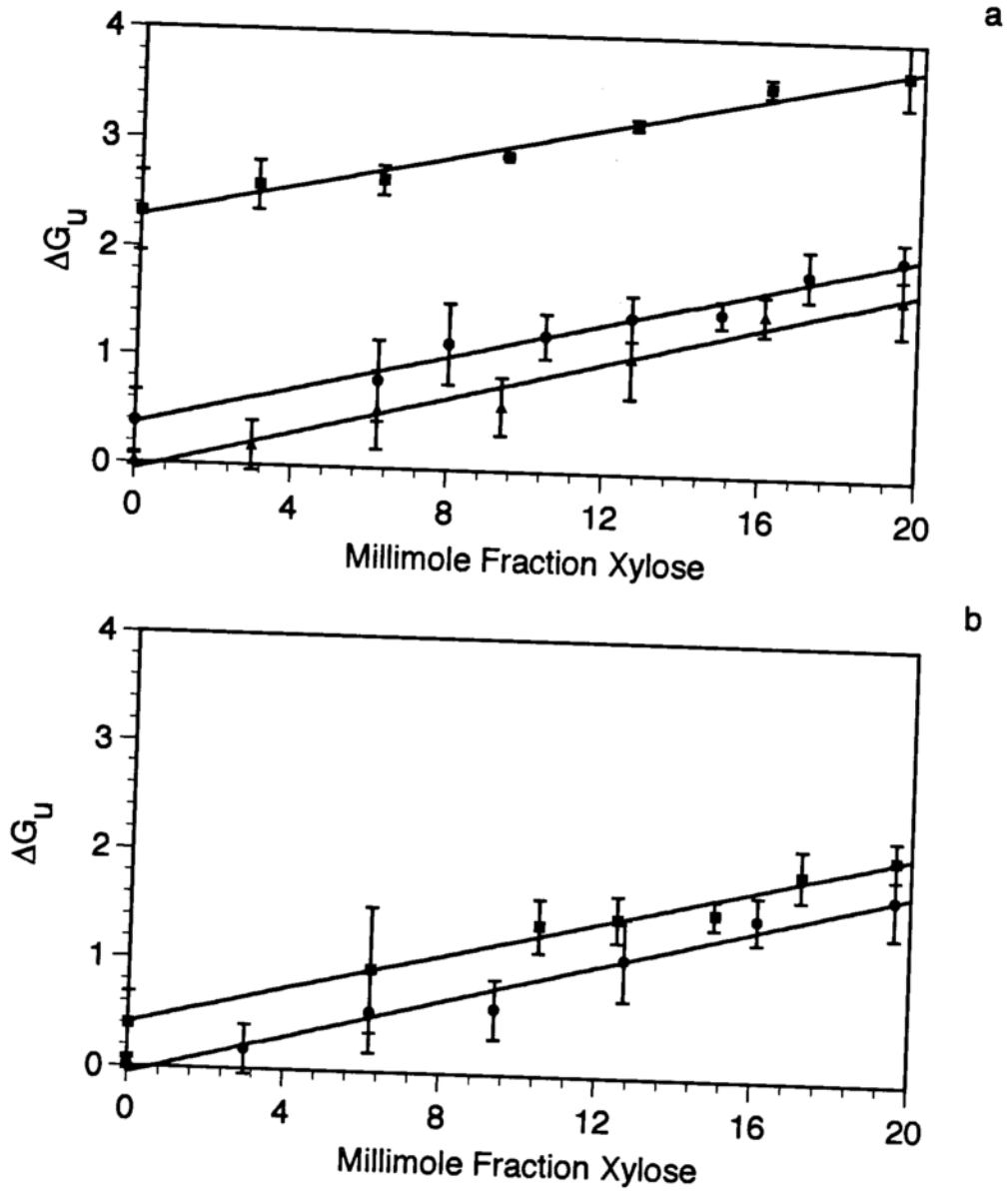

Figure 5-5. Free Energy of Unfolding vs. Millimole Fraction Xylose. At the xylose concentration used here the activity coefficient is negligible and millimole fraction is used since it is independent of temperature and pressure. a) From the pressure unfolding profiles b) From the intensity values at atmospheric pressure. (■) WT at pH 4.5, (●) H121P and (▲) A69T + A90S, both at pH 7.0. The solid lines represent linear fits to the data.

atmospheric pressure are reported in Table 5-1 as the xylose *m*-value (m_{xy}). Since the WT is completely folded in the absence of xylose, it is not possible to calculate a xylose *m*-value for the WT from the atmospheric pressure data alone. Regardless of the method for obtaining the free energy of unfolding (the pressure unfolding profiles with linked or unlinked ΔV_u values or atmospheric pressure), the slopes for both the m^+ mutant and the m^- mutant are larger than that obtained for WT. In the case of the m^+ mutant, the m_{xy} value is 21% larger than that of WT, similar to the 28% difference observed for the cooperativity of unfolding by guanidine. This observation is consistent with a surface area effect for the increased cooperativity of unfolding of this mutant compared to WT. On the other hand, the correlation between ΔA_u and *m*-value does not appear to hold for the m^- mutant. Its m_{xy} value is 14% larger than that of WT and only 6% smaller than that of the m^+ mutant. While calorimetric studies (Carra et al., 1994), circular dichroism (CD) and fluorescence melt comparisons (Eftink, 1995) and pressure-jump relaxation studies (Vidugiris et al., 1995) indicate WT nuclease equilibrium unfolding profiles are well described by a two-state model, Creighton and Shortle (Creighton & Shortle, 1994) have shown that the altered *m*-values measured for solvent denaturation of certain m^- mutants of nuclease may be due to the presence of a partially folded state which becomes significantly populated. Such complexity for m^- mutants has also been noted from calorimetric studies (Carra et al., 1994, Carra & Privalov, 1995).

Protein	m_{gdn}[a]	m_{xy}[b] atm	m_{xy}[b] pressure		ΔV_u (ml/mol)	
			linked	unlinked	linked	unlinked
WT	1	n.d.	73.3 ± 2.3	59.3 ± 11.3	-75.3 ± 1.3	-73.7 ± 5.9
H121P	0.72	82.8 ± 0.4	83.7 ± 0.4	81.0 ± 13.5	-70.5 ± 2.8	-69.9 ± 9.3
A69T + A90S	1.28	88.9 ± 0.1	88.6 ± 0.1	99.0 ± 14.4	-78.0 ± 8.8	-81.8 ± 10.6

Table 5-1. Guanidine *m*-values, xylose *m*-values and ΔV_u.

n.d. - not determined

[a](Shortle et al., 1989). m_{gdn} relative to the WT in kcals/mol per M.

[b]m_{xy} in kcals/mol per mole fraction xylose.

Both the m^- and m^+ mutant used here, H121P and A69T + A90S, were too unstable for calorimetric studies, however their CD melt profiles with and without xylose can be seen in Figures 5-7 and 5-8 along with the WT in Figure 5-6 (the entire CD spectra as a function of temperature for all three proteins with and without xylose can be seen in Appendix II). As seen with pressure denaturation, xylose pushes the transition to higher temperatures for all three proteins. In fact, based on the CD spectra for the mutants with and without xylose at room temperature, both mutants appear to gain secondary structure, specifically more alpha helix, with the addition of xylose (Figures 5-9 a and b). WT nuclease and the m^+ mutant, A69T + A90S, were both well represented by a simple two-state transition (Figures 5-6 and 5-8), whereas the m^- mutant, H121P, exhibited non-two-state character (Figure 5-7). In fact, H121P fit well to a three state transition with two melting point transitions and two enthalpic terms. Thus, it can be concluded that the m^+ mutant exposes more surface area in the unfolded state than does the WT. However, it cannot be concluded that the m^- mutant exposes less surface area. Rather, its altered *m*-value probably arises from the population of intermediates.

Given that the m^+ mutant exposes more surface area upon unfolding than WT nuclease, it would be a perfect mutant to determine whether this increase in exposed surface area would correlate with a larger negative volume change upon unfolding of this mutant by pressure. The values of ΔV_u from the linked and unlinked analyses of the pressure unfolding of WT nuclease and the two

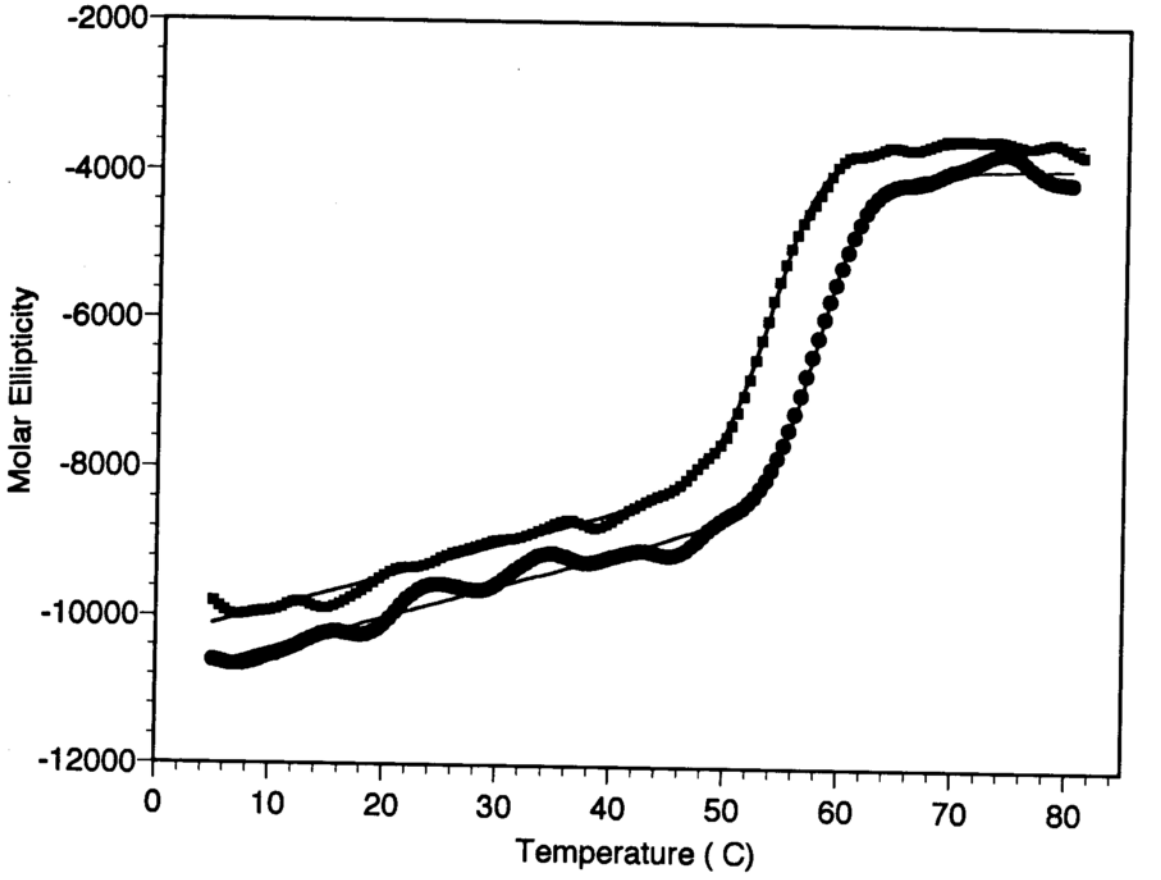

Figure 5-6. CD thermal melt data for WT nuclease monitored at 222 nm and pH 5.5. The symbols are the data points and the solid lines represent a two-state fit to the data. (■) no xylose (●) 19.6 millimole fraction xylose.

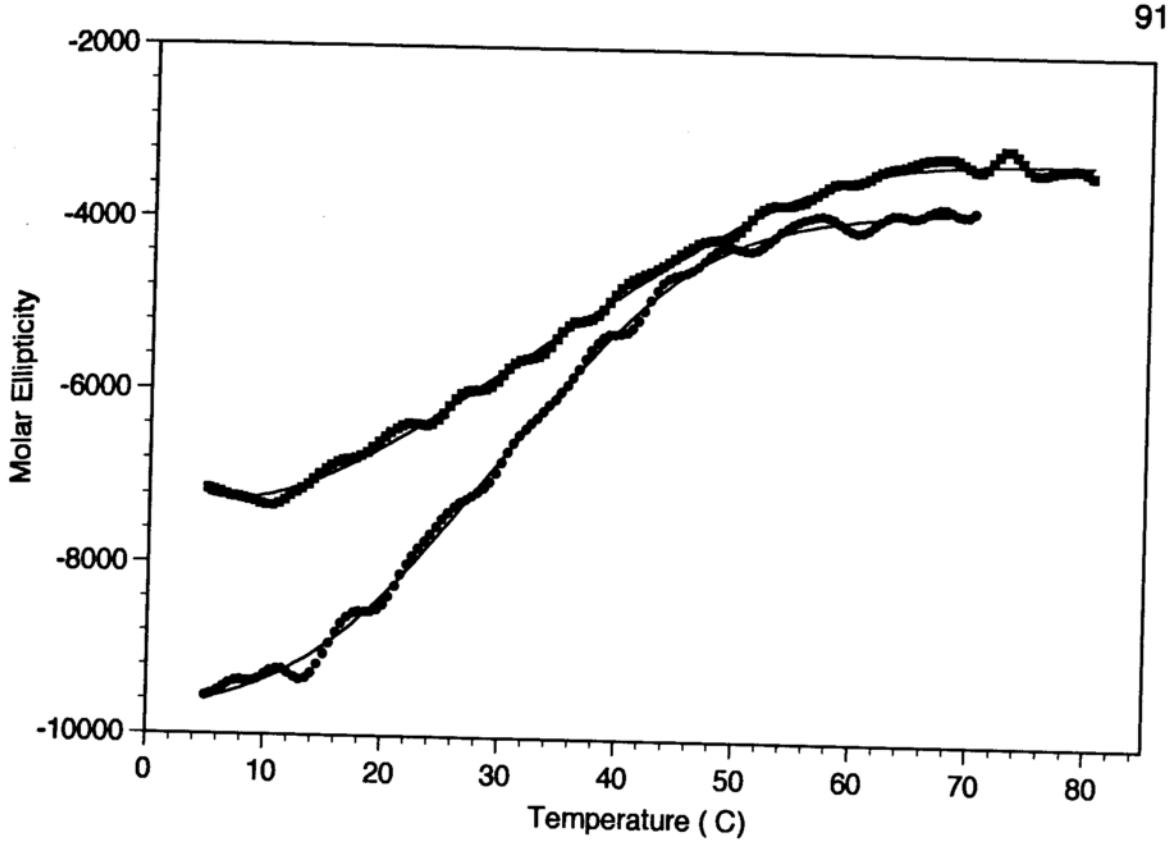

Figure 5-7. CD thermal melt data for H121P monitored at 222 nm and pH 7.0. The symbols are the data points and the solid lines represents a three-state fit to the data. (■) no xylose (●) 19.6 millimole fraction xylose.

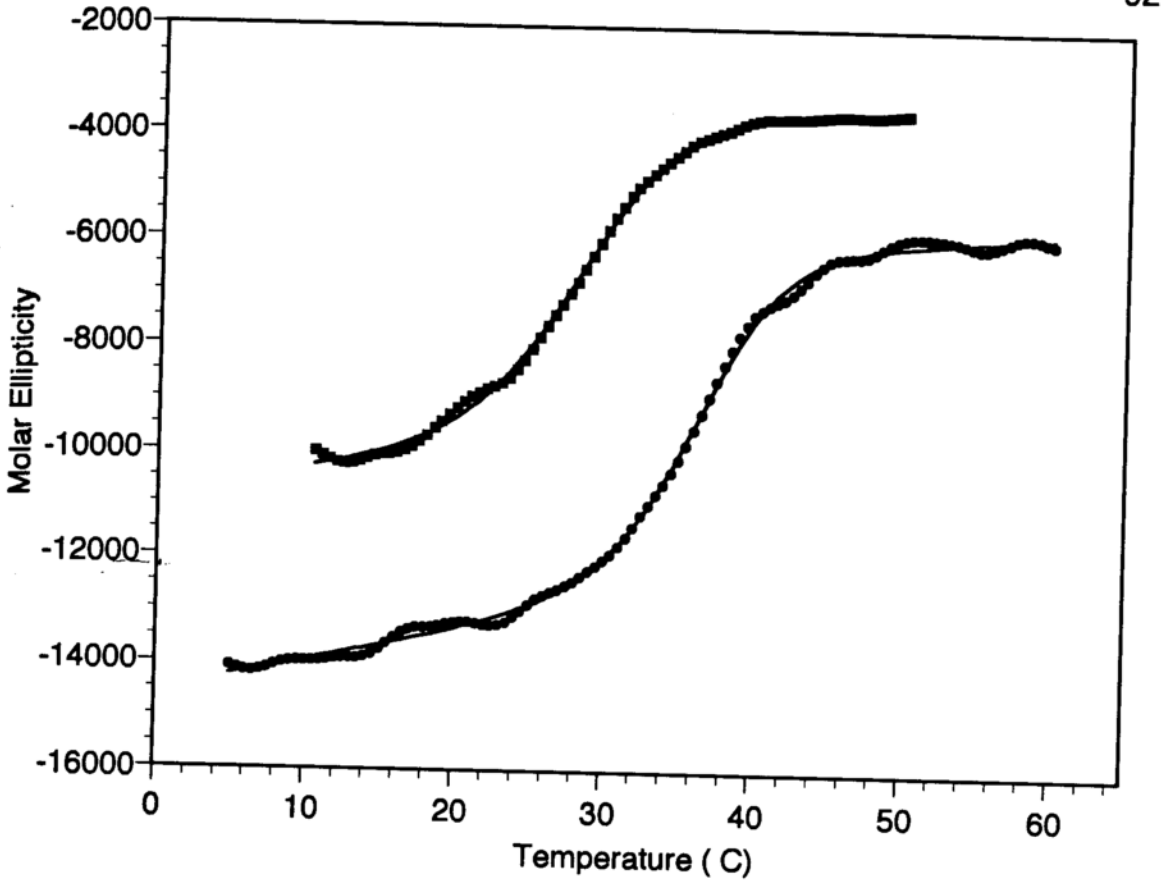

Figure 5-8. CD thermal melt data for A69T + A90S monitored at 222 nm and pH 7.0. The symbols are the data points and the solid lines represents a two-state fit to the data. (■) no xylose (●)19.6 millimole fraction xylose.

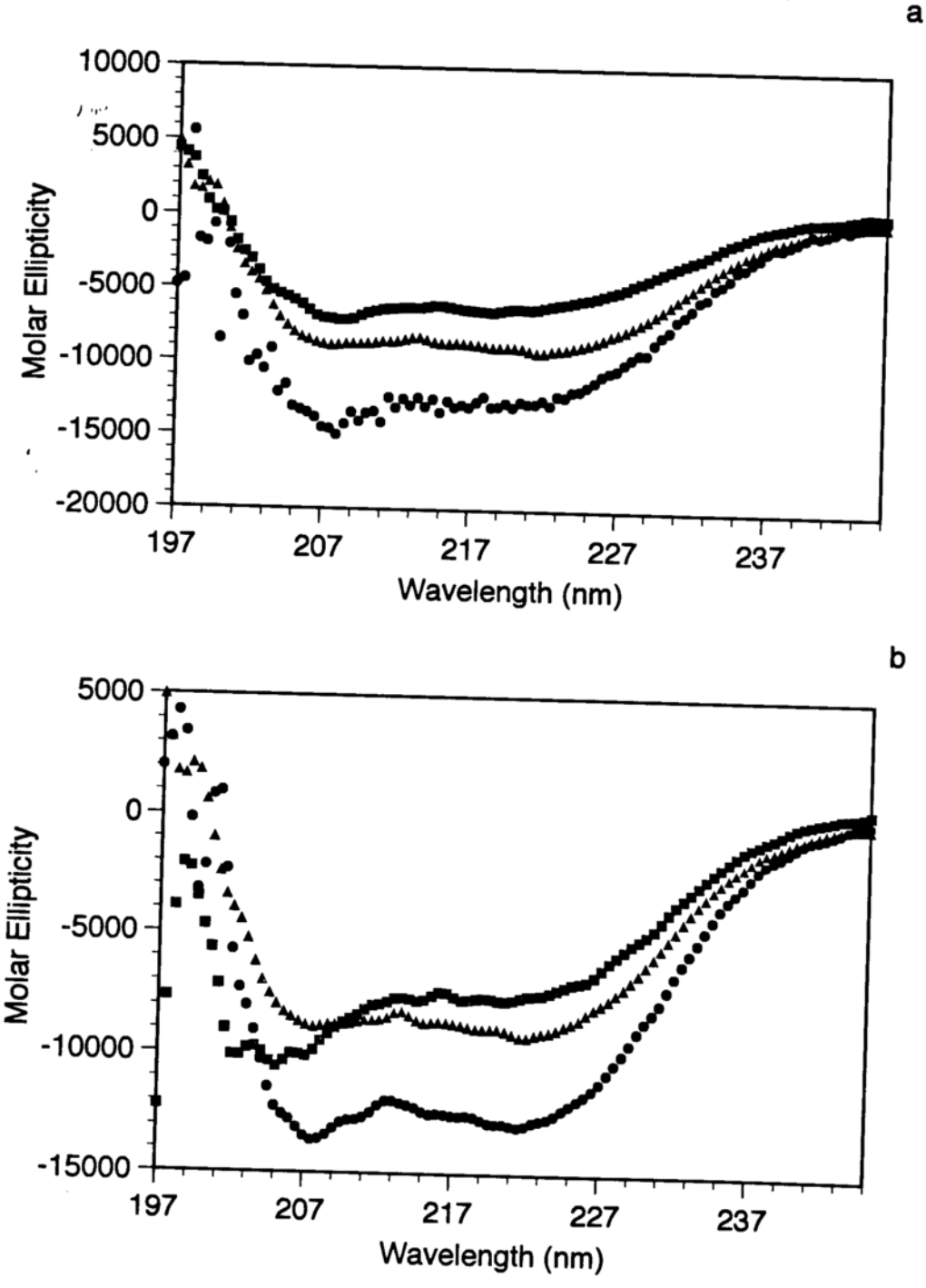

Figure 5-9. CD spectra at room temperature and pH 7.0 for (a) H121P and (b) A69T + A90S. (■) no xylose (●) 19.6 millimole fraction xylose (▲) WT nuclease without xylose.

mutants were averaged together for each replicate set of xylose concentrations for each protein and are given in Table 5-1 with their standard deviations. No trend was observed with xylose concentration in the value of ΔV_u recovered from the unlinked analyses as seen in Chapter 3 for the WT and Figure 5-10 for the mutants. The value obtained for WT in these studies (75.3 ml/mol linked and 73.7 ml/mol unlinked) is identical within error of that obtained in earlier work (Vidugiris et al., 1995, Vidugiris et al., 1996). Regardless of the method of analysis (linked or unlinked), the ΔV_u values are within experimental error for the three proteins, differing from one another by less than 10%, nearly 3-fold less than the 28% deviations in the denaturant *m*-values. For example, the ΔV_u of the m^+ mutant is only 3% larger than that of WT, while the guanidine *m*-value and xylose *m*-value differ by 28% and 21%, respectively. Thus, the volume change upon unfolding does not appear to correlate with the amount of surface area exposed upon unfolding.

DISCUSSION

The goal of this study was to evaluate the contribution of exposed surface area to the ΔV of unfolding using cooperativity mutants of staphylococcal nuclease. First, it was necessary to establish that the difference in cooperativity of unfolding of these mutants originates from differences in exposed surface area in the unfolded state. A relationship between ΔA and the *m*-value is still

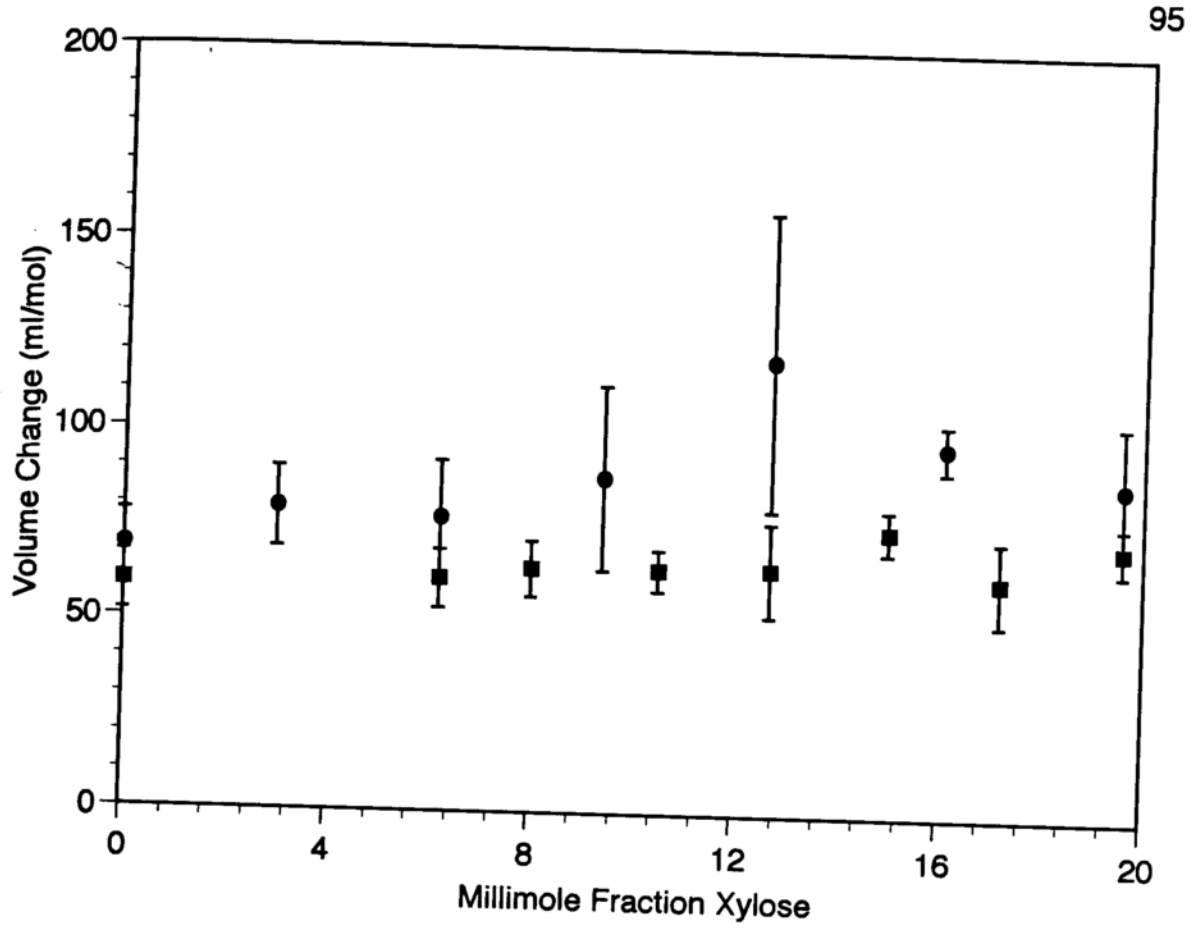

Figure 5-10. ΔV_u as a function of millimole fraction xylose for all raw data repetitions of (■) H121P and (●) A69T + A90S.

suspect even with evidence such as: (1) Schellman's derivation in which the pseudo binding constant is affected by the number of binding sites exposed on the protein surface, and therefore the amount of surface area exposed (Schellman, 1987) and (2) experimental data suggesting that ΔC_p and ΔH correlate with the *m*-value (Shortle et al., 1988). Based on temperature studies monitored by intrinsic tryptophan fluorescence, the apparent van't Hoff enthalpy (ΔH) and the heat capacity change (ΔC_p) both increase for m^+ mutants and decrease for m^- mutants. Since ΔC_p is known to be a function of ΔA (equation 1), the *m*-value should also be a function of ΔA if the *m*-value correlates with ΔC_p.

The hypothesis that *m*-value corresponds to the amount of exposed surface area implies that there must be a change in the amount of exposed surface area in either the native or denatured state. For an m^+ mutant either the exposed surface area of the denatured state must increase or that of the native state must decrease. It is physically unrealistic to expect a further decrease in exposed surface area for the native state since this state is energetically the most stable state and thus already minimizes exposed surface area. A very large change in structure of the native state would be required to yield a decrease of 28%. Therefore, there must be an increase in exposed surface area of the denatured state. In spite of this, at first glance it would seem unlikely that there could actually be an increase in exposed surface area of as much as 28% since it has previously been assumed that a protein unfolds to a random coil.

FTIR and SAXS data from Chapter 3 do show that it is indeed possible to increase the amount of exposed surface area for the denatured state by a magnitude of 22% (Panick et al., 1997). For an m^- mutant, there must be either an increase in exposed surface area for the native state or a decrease in that for the denatured state. Realistically both cases are possible, however evidence from x-ray crystal structures of the most pronounced m^- mutant (V66L + G79S + G88V) as well as another m^- mutant (L103F) show that no change in ΔA for the native state is observed (Loll et al., 1988). Along with the fact that the ΔA for an m^+ mutant occurs in the denatured state, the x-ray crystal structures suggest that ΔA for the denatured state decreases for the m^- mutant instead of increasing for the native state. However as mentioned previously, m^- mutants are a result of non-two-state behavior.

It appears from the effects of xylose on the stability of the nuclease mutants shown here that a correlation between m-value and surface area exposed upon unfolding exists for the m^+ mutant. The percentage difference in m_{xy} between the WT and the m^+ mutant is about 21%, close to the 28% difference in guanidine m-values. However, this correlation does not appear to hold for the m^- mutant; the m_{xy} value for H121P is actually slightly larger than that of WT, rather than smaller. The percentage difference in m_{xy} between the m^- and m^+ mutants is about 6%, whereas the guanidine m-values differ by a factor of 1.6 (Shortle et al., 1989). The small difference observed in m_{xy} between the m^- and m^+ mutants leads to the conclusion that a correlation between

guanidine *m*-value and surface area for the m^- mutant is unlikely. The lack of correlation between *m*-value and ΔA for the m^- mutant can be attributed to its non-two-state behavior as is evident in the CD thermal melt data (Figure 5-7).

A study of the differences between m^+ and m^- mutants lead to the fact that the m^+ mutants are located in the hydrophobic β-barrel (core I) of the protein, while the m^- mutants are found in a second cluster (core II) as shown in Figure 5-11 (Shortle et al., 1990). The non-two-state behavior of m^- mutants is attributed to enhancement of the segregation of the core I residues into an independent cluster, mostly through indirect effects, while the m^+ mutants reduce the stability of core I interactions (Shortle, 1995). Since m^+ mutations reduce the stability of this independent core, they result in an increase in exposed surface in the unfolded state and the correlation between *m*-value and ΔA_u holds. In contrast, m^- mutants can either stabilize this independent cluster, destabilize core II, decrease interactions maintaining cooperativity between the subdomains, or destabilize the native state and stabilize intermediate states at positions integral to the hydrophobic core resulting in an increase in the number of states populated between the native and denatured states (Carra et al., 1994, Carra & Privalov, 1995). The population of such intermediate states has been demonstrated for several m^- mutants by micro-calorimetry (Carra et al., 1994, Carra & Privalov, 1995). In such cases the correlation between *m*-value and ΔA_u may not apply because the two-state approximation is not valid. We believe this to be the case for the m^- mutant studied here, H121P.

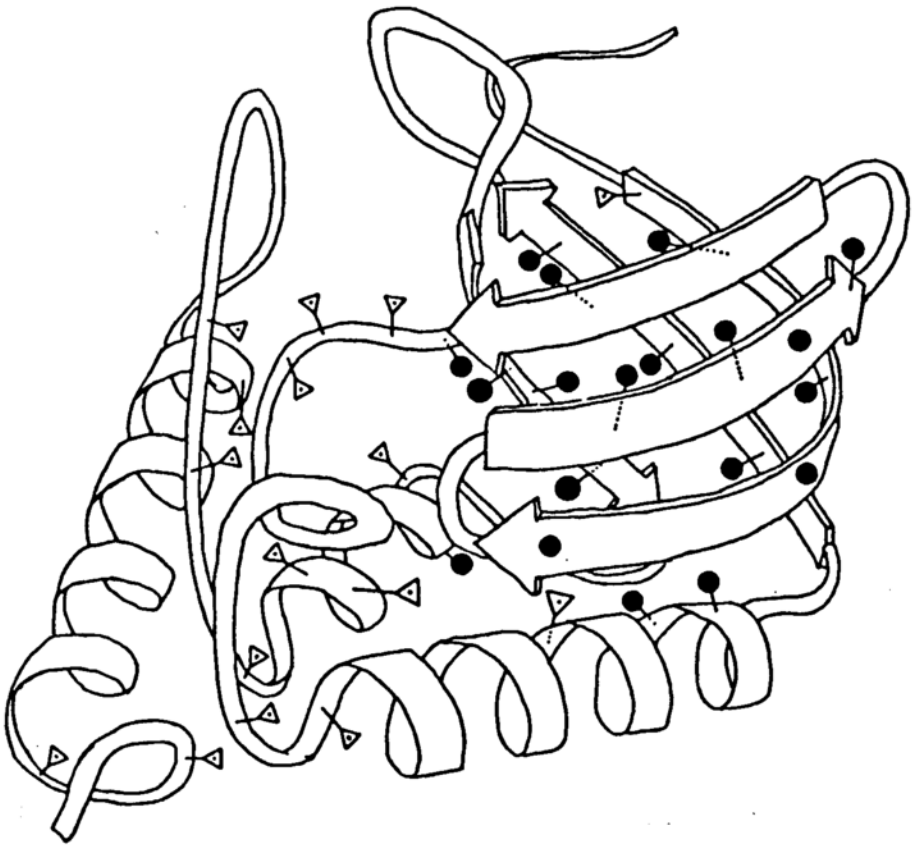

Figure 5-11. Ribbon diagram showing the approximate position of the WT side chain for m^+ (•) and m^- (△) mutants involving the 39 large hydrophobic residues. Reprinted from Shortle and coworkers (Shortle et al., 1990).

Since surface area, ΔA_u, and *m*-value do correlate for the m^+ mutant, A69T + A90S, it provides a clear test of the correlation between ΔA_u and ΔV_u. The volume change for this mutant has been clearly determined and is within experimental error (≤10%) of that obtained for WT (Table 5-1). The ΔV_u for the m^- mutant was found to be nearly identical to that of WT as well. Thus, it was concluded that for Staphylococcal nuclease unfolding there is no correlation between ΔV_u and ΔA_u.

It has long been assumed in high pressure biochemistry that the exposure of hydrophobic surface area results in a decrease in system volume (Nemethy & Scheraga, 1962, Weber & Drickamer, 1983). However, it has been noted that the volume changes observed upon pressure-induced protein unfolding are much smaller than expected from model compound studies (Dill, 1990). More recently, alternative explanations for ΔV_u have been proposed. Prehoda & Markley (Prehoda & Markley, 1996) have proposed compensation between a positive contribution from hydrophobic hydration and a negative contribution of elimination of excluded volume upon unfolding. On the other hand, the observed volume change could result from compensating positive and negative contributions from nonpolar and polar hydration as suggested by Chothia and coworkers (Harpaz et al., 1994). The compensating effect could also be credited to the thermal volume due to cavity creation as noted in the scaled particle theory (Chalikian & Bresiauer, 1996).

Identical values for ΔV_u for WT nuclease and the m^+ mutant, A69T + A90S, provides strong evidence that hydrophobic hydration does not make a large, negative contribution to the volume change of protein unfolding. The change in total accessible surface area upon unfolding for WT nuclease assuming a completely solvent exposed chain in the unfolded state, was calculated to be 12,058 Å^2 and can be broken down to ΔASA_{polar} = 3593 Å^2 and $\Delta ASA_{nonpolar}$ = 8465 Å^2 (Myers et al., 1995). Although the majority of ΔASA is due to the nonpolar residues, their positive contributions to ΔV_u may be offset by a larger negative contribution from the polar groups and backbone. In addition, since it is now known that the unfolded state for nuclease is not a random coil, the estimation for ΔASA is over exaggerated so there may not be as large of a difference between nonpolar and polar surface area. If compensation between exposure of polar and nonpolar surfaces gives rise to the relatively small values observed for the volume changes upon unfolding, then it must be concluded that this compensation remains essentially unchanged for the mutants used in this study as compared to nuclease WT, since the volume changes were found to be essentially identical. Another possibility is that exposed surface area, polar or nonpolar, contributes very little to the ΔV_u. In either case, the remaining contribution to ΔV_u, the excluded volume of the folded chain due to imperfect packing, should contribute significantly to the value of ΔV_u.

CHAPTER 6: THE ROLE OF CAVITIES IN THE PRESSURE DENATURATION OF STAPHYLOCOCCAL NUCLEASE

The decrease in system volume upon unfolding is thought to be a consequence of electrostriction of charged residues, hydration of exposed surface area upon unfolding, and packing defects (Weber & Drickamer, 1983). Royer and coworkers (Royer et al., 1993) ruled out electrostriction as a significant contribution in nuclease and Chapter 5 of this thesis presented data that rules out hydration of exposed surface area. This leaves packing defects as the predominant factor in the overall change in volume upon unfolding. As referenced in Chapter 1, Honig and coworkers (Rashin et al., 1986) found that cavities make up approximately 0 - 2% of the total volume of a protein. The observed change in partial molar volume upon unfolding for nuclease is about 0.5% of the total hydrated volume of the protein (Royer et al., 1993). Therefore, the cavities in the interior of nuclease could account for the total volume change upon unfolding.

Proteins consist of a tightly packed hydrophobic core with a packing density roughly similar to that of crystals of amino acids (Richards, 1977). These tightly packed cores are thought to contribute significantly to the overall stability of the native state, *i.e.*, the energy of stabilization provided by the transfer of a hydrophobic residue from an aqueous solvent to the interior of the protein, is about 25-30 cal mol^{-1} $Å^{-2}$ (Richards, 1977). A study in nuclease in which every large hydrophobic amino acid residue was mutated to alanine and glycine showed that the mutant proteins were more unstable than the WT (Shortle et al., 1990). The decrease in stability was larger than that expected for the transfer

free energy alone suggesting that the stability was decreased by more than just the decrease in hydrophobicity of the side chain. It was later demonstrated in T4 lysozyme that there is a linear relationship between the size of cavity created by a given mutation and the loss of protein stability (Eriksson et al., 1992). That is the larger the cavity which is created, the less stable the mutant. This is thought to occur due to the loss of important van der Waals interactions. Lattman and coworkers have demonstrated that the insertion of amino acids into the structure of nuclease do not cause as large of a decrease in stability as expected (Keefe et al., 1993). In fact, the decrease in stability was similar to that observed for substitution mutations made in the same area. Furthermore, insertions made within the interior of the protein did not cause as large of a decrease in stability as those made at the protein surface (Keefe et al., 1994). Therefore, the overall stability of mutations within a protein depends on the location of the mutation and the degree of local rearrangements made to accommodate the mutation.

Three cavity mutants of nuclease were studied to determine the differences in the change in volume upon unfolding, ΔV_u, relative to WT nuclease. All three mutants occurred at valine 66 which is located in helix 1 and packs into the β-barrel and hydrophobic core of the protein (Figure 6-1). Mutations at this position could potentially disrupt the packing of helix 1 against the β-barrel which may alter the protein stability. Two of the mutations were changes to smaller amino acid side chains (glycine and alanine) while the third

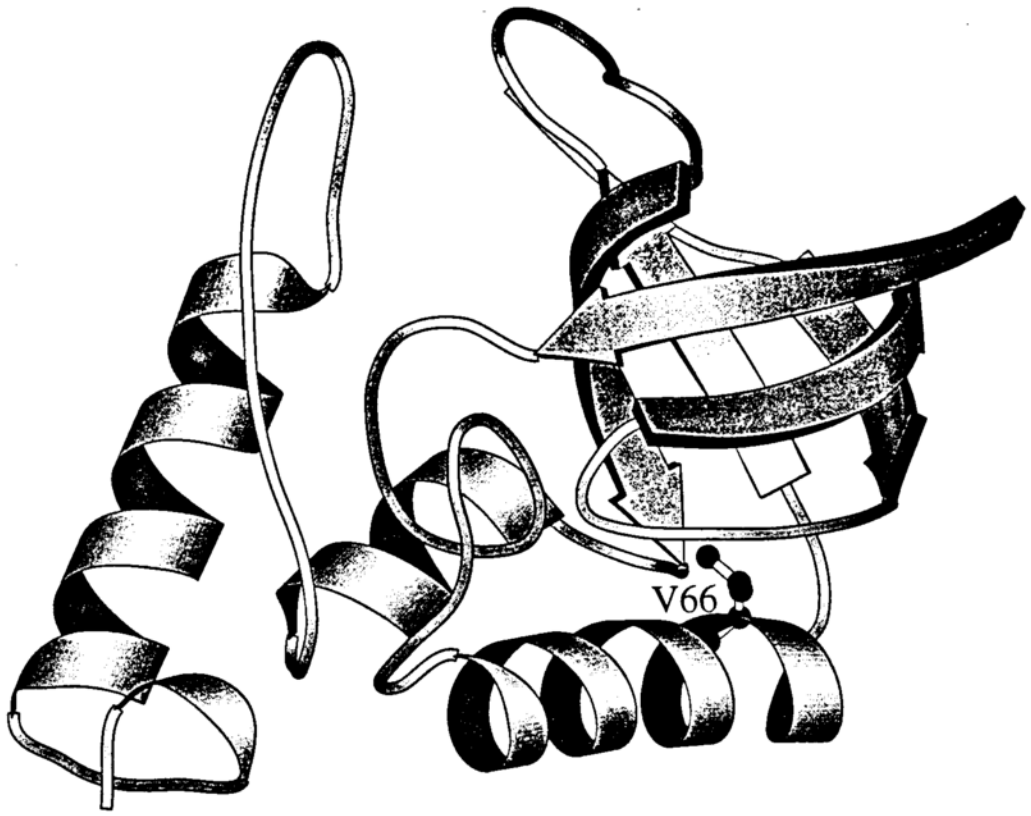

Figure 6-1. The three dimensional structure of Staphylococcal Nuclease determined from x-ray crystallographic data (Hynes & Fox, 1991). The figure was drawn using the program Molscript (Kraulis, 1991). Valine 66 is shown in ball-and-stick presentation.

involved a mutation to a larger amino acid side chain (leucine). The crystal structures have been solved for these mutants. Rather than collapsing around the smaller amino acids, the protein exposes cavities at the site of the mutations and these cavities do not contain any water molecules (personal communication, Ed Lattman). It was therefore expected that the valine to glycine and alanine mutations should result in an increase in the change in volume with respect to the WT protein. On the other hand, the valine to leucine substitution which introduces a larger amino acid might conceivably result in a decrease in the magnitude of the volume change of unfolding.

RESULTS

Figure 6-2, 6-3, and 6-4 show representative high pressure unfolding experiments for the three mutants at position 66. Due to its decreased stability the pressure unfolding of V66G was carried out in the presence of 19.6 millimole fraction xylose at pH 7.0. Since V66A is also less stable than WT nuclease, the pressure denaturation was carried out at pH 7.0, rather than at pH 5.5. On the other hand, V66L is considerably more stable than WT nuclease and therefore the experiments with this mutant were performed in the presence of 0.5 M guanidine at pH 5.5. The data were analyzed for the volume change upon unfolding as described in Materials and Methods (Chapter 3) and the recovered

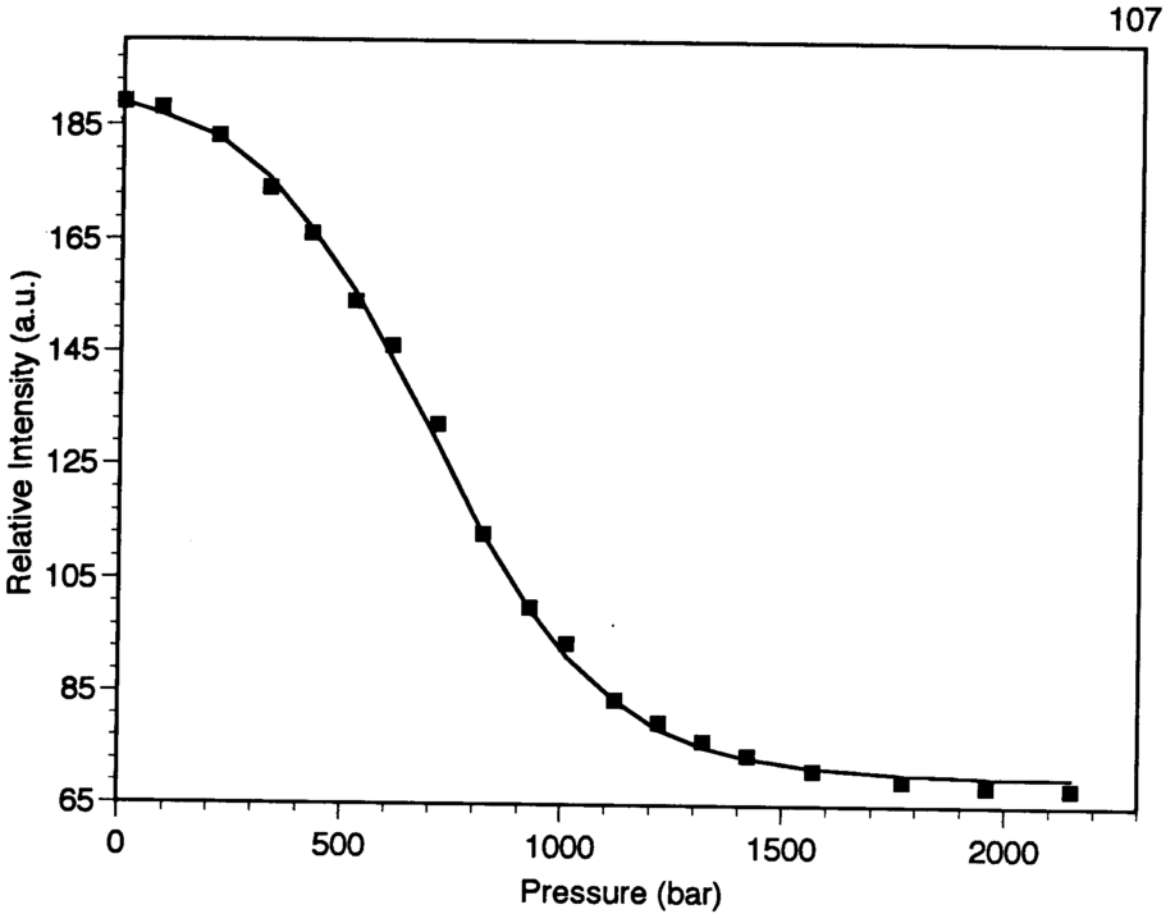

Figure 6-2. A representative experiment for the unfolding of V66G at pH 7.0 and 21°C with 19.1 millimole xylose. The solid line represents the fit to the data.

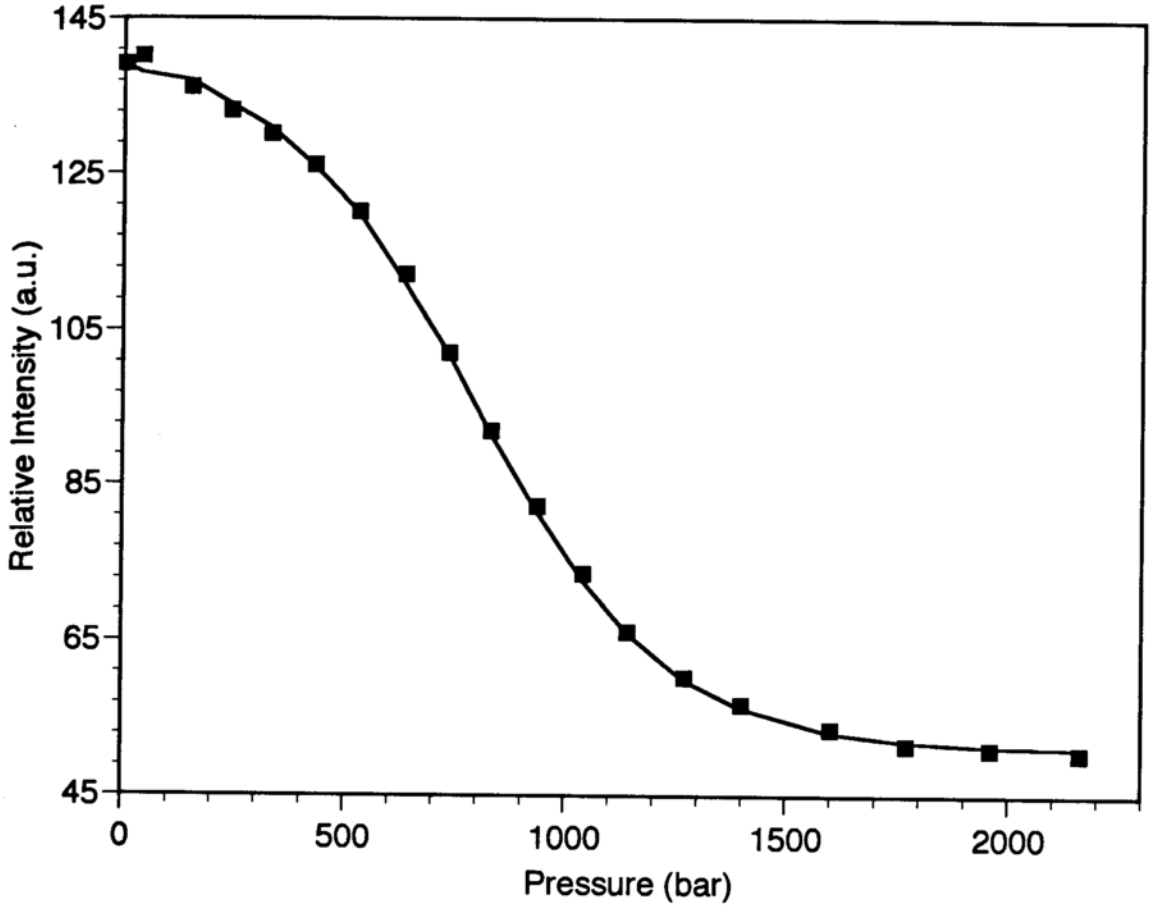

Figure 6-3. A representative experiment for the unfolding of V66A at pH 7.0 and 21°C. The solid line represents the fit to the data.

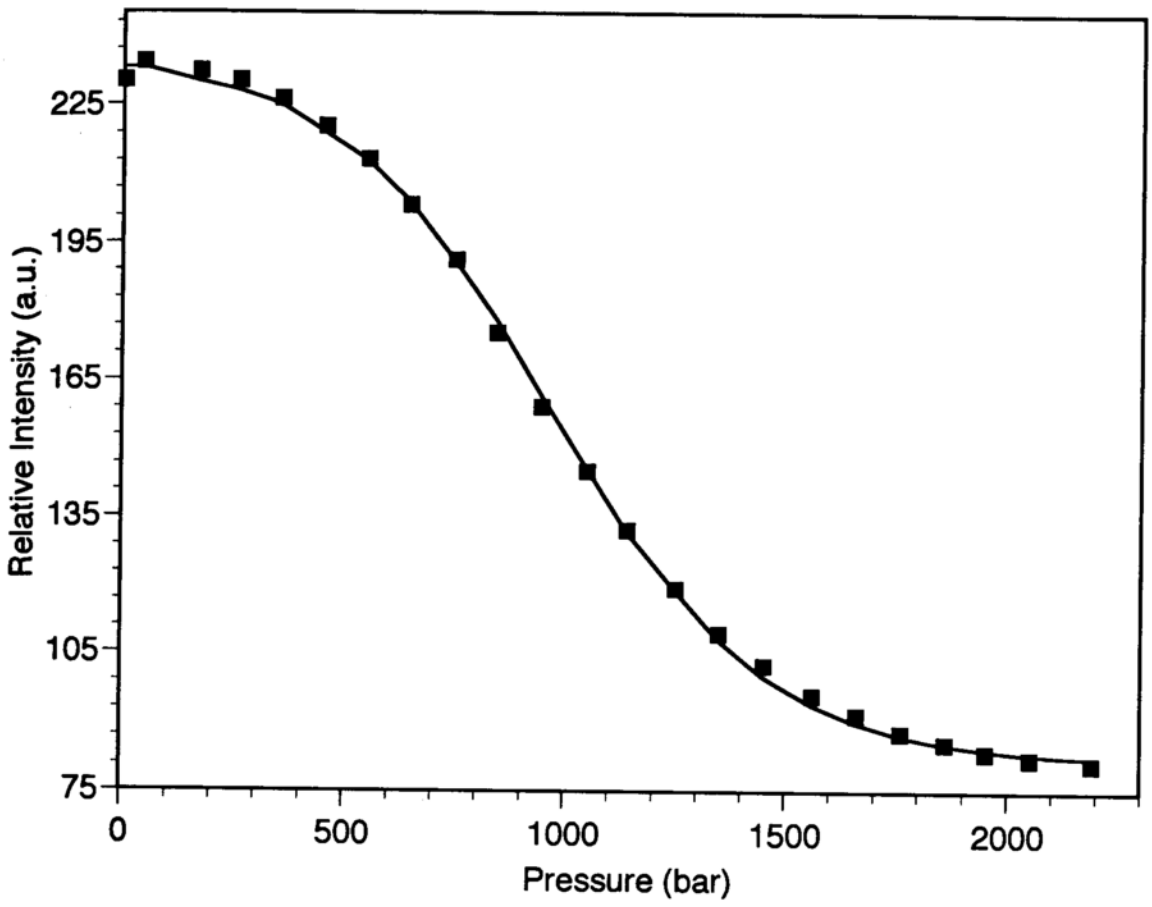

Figure 6-4. A representative experiment for the unfolding of V66L at pH 5.5 and 21°C with 0.5 M guanidine. The solid line represents the fit to the data.

parameter values of the volume changes of unfolding for the average of 4 to 5 experiments along with the values from the global analysis of the data are shown in Table 6-1. The lines through the data points in Figures 6-2, 6-3, and 6-4 represent the best fit of the particular data set shown. Additional experiments can be found in Appendix III. The free energies of unfolding cannot be compared since the denaturation conditions for all three mutants were quite different. Nonetheless, they are consistent with the known relative stabilities of these mutants.

As demonstrated in Chapters 4 and 5, the value of volume upon unfolding does not change in the presence of xylose or guanidine or with differences in pH (Royer et al., 1993). Thus, their magnitudes can be compared between the three mutants and WT nuclease, regardless of experimental conditions. The volume change upon unfolding for WT is -75.3 ± 1.3 ml/mol. The values of ΔV_u for V66G and V66A are within error of one another but are both significantly larger in absolute magnitude than that found for WT, as would be expected from creating larger cavities within the interior of the protein. Unexpectedly, the V66L mutant also has a volume change larger in absolute magnitude than WT.

DISCUSSION

Although proteins have been shown to be as tightly packed as small organic crystal molecules

Protein	ΔG_u (kcal/mol)		ΔV_u (ml/mol)	
	average	global	average	global
V66G	2.0 ± 0.2	2.0 ± 0.2	-112.6 ± 8.2	-111.9 ± 7.7
V66A	2.2 ± 0.2	2.1 ± 0.2	-105.7 ± 7.6	-103.8 ± 6.1
V66L	2.4 ± 0.3	2.3 ± 0.4	-95.7 ± 4.1	-94.2 ± 11.7

Table 6-1. The volume change and free energy change upon unfolding.

(Finney, 1979, Richards, 1974, Schulz & Schirmer, 1979), Honig and coworkers determined that out of 12 proteins, all but one contained internal cavities (Rashin et al., 1986). In addition they found that the volume of the cavities were between 0 to 600 $Å^3$ (0 - 361 ml/mol) and increases with molecular weight so that the cavities make up less than 2% of the total protein volume (Rashin et al., 1986). Since the change in volume upon unfolding for nuclease is 0.5% of the total protein volume, the cavities could account for the observed volume change upon unfolding (Royer et al., 1993). The mutants involved in this study change the size of the internal cavity near amino acid 66 which is located in the hydrophobic core of nuclease and is adjacent to two cavities with volumes of 59 $Å^3$ and 18 $Å^3$ (35.5 ml/mol and 10.8 ml/mol) (Wynn et al., 1996). Figure 6-5 shows the crystal structure of V66G superimposed on top of the WT structure. It can be seen that the cavity does still exist and that there has only been a minimum amount of local readjustment of the neighboring side chains. Through personal communications with Dr. Lattman, it is known that the cavity remains intact for the other two mutants as well and that there are no waters present in the cavity.

A crude calculation can be completed to determine the change in volume for the substitution of the valine at position 66 to glycine, alanine, and leucine by using the van der Waals volumes determined by Richards (Richards, 1974). Table 6-2 shows the values for such a calculation. The predicted volume change upon unfolding for the three mutants would be -107, -96, and -62 ml/mol for V66G, V66A, and V66L, respectively. The actual experimental values for

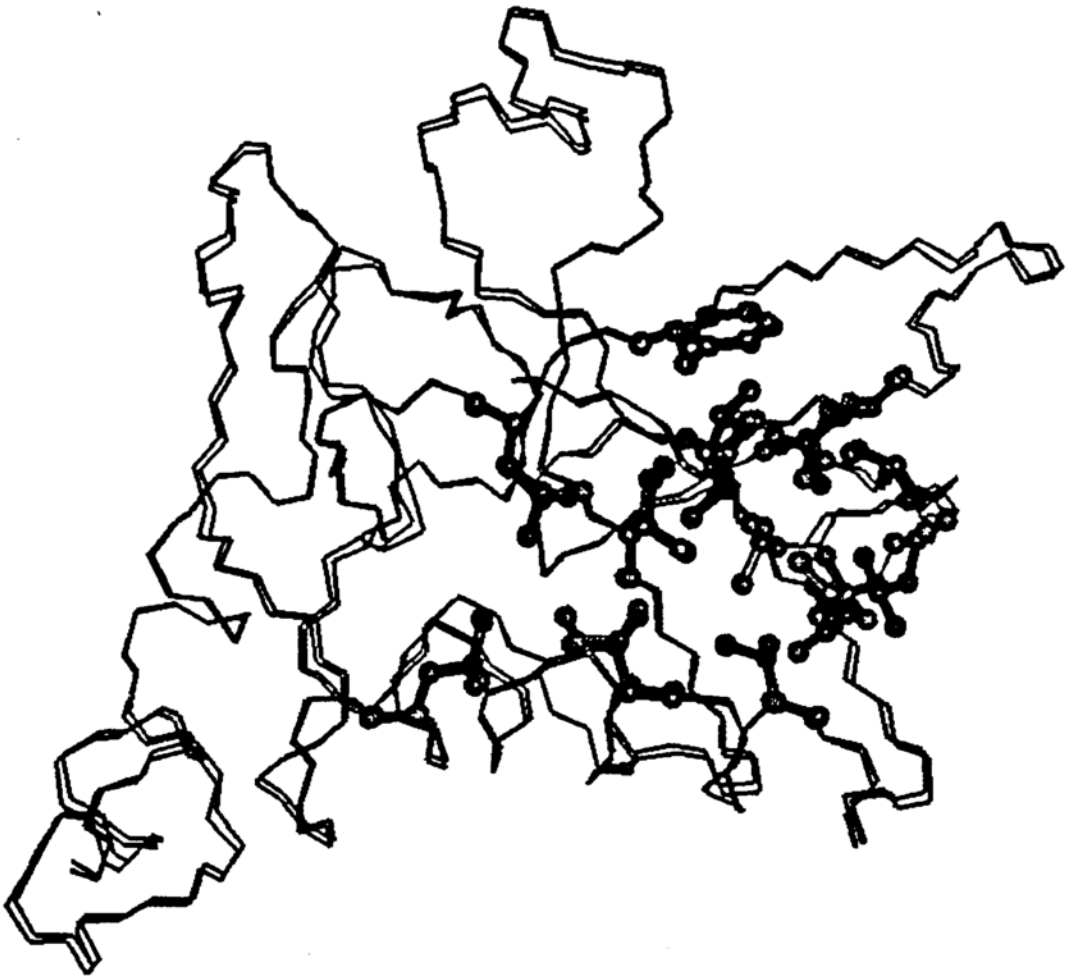

Figure 6-5. The crystal structure of V66G (gray) superimposed on top of the WT crystal structure (black). (The crystal structure of V66G was a gift from Ed Lattman).

Amino Acid	van der Waals Volume (ml/mol)	$\Delta V_{mutation}$ (ml/mol)	Predicted $\Delta V_{unfolding}$ (ml/mol)
Valine	63.2	0	-75
Glycine	28.9	34.3	-107
Alanine	40.3	22.9	-96
Leucine	74.7	-11.4	-62

Table 6-2. Side chain van der Waals volumes (Richards, 1974) and predicted volume change upon unfolding.

V66G and V66A are -111.9 and -103.8 ml/mol. Although the predicted calculations are crude, they are comparable with the observed experimental values. As seen in Figure 6-5, there is a slight amount of local rearrangement which would most likely result in a small difference in the size of the cavity, but it is not significant. The V66G and V66A mutants of nuclease are m^+ mutants (Shortle et al., 1990) which means that they expose a larger amount of surface area in the unfolded state than that of the WT. Since it was demonstrated in Chapter 5 that the amount of surface area exposed upon unfolding does not correspond to the change in volume upon unfolding and since the only other modification in these two mutants is the change in cavity size, these results suggest that it is most likely the cavity size which plays a vital role in the change in volume upon unfolding for nuclease. This was predicted to be the case by Weber & Drickamer (Weber & Drickamer, 1983).

Although there was good agreement between the predicted and experimental values for V66G and V66A, the experimental value for V66L was unexpectedly found to be -94.2 ml/mol which is a larger change in volume than observed for WT. This was unexpected because a large side chain was replaced with an even larger side chain which was predicted to fill in the cavity resulting in a smaller change in volume. One possible explanation may be a consequence of V66L being an m^- mutant and therefore exhibiting non-two-state behavior at acidic pH (Carra et al., 1994). However, once again non-two-state behavior is not observed in the present results. In addition, if an intermediate

were present, it should have a volume larger than that of the unfolded protein since the intermediate would have more secondary structure remaining. In other words, the volume change for the transition from the native to an intermediate should be smaller in magnitude than that from the native to the unfolded state. Therefore, this explanation is improbable.

Another explanation could be local rearrangements in the structure which may create one or more new cavities. This has been shown to occur with a cavity mutants of lysozyme (Eriksson et al., 1992) and nuclease (Wynn et al., 1997). The nuclease mutants occurred at valine 23 which is located on the first strand of the β-barrel and is one of the side chains which surrounds the cavity adjacent to valine 66 in WT nuclease. In that study a series of unnatural amino acids with increasingly larger side chains were placed at position 23. The limit in volume that can be accommodated at position 23 without significant rearrangement was a 1-n-propyl cysteine disulfide side chain (Wynn et al., 1996). As the size of the side chain was increased, helix 1 became displaced from the main body of the β-barrel resulting in the creation of a cavity with a variation in size from 17-29 $Å^3$ depending on the side chain (Wynn et al., 1997). It is uncertain whether such a rearrangement occurs with the V66L mutant of nuclease studied here. Given that this mutant is more stable than WT nuclease, it is unlikely that replacement of valine by leucine at this position results in a rearrangement that leads to creation of a large cavity since this would be highly destabilizing, as is the case with the V66G and V66A mutants. However,

changes in orientation such as those observed by Fox could lead to creation of a number of smaller cavities that would be below the threshold for destabilization. Additional structural information would be necessary to determine whether the larger ΔV_u observed for the V66L mutant truly arises from cavity creation as well.

Although it could be serendipity which caused the different volume change upon unfolding for the three mutants studied here, the pressure denaturation of many nuclease mutants have been studied (Royer et al., 1993; Vidugiris et al., 1995; Vidugiris et al., 1996; Frye et al., 1996) and all show the same volume change upon unfolding as WT nuclease. In any case, the introduction of cavities within the protein has been the only factor that causes a change in volume upon unfolding. It can therefore be concluded that cavities play a very important role in the change in protein system volume upon unfolding.

CHAPTER 7: THE KINETIC BASIS FOR THE STABILIZATION OF STAPHYLOCOCCAL NUCLEASE BY XYLOSE

Sugars have been used as protein stabilizers for many years but it was not until recently that the mechanism of stabilization was established to involve the preferential exclusion of sugars from the surface of proteins (Timasheff, 1993). That is, in a three component solution of water, sugar, and protein, proportionally more water molecules and fewer sugar molecules are found at the surface of the protein than in the bulk. Addition of sugar to a protein solution therefore results in a net increase in free energy which is proportional to the amount of protein surface area that must be preferentially hydrated. Since the protein native state exposes less surface area than the denatured state, the addition of sugars favors folding. Glycerol may be an exception, since in certain cases it binds to proteins at specific sites, and its effects may be stabilizing or destabilizing depending upon the observed property. The stabilization of proteins by sugars must involve modifications in either the rate of folding, unfolding, or both, but the kinetic basis for this stabilization has never been demonstrated. This study addressed the stabilization of proteins by sugars. The effects of a xylose on the folding and unfolding rate constants and information about the degree of exposed surface area in the transition state were determined.

In order to determine the effects of xylose on the rates of folding and unfolding of Staphylococcal nuclease (nuclease), pressure induced unfolding was studied as a function of xylose concentration. High pressure leads to the unfolding of proteins because the volume of the protein-solvent system is smaller

when the protein is in the unfolded state. Pressure jump relaxation kinetics have revealed that the destabilization of the folded state with increasing pressure occurs due to a large positive activation volume for folding, leading to a significant decrease in the rate of folding upon increasing pressure. The rate of unfolding is also slowed by pressure, but to a much lesser degree (Vidugiris et al., 1995). Nuclease was chosen as our model protein since the wild type (WT) has been shown to be well represented by a simple two-state equilibrium from the native to the denatured state without any stable intermediates by a number of methods (Eftink, 1995, Eftink et al., 1991a, Royer et al., 1993, Schechter et al., 1970, Shortle & Meeker, 1986, Shortle et al., 1988, Shortle et al., 1990, Vidugiris et al., 1995), although kinetic (Chen et al., 1992a, Chen et al., 1992b, Nakano et al., 1993), NMR (Alexandrescu et al., 1990, Alexandrescu et al., 1989, Evans et al., 1987, Evans et al., 1989, Fox et al., 1986, Jacobs & Fox, 1994, Loh et al., 1991) and calorimetric (Carra et al., 1994) evidence has revealed small populations of intermediates under certain conditions. Previous high-pressure studies of WT nuclease were well described by a two-state transition except at low pressures where little unfolding occurs (Royer et al., 1993, Vidugiris et al., 1995, Vidugiris et al., 1996). Thus, the fluorescence signal of nuclease, which decreases in intensity upon unfolding is representative of the unfolding of the entire protein even though it emanates from a single residue, tryptophan 140 (Royer et al., 1993, Shortle & Lin, 1985, Vidugiris et al., 1995). This is not the case for all proteins. Non-two-state behavior has been observed

by comparing pressure effects on the NMR signals of individual residues of hen egg white lysozyme (Samarasinghe et al., 1992) and the NMR and fluorescence signals of *arc* repressor (Peng et al., 1993).

RESULTS

The equilibrium unfolding of WT nuclease is displaced to higher pressures with increasing xylose concentrations (Figure 7-1) consistent with results discussed in Chapters 4 and 5 (Frye et al., 1996). The degree to which the equilibrium free energy depends upon the xylose concentration is termed the xylose *m*-value. It was found to be 153 ± 34 which is slightly larger than previously reported in Chapter 5, but is not as well determined (Frye et al., 1996), and is within error of the previous value. The observed change in volume upon unfolding is independent of xylose concentration as demonstrated in Chapter 4. The equilibrium free energy and volume change of unfolding at various xylose concentrations are shown in Table 7-1.

Representative kinetic traces of the pressure-jump relaxation profiles at 6.2 millimole fraction xylose for the denaturation of nuclease monitored by intrinsic tryptophan fluorescence, along with the fits to the data as described by equation 7 in Chapter 3, can be seen in Figure 7-2. Figure 7-3 shows a close up of the fit to the data at 1500 bar from Figure 7-2 in order to demonstrate the accuracy of the fit. The time scale for reaching equilibrium increases

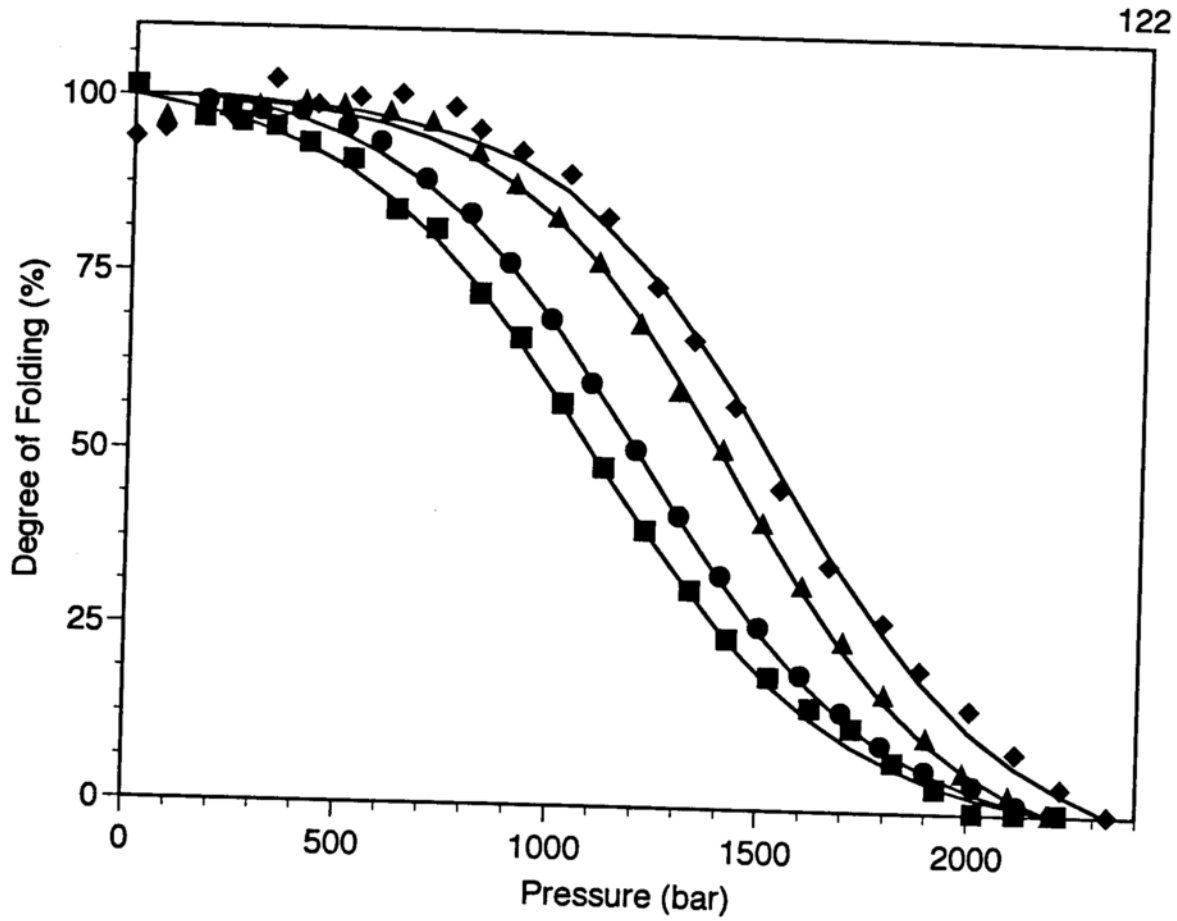

Figure 7-1. Unfolding profiles for WT nuclease as a function of pressure and mole fraction xylose at pH 4.5 and 21°C. The symbols are data from a representative set of experiments, and the solid lines represent the global curve analysis fits to the data. (■)1.5 millimole xylose; (●) 3 millimole xylose: (▲) 6.2 millimole xylose; (◆) 9.4 millimole xylose.

Millimole Fraction Xylose	ΔG_u kcal/mol		ΔV_u ml/mol	
	equilibrium	kinetics	equilibrium	kinetics
1.5	2.2 ± 0.2	2.4 ± 0.4	-76.8 ± 4	-95.8 ± 18
3.0	2.5 ± 0.2	2.4 ± 0.5	-79.1 ± 4	-89.1 ± 13
6.2	3.2 ± 0.3	3.0 ± 0.6	-86.4 ± 7	-98.9 ± 15
9.4	3.3 ± 0.4	3.6 +1.8/-0.8	-83.8 ± 8	-108.8 ± 38

Table 7-1. Comparison of equilibrium and kinetic changes in free energy and volume as a function of xylose concentration.

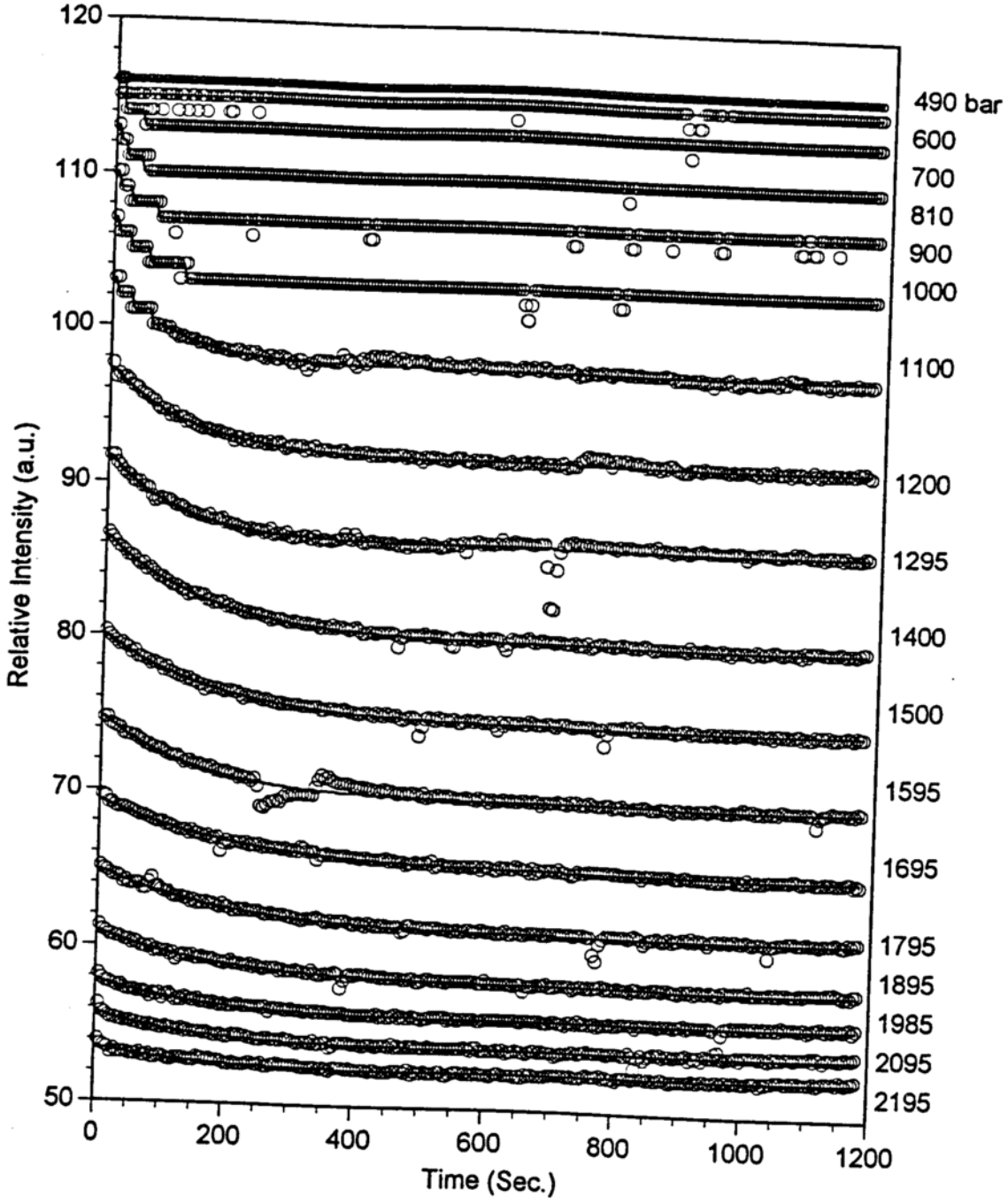

Figure 7-2. A representative pressure-jump relaxation profile at 6.2 millimole xylose for WT nuclease at pH 4.5 and 21°C. The fluorescence intensity is plotted on the left side of the y axis and the final pressure from each pressure jump is on the right side. Solid lines through the points represent the results of the global curve analysis fits to the data.

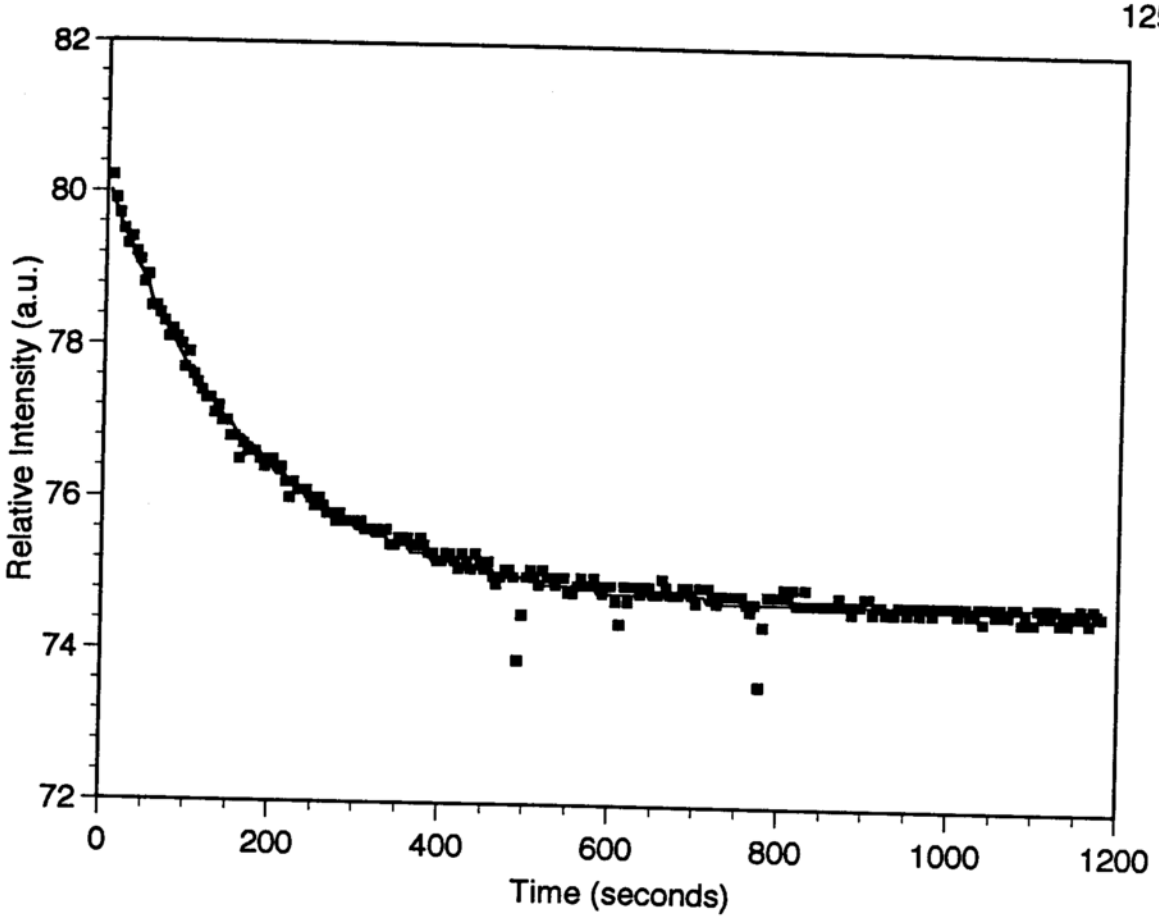

Figure 7-3. A close up of the fit to the data of intrinsic tryptophan intensity as a function of time at 1500 bar from Figure 7-2.

systematically as a function of pressure, as was observed previously (Vidugiris et al., 1995). The relaxation profiles were fit as described in Materials and Methods (Chapter 3) for their characteristic relaxation times, τ. Plots of the natural logarithm of τ as a function of pressure for the four tested xylose concentrations are depicted in Figures 7-4 a-d. It can be seen that ln τ increases linearly with pressure up to a break point that corresponds to the midpoint of the equilibrium unfolding curve (the point where $\Delta G_p = 0$), and then increases linearly with a much smaller slope. The values for the folding rate constants were obtained from the intercept of the linear regression of the ln τ plots below the midpoint (since k_f predominates in the sum in equation 9, Chapter 3), while those for unfolding are derived from the linear regression of the points above the midpoint. The activation volumes, $\Delta V_f^{\ddagger}$ and $\Delta V_u^{\ddagger}$, obtained from the slopes of the plots of ln τ vs. pressure (Figure 7-4) at each xylose concentration are within error of one another and within experimental error of those previously reported for nuclease (Vidugiris et al., 1995, Vidugiris et al., 1996) (Table 7-2).

Figures 7-5 a-d show the nonlinear analysis fits to the data as described in Chapter 3 (equation 13) for the four xylose concentrations studied fixing the values of the equilibrium constants to those obtained from the equilibrium data analyses. The values of the equilibrium constants from the nonlinear analysis were within error of one another for the data at 3 and 6.2 millimole fraction xylose. The values for the data at 1.5 millimole fraction xylose were slightly

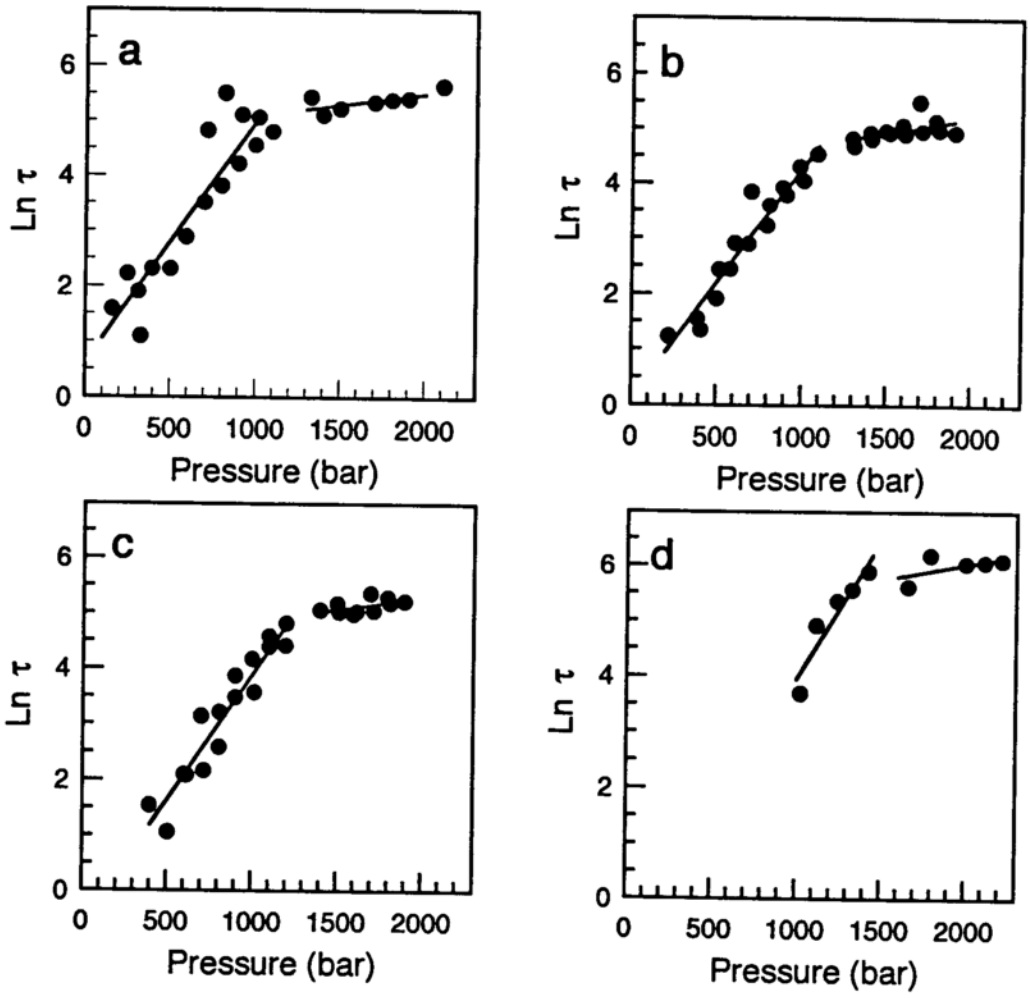

Figure 7-4. Natural logarithm of the relaxation time, ln τ, as a function of pressure. The relaxation times are those obtained from the global analysis of the relaxation data according to a single exponential decay model as described in Materials and Methods. Solid lines through the points represent the results of linear regression analysis of the points above and below the midpoint of the transition as described in the Materials and Methods. (a) 1.5 millimole xylose, (b) 3 millimole xylose, (c) 6.2 millimole xylose, (d) 9.4 millimole xylose.

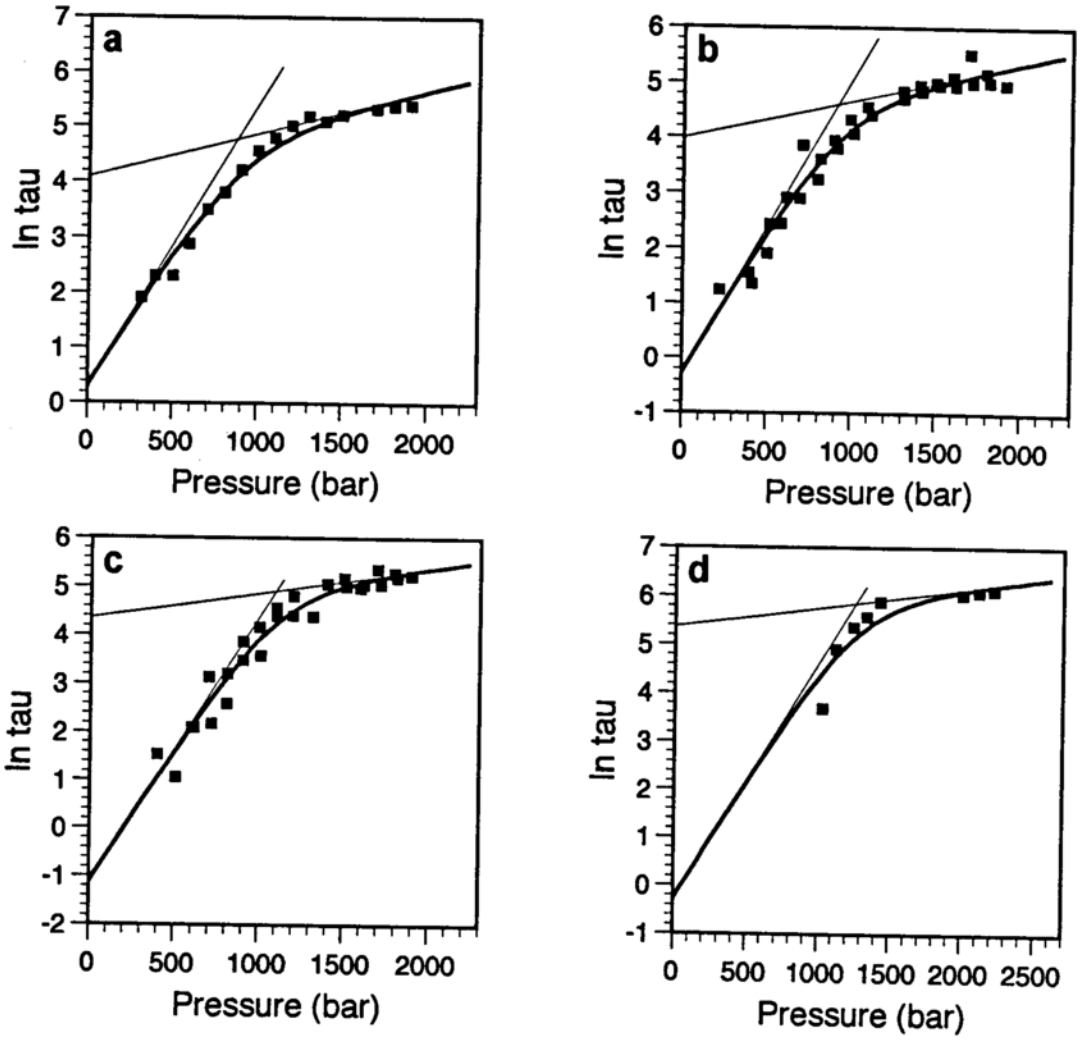

Figure 7-5. Natural logarithm of the relaxation time, ln τ, as a function of pressure. The relaxation times are those obtained from the global analysis of the relaxation data according to a single exponential decay model as described in Materials and Methods. Solid lines through the points represent the results of nonlinear regression analysis fixing the equilibrium constant and equilibrium volume change to those values obtained from the equilibrium data analysis. (a) 1.5 millimole xylose, (b) 3 millimole xylose, (c) 6.2 millimole xylose, (d) 9.4 millimole xylose.

Millimole fraction xylose	$\Delta V_f^{\ddagger}$ (ml/mol)		$\Delta V_u^{\ddagger}$ (ml/mol)		k°_f (s^{-1})		k°_u (s^{-1})	
	linear	nonlinear	linear	nonlinear	linear	nonlinear	linear	nonlinear
1.5	106.0 ± 13.2	123.8 ± 17.3	10.2 ± 4.6	19.2 ± 13.4	0.54 ± 0.26	0.72 ± 0.24	0.010 ± .003	0.017 ± 0.013
3.0	102.2 ± 7.7	130.0 ± 15.0	13.1 ± 6.1	16.4 ± 11.2	0.91 ± 0.2	1.3 ± 0.4	0.016 ± .008	0.018 ± 0.014
6.2	109.8 ± 9.2	134.7 ± 18.5	10.9 ± 5.8	12.5 ± 12.5	1.9 ± 0.7	3.1 ± 1.5	0.012 ± .006	0.013 ± 0.016
9.4	122.7 ± 26.4	118.6 ± 204	13.9 ± 11.2	9.2 ± 123	3.0 +8.0/- 2.2	1.3 ± 9.5	0.007 ± .010	0.005 ± 0.037

Table 7-2. Rate constants and activation volumes of folding and unfolding as a function of xylose concentration for the linear and nonlinear analysis.

outside of error with one another. Since there was good agreement between the equilibrium constants from the equilibrium analysis and nonlinear kinetic analysis at the other two xylose concentrations which were better determined, to a first approximation the two-state model for the pressure denaturation of nuclease holds. Therefore, the values for the equilibrium constants in the nonlinear analysis were fixed to the values obtained from the equilibrium data analyses for each xylose concentration. The values for k°_f, k°_u, $\Delta V_f^\ddagger$, and $\Delta V_u^\ddagger$ from the nonlinear analysis are shown in Table 7-2 along with those values from the linear analysis. The numbers from the linear and nonlinear analyses are in fairly good agreement except for the values of $\Delta V_f^\ddagger$ at 3 millimole fraction xylose. Although the values look fairly similar, the linear analysis makes the assumption that the folding rate constant dominates at low pressures and the unfolding rate constant at high pressures. Making this assumption most likely causes a systematic error which underestimates the activation volumes and rate constants for the folding process. Therefore, the values from the nonlinear analysis are more accurate since this assumption is not made.

The rate constants and activation volumes from the linear kinetic analysis were used to calculate equilibrium values for the change in free energy, ΔG_u, and volume, ΔV_u upon unfolding in order to compare them to those obtained from analysis of the equilibrium profiles. Their values, given in Table 7-1, are within error of one another, further validating the two-state model of unfolding to a first approximation. The agreement of the kinetic data with the equilibrium data

offers support that the linear analysis of the relaxation times is a reasonable approximation.

In Figure 7-6 are shown the plots of the rate constants of folding and unfolding, $k°_f$ and $k°_u$, for the linear and nonlinear analyses as a function of the millimole fraction xylose. Both methods of analysis show that the rate of folding increases significantly with increasing xylose while that of unfolding decreases slightly, although the effect is smaller. The linear fits to the data points help demonstrate this point.

The natural logarithm of the rate constants as a function of the natural logarithm of water activity is shown in Figure 7-7a. The activity of water was calculated by the equation:

$$\ln(a_w) = -\frac{[solute]_{osmolal}}{55.5} \qquad (1)$$

where $[solute]_{osmolal}$ is the osmolal concentration of solute and 55.5 is the number of water molecules in 1 kg. The slope of the linear fit to the data yields the change in the number of water molecules by the equation:

$$\ln K = (\Delta n_w)[\ln a(w)] \qquad (2)$$

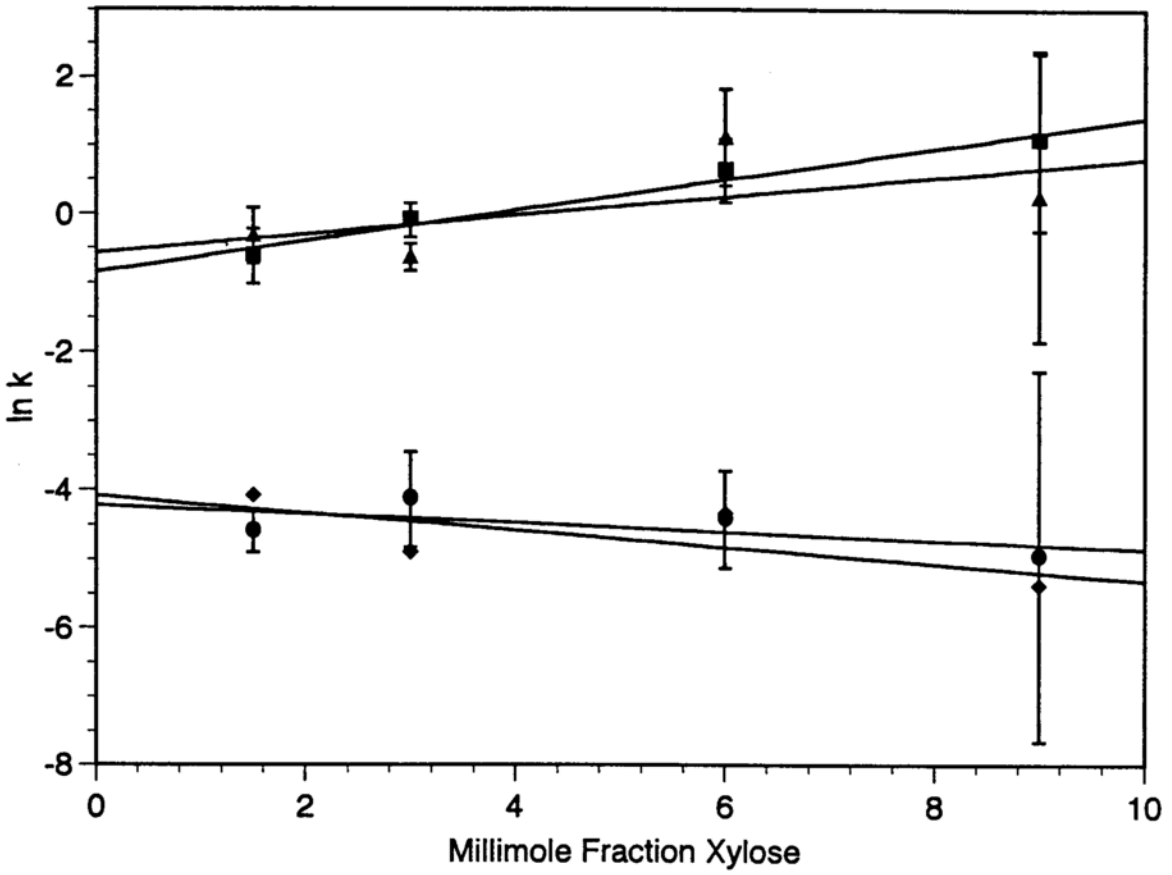

Figure 7-6. Natural logarithm of the rate of folding and unfolding, ln k°_f and ln k°_u, as a function of xylose concentration. The rate constants are those obtained from the linear and nonlinear plots of the relaxation time as a function of pressure as described in Materials and Methods. The solid lines represent linear regression analysis of the points. (■) ln k_f° from linear analysis, (●) ln k_u° from nonlinear analysis, (▲) ln k_f° from linear analysis, and (◆) ln k_u° from nonlinear analysis.

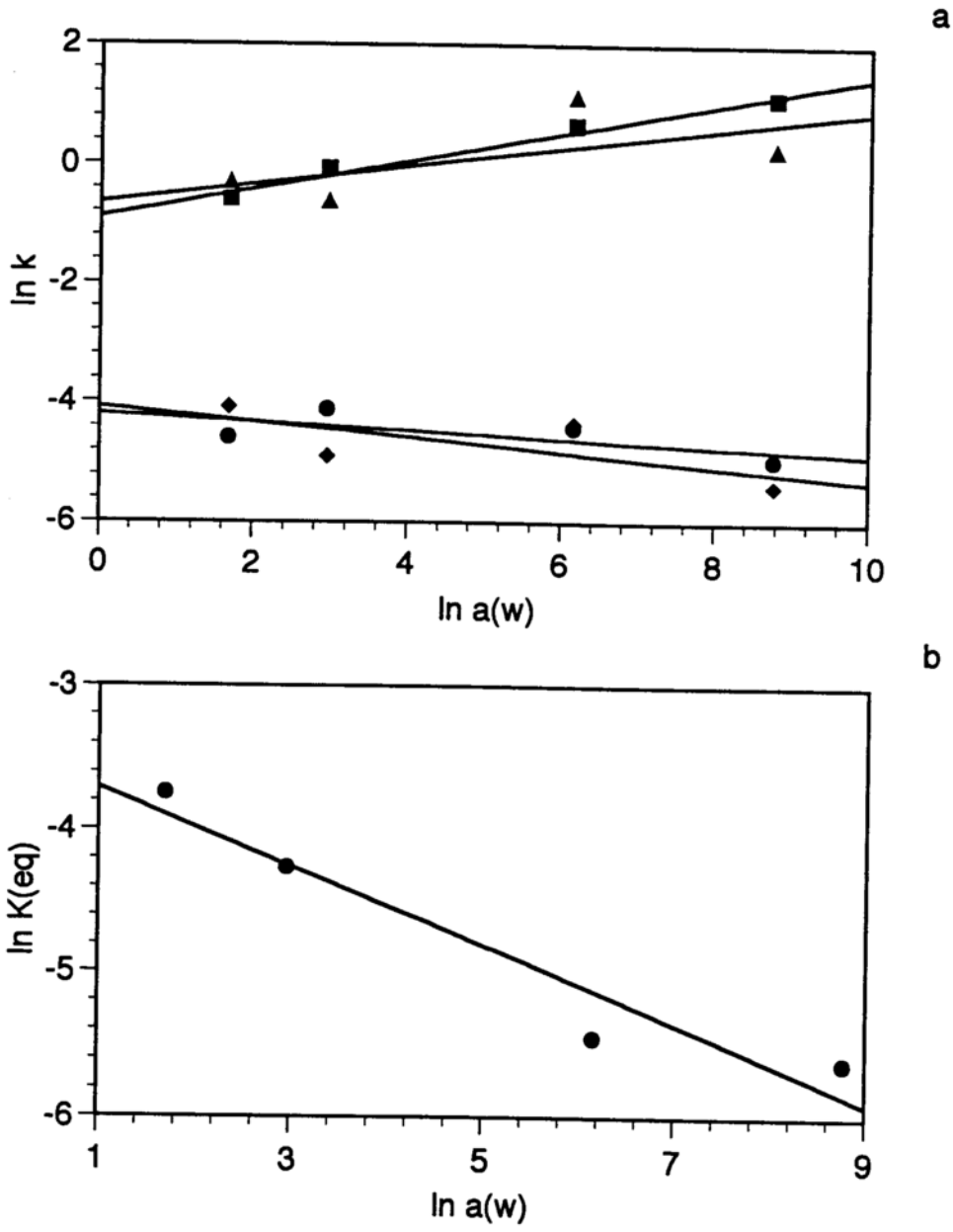

Figure 7-7. (a) (■) ln $k_f°$ & (●) ln $k_u°$ (linear analysis) and (▲) ln $k_f°$ & (◆) ln $k_u°$ (nonlinear analysis) as a function of the ln water activity. The rate constants are those obtained from the linear and nonlinear plots of the relaxation time as a function of pressure as described in Materials and Methods. (b) The equilibrium constant of unfolding as a function of the natural logarithm of water activity. The equilibrium constants are from the fits to the equilibrium unfolding profile.

The results from the linear analysis indicate that 236 ± 25 water molecules are released from the surface of the protein upon folding while 67 ± 60 molecules are involved in the unfolding of nuclease. Whereas the results from the nonlinear analysis indicate that 153 ± 132 water molecules are released from the surface of the protein upon folding while 123 ± 94 molecules are involved in the unfolding of nuclease. The rate constants obtained at the highest concentration of xylose (9.4 millimole fraction xylose) from both the linear and nonlinear analyses are not well-determined (see standard deviations in Table 7-2). This lack of precision is due to the small number of data points in the transition region over the available pressure range for a protein that is stabilized by sugar to such a large extent (see Figure 7-5 d). If this value is not included in the linear regression, then the number of water molecules released upon folding becomes 367 ± 176 for the nonlinear analysis and 271 ± 40 from the linear analysis, whereas for unfolding the values are 12 ± 180 and 15 ± 102, respectively for the nonlinear and linear analyses. Based on these numbers, it can be postulated that a significant number of water molecules is released from the surface of the protein upon folding, while a lesser degree of hydration is involved in the transition between folded state and transition state. The natural logarithm of the equilibrium constant as a function of the natural logarithm of water activity is plotted in Figure 7-7b. The change in the number of waters between the folded and unfolded states is 276 which is within standard deviation of the change in the number of water molecules between the rates of folding and unfolding.

DISCUSSION

The energetic basis for the stabilization of proteins by osmolytes such as xylose is accepted generally to arise from a preferential exclusion of sugar from protein surfaces that increases the free energy of all states of the protein (Timasheff, 1993). This net increase in free energy for all of the states of the protein is necessarily proportional to the amount of protein surface area exposed in these states. Those states which expose the most surface area are destabilized to the greatest extent as depicted in Figure 7-8. Therefore, the free energy of the unfolded state increases much more than that of the folded state which is preferentially populated in the presence of xylose. The kinetic basis for this increase in the free energy of unfolding depends upon the effect of xylose on the transition state relative to its effect on the native and denatured states. This in turn depends upon the degree of exposure of surface area of the transition state relative to the native and denatured states. The kinetic basis for the increase in the ΔG of unfolding upon increasing xylose concentration appears from the present results to be due primarily to an increase in the rate of folding, while the decrease in the rate of unfolding plays a less significant role. This indicates that a greater degree of surface area is buried between the unfolded and the transition states than between the latter and the folded state. This suggests that the transition state in nuclease folding lies closer along the folding

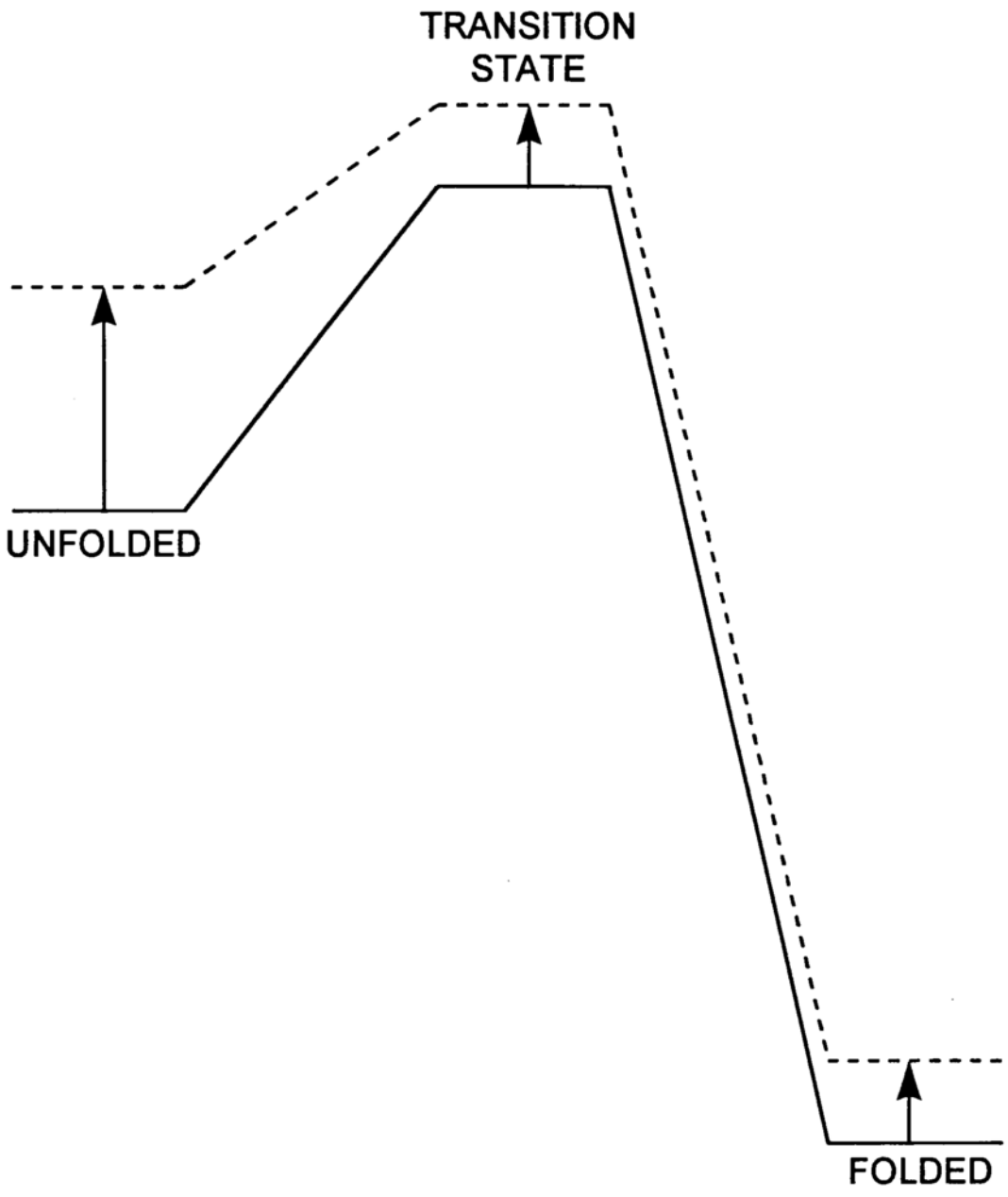

Figure 7-8. Free energy diagram of folded, unfolded and transition states for xylose stabilization of nuclease which emerges from the data presented. The dotted line represents the ensemble of protein states in the presence of xylose while the solid lines represent the ensemble of protein states without xylose.

coordinate to the folded rather than unfolded state in terms of amount of exposed surface area.

Fersht and coworkers have drawn similar conclusions for barnase based on the effects of denaturant on the rates of unfolding (Serrano et al., 1992). Based on activation *m*-values, they determined that the transition state buries approximately 70-75% of the surface exposed in the unfolded state for barnase and approximately 60% for CI-2 (Itzhaki et al., 1995, Otzen et al., 1994). Englander and coworkers determined that about 50% of the exposed surface in the unfolded state was buried in the transition state of cytochrome c (Sosnick et al., 1996). The transition state for all of these proteins involve the burial of a significant amount of surface area and the rate limiting step is cited as being molecular collapse of the peptide chain.

Molecular collapse is also named as the rate limiting step for the cold-shock protein CspB (Jacob et al., 1997). In this case however, the rationale was that protein folding is diffusion controlled as a result of the increase in solvent viscosity in the presence of increasing amounts of sucrose and ethylene glycol. Their results showed a decrease in the rates of folding and unfolding in the presence of sucrose and ethylene glycol which was interpreted as being a result of the increase in solvent viscosity. The results in this thesis disagree with theirs since the rate of folding was actually found to increase as a function of xylose. These inconsistencies could be a consequence of osmolytes behaving differently

for specific proteins or a function of differences in the osmolytes resulting from differences in the extent of increase in viscosity.

Previous pressure-jump relaxation kinetic experiments have been carried out on nuclease by Royer and coworkers (Vidugiris et al., 1995). These studies revealed that the folding rates slow down as a function of pressure as a result of a large positive activation volume of folding. A small positive activation volume of unfolding was also observed. The system volume in the transition state must therefore be larger than the volume of the folded and unfolded states. The rate limiting step in folding for nuclease was thus proposed to involve dehydration since pressure denaturation is a function of the differences in solvation. A swelling of the native chain as a result of disruption of tertiary chain contacts was proposed as the rate limiting step of unfolding. Figure 7-9 shows a schematic of the physical basis of the volume change (Vidugiris et al., 1995).

The present results on the effect of xylose on the rate constants provides additional evidence for this interpretation. The rate of folding is increased as a function of xylose because the unfolded state exposes a large amount of surface area. This exposed surface area is hydrated in the unfolded state which is energetically unfavorable. Therefore, the system prefers to dehydrate the exposed surface area and fold more quickly. These results also indicate that folding is accompanied by significant dehydration, while there is not a significant change in hydration upon unfolding. This suggest that the transition state and the native state are hydrated to a similar extent. Roder and coworkers reached

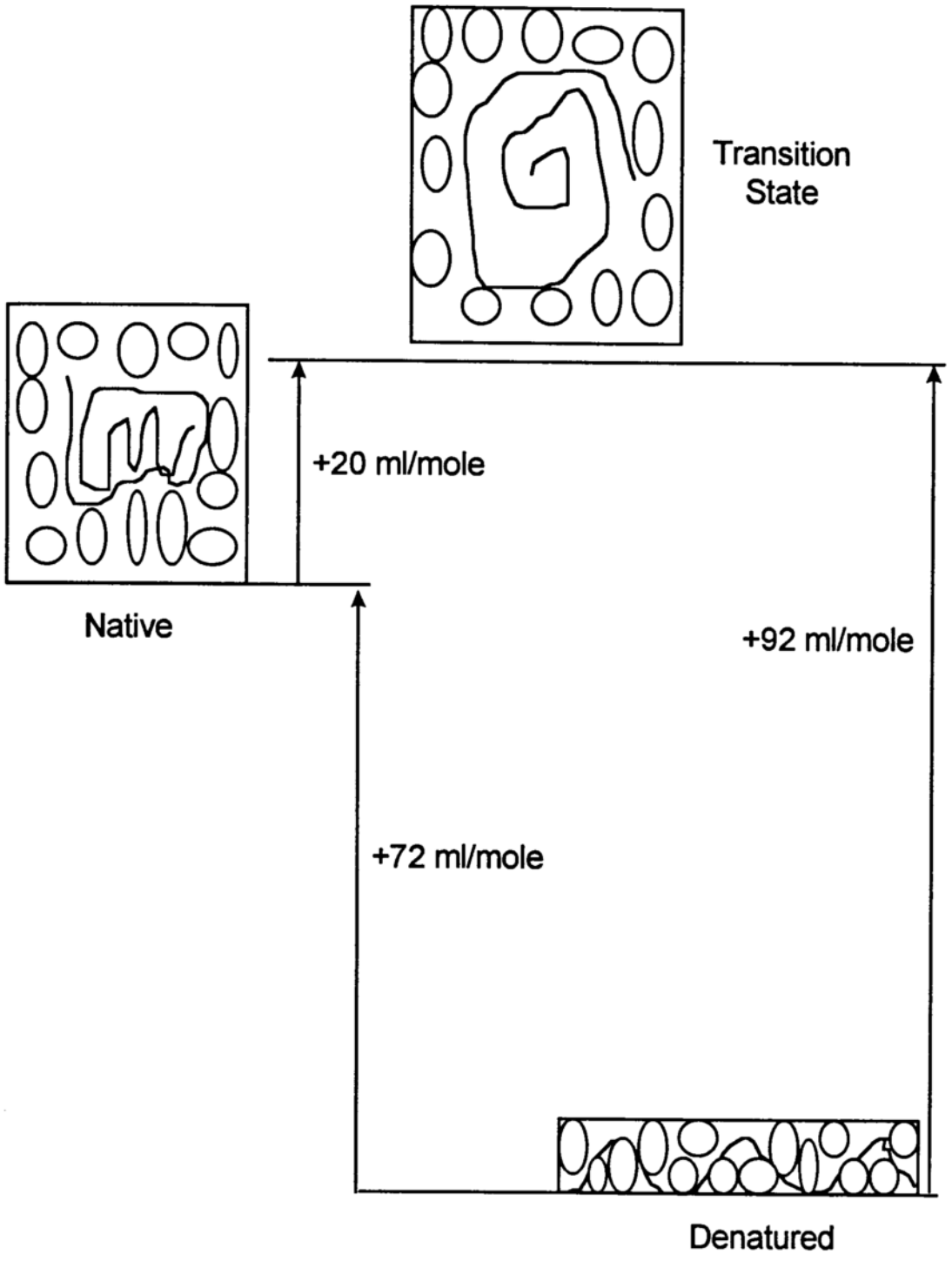

Figure 7-9. Schematic representation for the physical basis of the volume change adapted from Vidugiris et al., 1995.

a similar conclusion for ubiquitin folding (Khorasanizadeh et al., 1996). The resulting picture of the transition state in nuclease folding is consistent with what Finkelstein and Shakhnovich have termed a dry molten globule (Finkelstein & Shakhnovich, 1989), with dehydration constituting the rate limiting step in folding.

Dehydration as the rate limiting step in nuclease folding is not necessarily in disagreement with the finding of molecular collapse as the rate limiting step in the previously mentioned proteins. Since the molecular collapse involves the burial of a significant amount of surface area, this implies that the buried surface area must become dehydrated. In fact, recent pressure-jump SAXS and FTIR experiments suggest that the formation of secondary and tertiary structures and molecular collapse occur on similar time scales and therefore depend upon the same rate limiting step, dehydration (Panick et al., 1997).

Dehydration of protein surfaces manifests itself by a large difference in the heat capacity (ΔC_p) of the different states involved. In fact, Fersht and coworkers (Oliveberg et al., 1995) determined the ΔC_p of activation in barnase folding, implicating an enthalpic as well as entropic contribution to the activation energy. It will be interesting and challenging to incorporate these kinetic results and this picture of the transition state into the increasingly popular funnel theory of protein folding (Dill et al., 1995, Socci et al., 1996).

CHAPTER 8: FINAL CONCLUSIONS

Pressure denatures proteins because the protein system volume of the denatured state is smaller than that of the native state. This change in system volume upon unfolding is an important thermodynamic variable which can provide crucial information about the solvation of the protein. Pressure denaturation is the only reliable method which can be used to obtain the volume change. The volume change is not well understood but is thought to be due to the contributions of electrostriction, packing defects, and hydration of exposed surface area. Previous work by Royer and coworkers (Royer et al., 1993) showed that electrostriction does not contribute significantly to the volume change of unfolding for Staphylococcal nuclease, the model protein system used in the present work.

The major focus of this thesis was to further characterize the factors contributing to the magnitude of the observed volume change of unfolding for Staphylococcal nuclease. Using cooperativity mutants which expose significantly larger or smaller amounts of surface area in their unfolded states, it was demonstrated that hydration of exposed surface area to different extents does not correlate with the magnitude of the volume change upon unfolding. Although hydration is an important factor in the volume change, hydration of polar and nonpolar surfaces appear to compensate one another resulting in a null effect. Given that neither electrostriction or hydration of exposed protein surface area appeared to contribute significantly to the volume change observed upon unfolding of nuclease, the role of packing imperfections was investigated.

In contrast to the lack of effects of electrostriction and surface area, the work in this thesis demonstrates that packing defects in the protein interior most likely play a significant role in determining the magnitude of the observed volume change of unfolding. The volume change for unfolding was larger for those mutations which introduced a larger cavity into the protein interior. This is due to the penetration of solvent into the cavities which were void spaces in the native state such that the larger the cavity the larger the difference in volume between the native and denatured states.

To further explore the role of solvation in protein stability and in the folding process, the effects of water activity on the stability and on the rates of folding and unfolding for staphylococcal nuclease were investigated. It had been shown previously that the transition state for nuclease unfolding occupies a larger volume than either the native or denatured state (Vidugiris et al., 1995). Moreover, the activation volume for folding was much larger than for unfolding. Thus the rate limiting step in protein folding was interpreted in this previous work as dehydration of a significant amount of surface area. The rate limiting step in protein unfolding was interpreted as disruption of the internal non-covalent interactions in the protein structure without penetration of solvent into the interior, resulting in an expanded chain which occupies a larger system volume than the native state. By carrying out pressure-jump relaxation experiments in the presence of the colligative agent xylose, the underlying kinetic basis for the stabilization of nuclease by sugars was determined in this thesis to arise

primarily from an increase in the folding rate. This result implicates significant dehydration for the transition from the unfolded to the transition state. Furthermore, this result implies that the transition state exposes a similar amount of surface area as compared to the native state and thus lies closer to the native than the denatured state on the reaction coordinate.

While this work aids in the understanding of the volume change upon unfolding as well as general information regarding solvation, the volume change is not completely understood. More information about the compensating contributions is needed to understand all of the factors involved in the decrease in system volume upon unfolding. In addition, pressure denaturation of several proteins would be needed in order to test the generality of the present results. This would best be accomplished by using a combination of techniques such as, fluorescence, NMR, SAXS, and FTIR, to monitor the pressure denaturation of a number of small reversibly folding proteins.

REFERENCES

Alexandrescu, A. T., Hinck, A. P., & Markley, J. L. (1990) *Biochemistry 29*, 4516-25.

Alexandrescu, A. T., Ulrich, E. L., & Markley, J. L. (1989) *Biochemistry 28*, 204-11.

Beechem, J., Gratton, E., Ameloot, M., Knutson, J., & Brand, L. (1991) in *Topics in fluorescence spectroscopy* (Lakowicz, J., Ed.) pp 241-305, Plenum Publishing Corp, New York City.

Beechem, J. M. (1992) *Methods in Enzymology 210*, 37-54.

Benson, A. M., Jr, & Drickamer, H. G. (1957) *The journal of chemical physics 27*, 1164-1174.

Bigelow, C. C. (1967) *Journal of Theoretical Biology 16*, 187-211.

Boje, L., & Hvidt, A. (1972) *Biopolymers 11*, 2357-2364.

Brandts, J. (1969) in *Biological Macromolecules* (Fasman, G., & Timasheff, S., Eds.), Marcel Dekker, New York City.

Brandts, J. F., Oliveira, R. J., & Westort, C. (1970) *Biochemistry 9*, 1038-47.

Carra, J. H., Anderson, E. A., & Privalov, P. L. (1994) *Biochemistry 33*, 10842-50.

Carra, J. H., & Privalov, P. L. (1995) *Biochemistry 34*, 2034-41.

Chalikian, T. V., & Breslauer, K. J. (1996) *Biopolymers 39*, 619-26.

Chalikian, T. V., Totrov, M., Abagyan, R., & Breslauer, K. J. (1996) *Journal of Molecular Biology 260*, 588-603.

Chen, H. M., Markin, V. S., & Tsong, T. Y. (1992a) *Biochemistry 31*, 12369-75.

Chen, H. M., Markin, V. S., & Tsong, T. Y. (1992b) *Biochemistry 31*, 1483-91.

Christensen, L. K. (1952) *Compt. rend. trav. lab. carlsberg. ser. chim. 28*, 37.

Clery, C., Renault, F., & Masson, P. (1995) *FEBS Letters 370*, 212-4.

Creighton, T. E., & Shortle, D. (1994) *Journal of Molecular Biology 242*, 670-82.

Cuatrecasas, P., Fuchs, S., & Anfinsen, C. B. (1967) *Journal of Biological Chemistry 242*, 1541-7.

Dill, K. A. (1985) *Biochemistry 24*, 1501-9.

Dill, K. A. (1990) *Biochemistry 29*, 7133-55.

Dill, K. A., Bromberg, S., Yue, K., Fiebig, K. M., Yee, D. P., Thomas, P. D., & Chan, H. S. (1995) *Protein Science 4*, 561-602.

Dill, K. A., & Chan, H. S. (1997) *Nature Structural Biology 4*, 10-9.

Duggleby, R. G. (1984) *Computers in Biology & Medicine 14*, 447-55.

Eftink, M. (1995) *Methods in Enzymology 259*, 487-512.

Eftink, M. R., Ghiron, C. A., Kautz, R. A., & Fox, R. O. (1991a) *Biochemistry 30*, 1193-9.

Eftink, M. R., Gryczynski, I., Wiczk, W., Laczko, G., & Lakowicz, J. R. (1991b) *Biochemistry 30*, 8945-53.

Eftink, M. R., & Ramsay, G. D. (1997) *Proteins 28*, 227-40.

Eigen, M., & deMaeyer, L. (1963) in *Techniques of organic chemistry* (Weissberger, A., Ed.) pp 895-1054, Wiley, New York City.

Eriksson, A. E., Baase, W. A., Zhang, X. J., Heinz, D. W., Blaber, M., Baldwin, E. P., & Matthews, B. W. (1992) *Science 255*, 178-83.

Evans, P. A., Dobson, C. M., Kautz, R. A., Hatfull, G., & Fox, R. O. (1987) *Nature 329*, 266-8.

Evans, P. A., Kautz, R. A., Fox, R. O., & Dobson, C. M. (1989) *Biochemistry 28*, 362-70.

Fersht, A. R. (1995) *Proceedings of the National Academy of Sciences of the United States of America 92*, 10869-73.

Fink, A. L., Calciano, L. J., Goto, Y., Nishimura, M., & Swedberg, S. A. (1993) *Protein Science 2*, 1155-60.

Finkelstein, A. V., & Shakhnovich, E. I. (1989) *Biopolymers 28*, 1681-94.

Finney, J. (1979) in *Water: A Comprehensive Treatise* (Franks, F., Ed.) pp 47-122, Plenum Press, New York City.

Flanagan, J. M., Kataoka, M., Shortle, D., & Engelman, D. M. (1992) *Proceedings of the National Academy of Sciences of the United States of America 89*, 748-52.

Fox, R. O., Evans, P. A., & Dobson, C. M. (1986) *Nature 320*, 192-4.

Frank, H., & Evans, M. (1945) *J. Chem. Phys. 13*, 507.

Frye, K. J., Perman, C. S., & Royer, C. A. (1996) *Biochemistry 35*, 10234-9.

Frye, K. J., & Royer, C. A. (1997) *Protein Science 6*, 789-793.

Gladstone, S., Laidler, K., & Eyring, H. (1941) *The theory of rate processes*, McGraw-Hill Book Co., New York.

Harpaz, Y., Gerstein, M., & Chothia, C. (1994) *Structure 2*, 641-9.

Hawley, S. A. (1971) *Biochemistry 10*, 2436-42.

Hermans, J., Jr., & Acampora, G. (1967) *Journal of the American Chemical Society 89*, 1547-52.

Huang, G. S., & Oas, T. G. (1995) *Proceedings of the National Academy of Sciences of the United States of America 92*, 6878-82.

Hynes, T. R., & Fox, R. O. (1991) *Proteins 10*, 92-105.

Ikai, A., & Tanford, C. (1971) *Nature 230*, 100-2.

Itzhaki, L. S., Otzen, D. E., & Fersht, A. R. (1995) *Journal of Molecular Biology 254*, 260-88.

Jackson, S. E., & Fersht, A. R. (1991) *Biochemistry 30*, 10436-43.

Jacob, M., Schindler, T., Balbach, J., & Schmid, F. X. (1997) *Proceedings of the National Academy of Sciences of the United States of America 94*, 5622-7.

Jacobs, M. D., & Fox, R. O. (1994) *Proceedings of the National Academy of Sciences of the United States of America 91*, 449-53.

James, E., Wu, P. G., Stites, W., & Brand, L. (1992) *Biochemistry 31*, 10217-25.

Janin, J. (1976) *Journal of Molecular Biology 105*, 13-4.

Karplus, M., & Weaver, D. L. (1976) *Nature 260*, 404-6.

Kataoka, M., Flanagan, J., Tokunaga, F., & Engelman, D. (1994) in *Synchrotron Radiation in the Biosciences* (Chance, B., Deisenhofer, J., Ebashi, S., Goodhead, D., Helliwell, J., Huxley, H., Iizuka, T., Kirz, J., Mitsui, T., Rubenstein, E., Sakabe, N., Sasaki, T., Schmahl, G., Stuhrmann, H., Wuthrich, K., & Zaccai, G., Eds.) pp 187-194, Calendon Press, Oxford.

Kauzmann, W. (1959) *Adv. Protein Chem 16*, 1-63.

Keefe, L. J., Quirk, S., Gittis, A., Sondek, J., & Lattman, E. E. (1994) *Protein Science 3*, 391-401.

Keefe, L. J., Sondek, J., Shortle, D., & Lattman, E. E. (1993) *Proceedings of the National Academy of Sciences of the United States of America 90*, 3275-9.

Khorasanizadeh, S., Peters, I. D., & Roder, H. (1996) *Nature Structural Biology 3*, 193-205.

Kim, P. S., & Baldwin, R. L. (1982) *Annual Review of Biochemistry 51*, 459-89.

Kita, Y., Arakawa, T., Lin, T. Y., & Timasheff, S. N. (1994) *Biochemistry 33*, 15178-89.

Klapper, M. (1973) in *Progr. Biorg. chem.* pp 55-132.

Kraulis, P. (1991) *J. Appl. crystallog. 24*, 946-950.

Lakowicz, J. (1983) *Principles of Fluorescence Spectroscopy*, Plenum, New York.

Lee, J. C., & Timasheff, S. N. (1981) *Journal of Biological Chemistry 256*, 7193-201.

Lesser, G. J., & Rose, G. D. (1990) *Proteins 8*, 6-13.

Levinthal, C. (1968) *J Chim Phys 65*, 44-45.

Li, T. M., Hook, J. W. d., Drickamer, H. G., & Weber, G. (1976a) *Biochemistry 15*, 3205-11.

Li, T. M., Hook, J. W. d., Drickamer, H. G., & Weber, G. (1976b) *Biochemistry 15*, 5571-80.

Lin, T. Y., & Timasheff, S. N. (1996) *Protein Science 5*, 372-81.

Livingstone, J. R., Spolar, R. S., & Record, M. T., Jr. (1991) *Biochemistry 30*, 4237-44.

Loh, S., McNemar, C., & Markley, J. (1991) in *Techniques in protein chemistry* pp 275-282, Academic Press, San Diego.

Loll, P. J., Meeker, A. K., Shortle, D., Pease, M., & Lattman, E. E. (1988) *Journal of Biological Chemistry 263*, 18190-2.

Miller, W. G., & Goebel, C. V. (1968) *Biochemistry 7*, 3925-35.

Mirejovsky, D., & Arnett, E. M. (1983) *Journal of American Chemical Society 105*, 1112-1117.

Myers, J. K., Pace, C. N., & Scholtz, J. M. (1995) *Protein Science 4*, 2138-48.

Nakano, T., Antonino, L. C., Fox, R. O., & Fink, A. L. (1993) *Biochemistry 32*, 2534-41.

Nemethy, G., & Scheraga, H. (1962) *Journal of Chemical Physics 36*, 3401-3417.

Oliveberg, M., Tan, Y. J., & Fersht, A. R. (1995) *Proceedings of the National Academy of Sciences of the United States of America 92*, 8926-9.

Otzen, D. E., Itzhaki, L. S., elMasry, N. F., Jackson, S. E., & Fersht, A. R. (1994) *Proceedings of the National Academy of Sciences of the United States of America 91*, 10422-5.

Pace, C. N. (1975) *CRC Critical Reviews in Biochemistry 3*, 1-43.

Pace, C. N. (1986) *Methods in Enzymology 131*, 266-80.

Paladini, A., & Weber, G. (1981) *rev. Sci. Instrum. 52*, 419-427.

Panick, G., Malessa, R., Winter, R., Rapp, G., Frye, K., & Royer, C. (1997) *J. Mol. Bio. in press*.

Peng, X., Jonas, J., & Silva, J. L. (1993) *Proceedings of the National Academy of Sciences of the United States of America 90*, 1776-80.

Prehoda, K., & Markley, J. (1996) in *High Pressure Effects in Biophysics and Enzymology* (Markley, J., Northrop, D., & Royer, C., Eds.) pp 33-43, Oxford University Press, New York City.

Privalov, P. L. (1979) *Advances in Protein Chemistry 33*, 167-241.

Privalov, P. L., & Gill, S. J. (1988) *Advances in Protein Chemistry 39*, 191-234.

Privalov, P. L., & Khechinashvili, N. N. (1974) *Journal of Molecular Biology 86*, 665-84.

Ptitsyn, O. B. (1987) *Journal of Protein Chemistry 6*, 273-293.

Rashin, A. A., Iofin, M., & Honig, B. (1986) *Biochemistry 25*, 3619-25.

Richards, F. M. (1974) *Journal of Molecular Biology 82*, 1-14.

Richards, F. M. (1977) *Annual Review of Biophysics & Bioengineering 6*, 151-76.

Rose, G. D., & Wolfenden, R. (1993) *Annual Review of Biophysics & Biomolecular Structure 22*, 381-415.

Royer, C. A. (1993) *Analytical Biochemistry 210*, 91-7.

Royer, C. A., & Beechem, J. M. (1992) *Methods in Enzymology 210*, 481-505.

Royer, C. A., Hinck, A. P., Loh, S. N., Prehoda, K. E., Peng, X., Jonas, J., & Markley, J. L. (1993) *Biochemistry 32*, 5222-32.

Royer, C. A., Smith, W. R., & Beechem, J. M. (1990) *Analytical Biochemistry 191*, 287-94

Samarasinghe, S. D., Campbell, D. M., Jonas, A., & Jonas, J. (1992) *Biochemistry 31*, 7773-8.

Sawamura, S., Kitamura, K., & Taniguchi, Y. (1989) *J. Phys. Chem. 93*, 4931-4935.

Schechter, A. N., Chen, R. F., & Anfinsen, C. B. (1970) *Science 167*, 886-7.

Schellman, J. A. (1978) *Biopolymers 17*, 1305-1322.

Schellman, J. A. (1987) *Biopolymers 26*, 549-59.

Schindler, T., Herrler, M., Marahiel, M. A., & Schmid, F. X. (1995) *Nature Structural Biology 2*, 663-73.

Schulz, G., & Schirmer, R. (1979) *Principles of Protein Structure*, Springer-Verlag, New York City.

Semisotnov, G. V., Rodionova, N. A., Razgulyaev, O. I., Uversky, V. N., Gripas, A. F., & Gilmanshin, R. I. (1991) *Biopolymers 31*, 119-28.

Serrano, L., Matouschek, A., & Fersht, A. R. (1992) *Journal of Molecular Biology 224*, 805-18.

Shortle, D. (1995) *Advances in Protein Chemistry 46*, 217-47.

Shortle, D., & Lin, B. (1985) *Genetics 110*, 539-55.

Shortle, D., & Meeker, A. K. (1986) *Proteins 1*, 81-9.

Shortle, D., & Meeker, A. K. (1989) *Biochemistry 28*, 936-44.

Shortle, D., Meeker, A. K., & Freire, E. (1988) *Biochemistry 27*, 4761-8.

Shortle, D., Meeker, A. K., & Gerring, S. L. (1989) *Archives of Biochemistry & Biophysics 272*, 103-13.

Shortle, D., Stites, W. E., & Meeker, A. K. (1990) *Biochemistry 29*, 8033-41.

Sjoberg, M., Silveston, R., & Kronberg, B. (1993) *Langmuir 9*, 973-979.

Smith, W., & Missen, R. (1982) *Chemical Reaction Equilibrium Analysis*, John Wiley & Sons, New York.

Socci, N. D., Onuchic, J. N., & Wolynes, P. G. (1996) *J Chem Phys 104*, 5860-5868.

Sosnick, T. R., Mayne, L., & Englander, S. W. (1996) *Proteins 24*, 413-26.

Sosnick, T. R., Mayne, L., Hiller, R., & Englander, S. W. (1994) *Nature Structural Biology 1*, 149-56.

Tanford, C. (1970) *Advances in Protein Chemistry 24*, 1-95.

Teller, D. C. (1976) *Nature 260*, 729-31.

Timasheff, S. N. (1993) *Annual Review of Biophysics & Biomolecular Structure 22*, 67-97.

Tsong, T. Y., Baldwin, R. L., & Elson, E. L. (1971) *Proceedings of the National Academy of Sciences of the United States of America 68*, 2712-5.

Vidugiris, G. J., Markley, J. L., & Royer, C. A. (1995) *Biochemistry 34*, 4909-12.

Vidugiris, G. J., Truckses, D. M., Markley, J. L., & Royer, C. A. (1996) *Biochemistry 35*, 3857-64.

Visser, A. J., Li, T. M., Drickamer, H. G., & Weber, G. (1977) *Biochemistry 16*, 4879-82.

Wang, J. F., LeMaster, D. M., & Markley, J. L. (1990) *Biochemistry 29*, 88-101.

Wang, Y., Alexandrescu, A. T., & Shortle, D. (1995) *Philosophical Transactions of the Royal Society of London - Series B: Biological Sciences 348*, 27-34.

Wang, Y., & Shortle, D. (1996) *Protein Science 5*, 1898-906.

Weber, G., & Drickamer, H. G. (1983) *Quarterly Reviews of Biophysics 16*, 89-112.

Wyman, J. j. (1964) *Adv. Protein Chem. 19*, 223-286.

Wynn, R., Harkins, P. C., Richards, F. M., & Fox, R. O. (1996) *Protein Science 5*, 1026-31.

Wynn, R., Harkins, P. C., Richards, F. M., & Fox, R. O. (1997) *Protein Science 6*, 1621-1626.

Zipp, A., & Kauzmann, W. (1973) *Biochemistry 12*, 4217-28.

Zwanzig, R., Szabo, A., & Bagchi, B. (1992) *Proceedings of the National Academy of Sciences of the United States of America 89*, 20-2.

APPENDIX I: ADDITIONAL DATA FROM CHAPTER 4

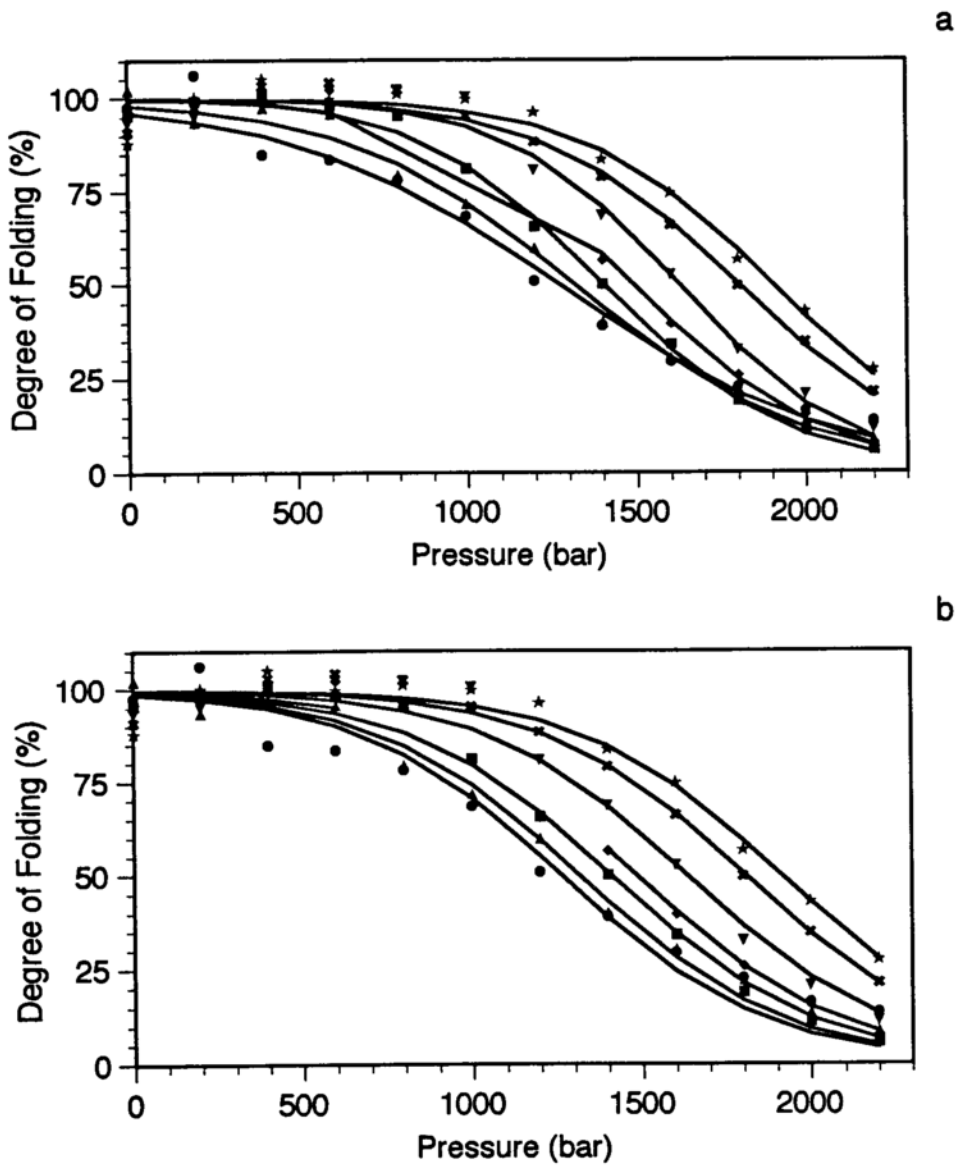

Figure I-1. Unfolding profiles for WT nuclease as a function of pressure and millimole fraction xylose at pH 4.5 and 21°C. The symbols are data from a representative set of experiments and the solid lines represent the (a) unlinked curve analysis and (b) global curve analysis fits to the data. (■) 0 mole fraction xylose, (●) 3 millimole fraction xylose, (▲) 6.2 millimole fraction xylose, (◆) 9.4 millimole fraction xylose, (▼) 12.7 millimole fraction xylose, (✖) 16.1 millimole fraction xylose, (★) 19.6 millimole fraction xylose.

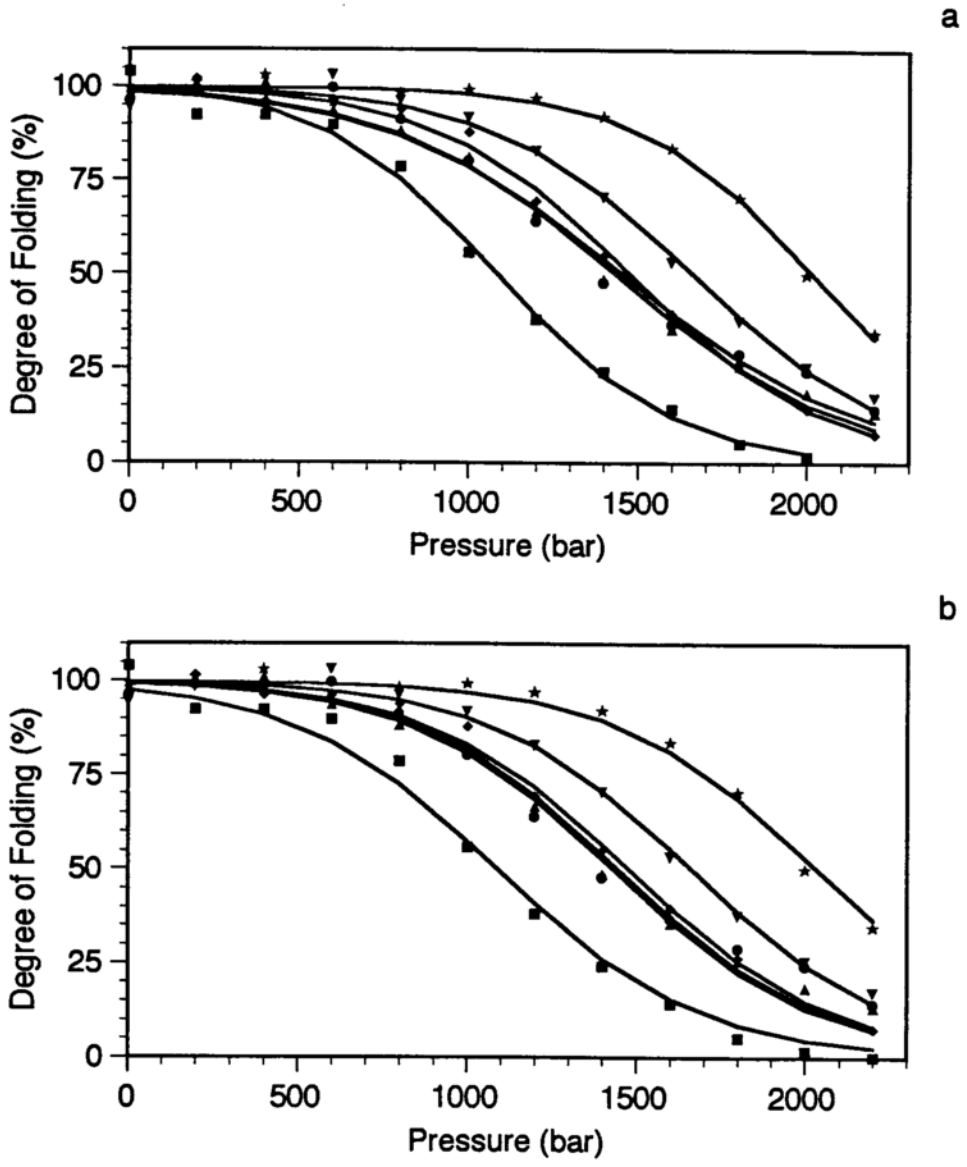

Figure I-2. Unfolding profiles for WT nuclease as a function of pressure and millimole fraction xylose at pH 4.5 and 21°C. The symbols are data from a representative set of experiments and the solid lines represent the (a) unlinked curve analysis and (b) global curve analysis fits to the data. (■) 0 mole fraction xylose, (●) 3 millimole fraction xylose, (▲) 6.2 millimole fraction xylose, (◆) 9.4 millimole fraction xylose, (▼) 12.7 millimole fraction xylose, (★) 19.6 millimole fraction xylose.

APPENDIX II: ADDITIONAL DATA FROM CHAPTER 5

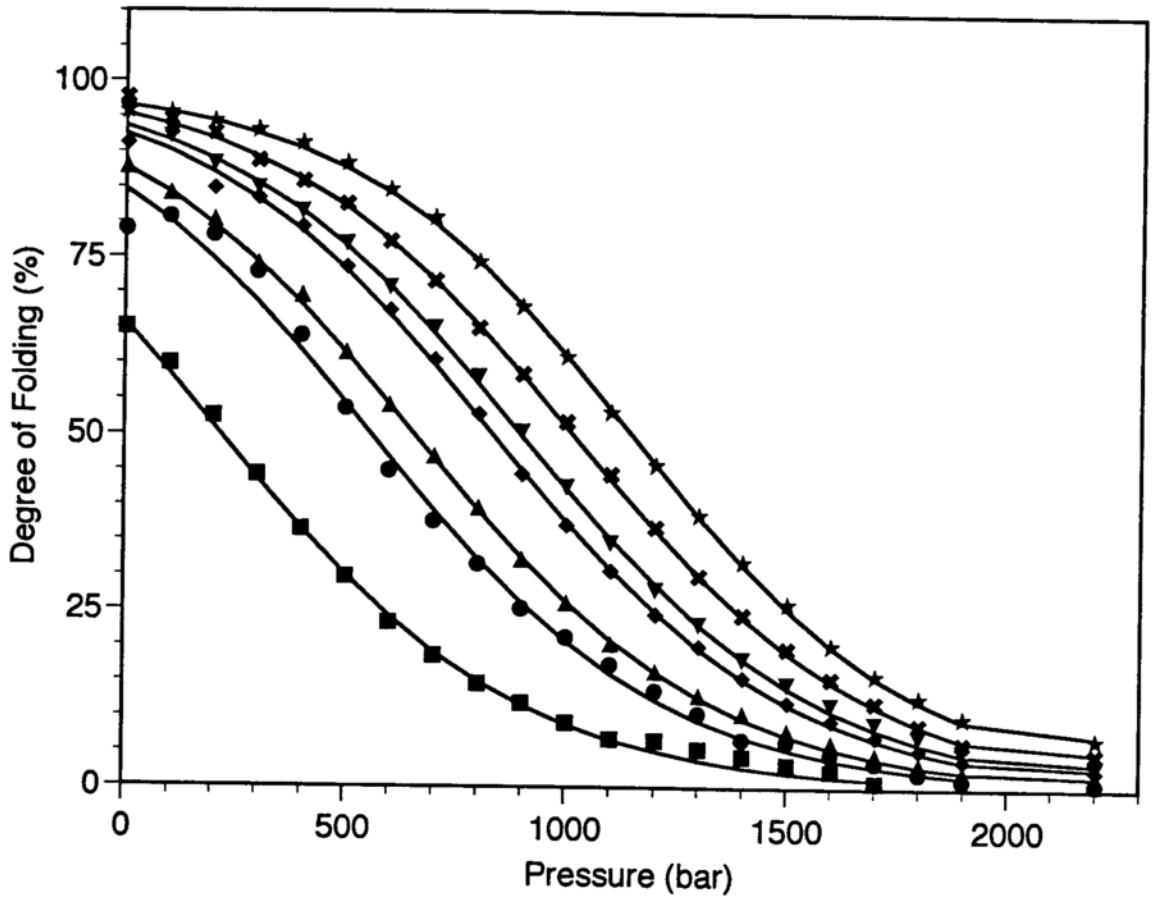

Figure II-1. Unfolding profiles for H121P as a function of pressure and millimole fraction xylose at pH 7.0 and 21°C. The symbols are the data from a representative set of experiments and the solid lines represent the unlinked curve analysis fits to the data (global curve analysis fits to the data are shown in Figure 5-2). (■) 0 mole fraction xylose, (●) 6.2 millimole fraction xylose, (▲) 10.5 millimole fraction xylose, (◆) 12.7 millimole fraction xylose, (▼) 15.0 millimole fraction xylose, (✖) 17.2 millimole fraction xylose, (★) 19.6 millimole fraction xylose.

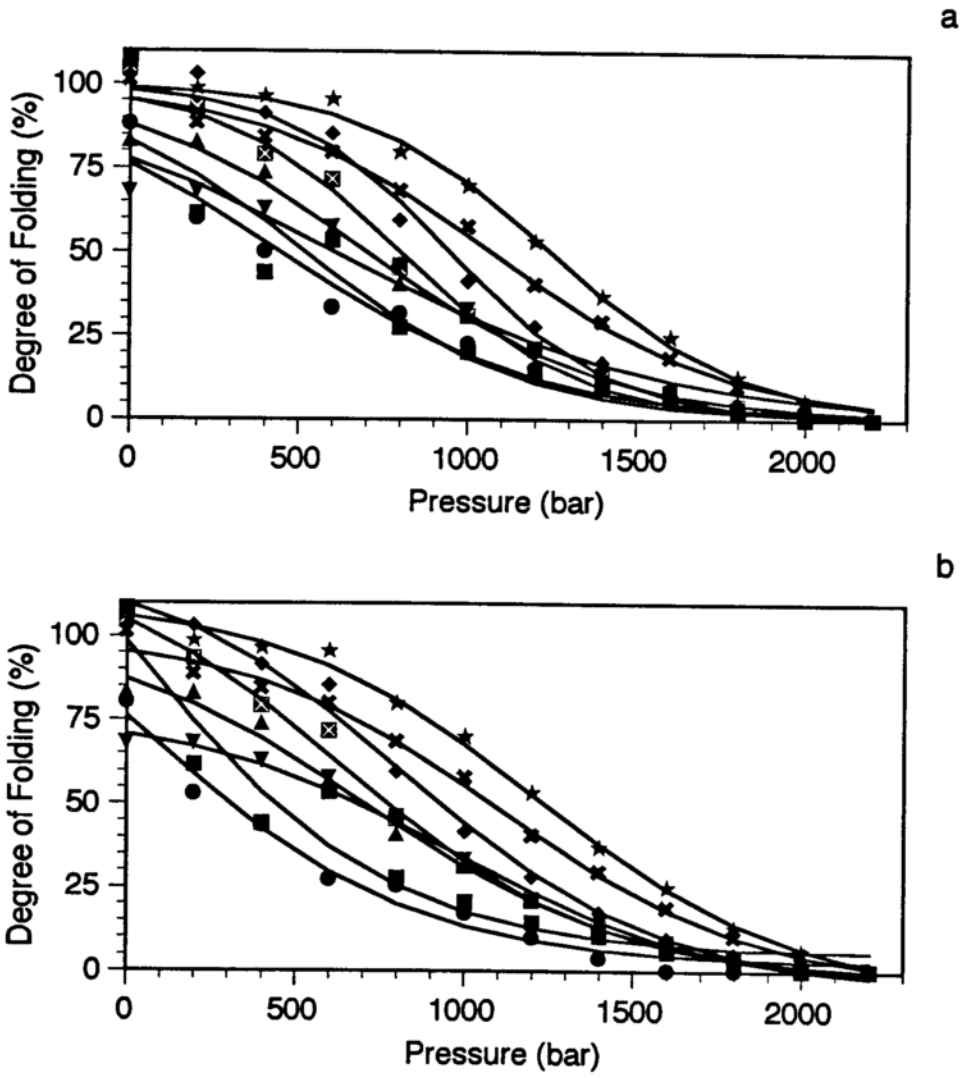

Figure II-2. Unfolding profiles for H121P as a function of pressure and millimole fraction xylose at pH 7.0 and 21°C. The symbols are the data from a representative set of experiments and the solid lines represent the (a) unlinked curve analysis and (b) global curve analysis fits to the data. (■) 0 mole fraction xylose, (●) 6.2 millimole fraction xylose, (⊠) 8 millimole fraction xylose, (▲) 10.5 millimole fraction xylose, (◆) 12.7 millimole fraction xylose, (▼) 15.0 millimole fraction xylose, (✖) 17.2 millimole fraction xylose, and (★) 19.6 millimole fraction xylose.

a

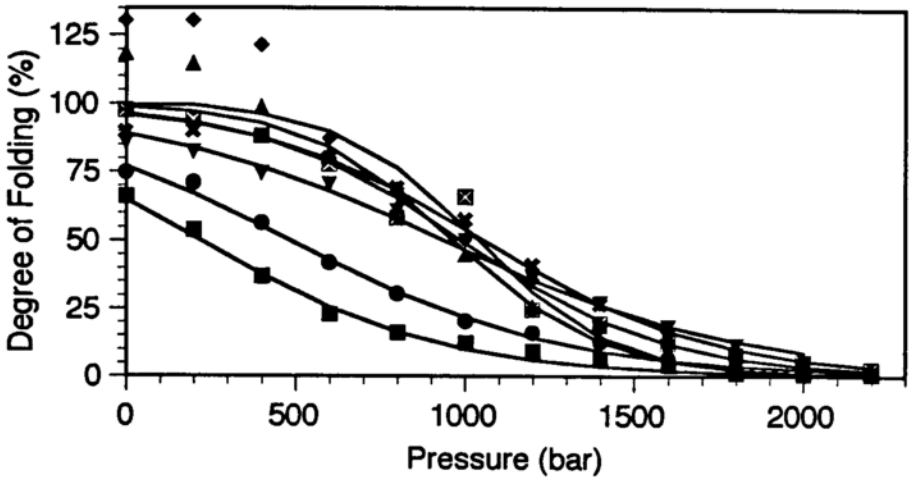

b

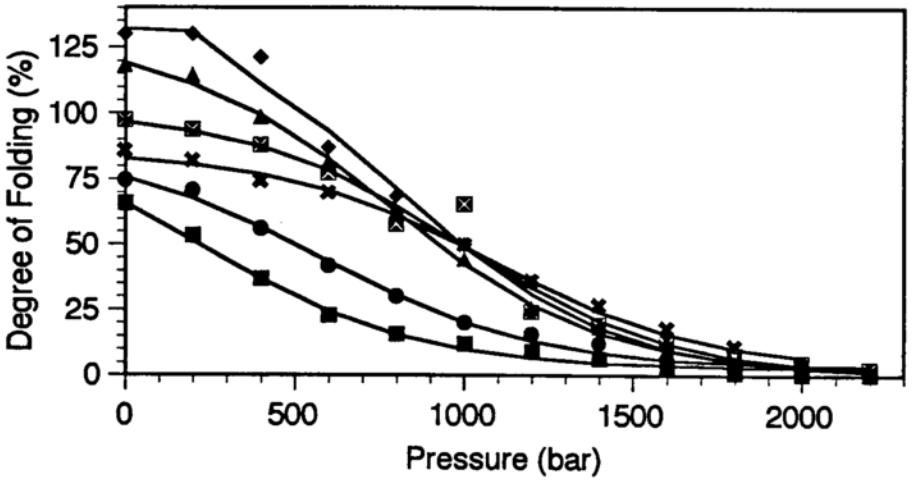

Figure II-3. Unfolding profiles for H121P as a function of pressure and millimole fraction xylose at pH 7.0 and 21°C. The symbols are the data from a representative set of experiments and the solid lines represent the (a) unlinked curve analysis and (b) global curve analysis fits to the data. (■) 0 mole fraction xylose, (●) 6.2 millimole fraction xylose, (⊠) 8 millimole fraction xylose, (▲) 10.5 millimole fraction xylose, (◆) 12.7 millimole fraction xylose, (✖) 17.2 millimole fraction xylose, and (★) 19.6 millimole fraction xylose.

a

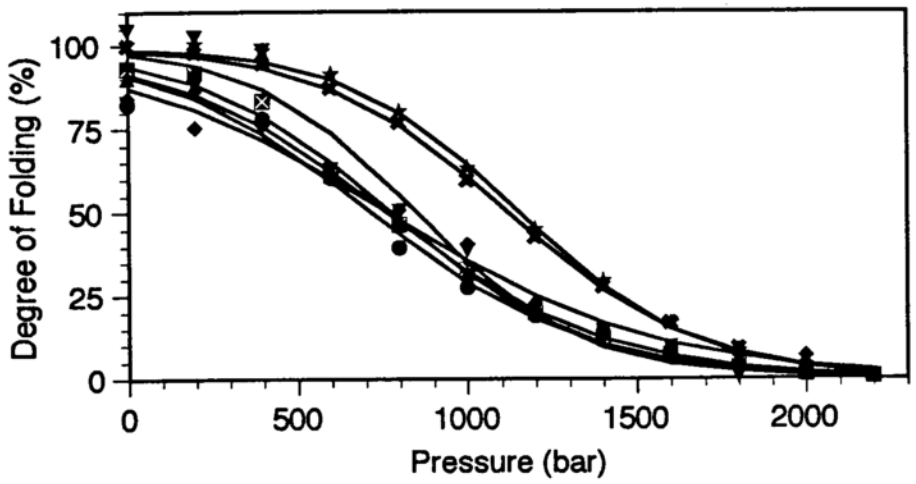

b

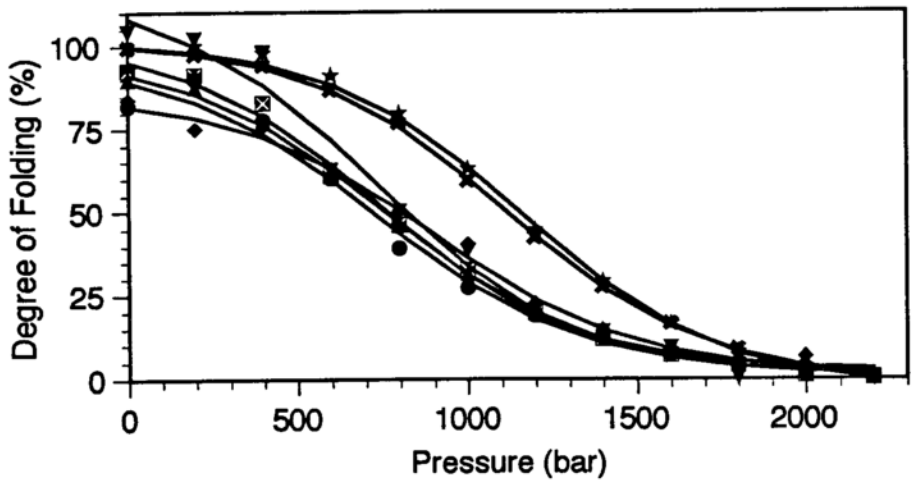

Figure II-4. Unfolding profiles for H121P as a function of pressure and millimole fraction xylose at pH 7.0 and 21°C. The symbols are the data from a representative set of experiments and the solid lines represent the (a) unlinked curve analysis and (b) global curve analysis fits to the data. (●) 6.2 millimole fraction xylose, (⊠) 8 millimole fraction xylose, (▲) 10.5 millimole fraction xylose, (◆) 12.7 millimole fraction xylose, (▼) 15.0 millimole fraction xylose, (✖) 17.2 millimole fraction xylose, and (★) 19.6 millimole fraction xylose.

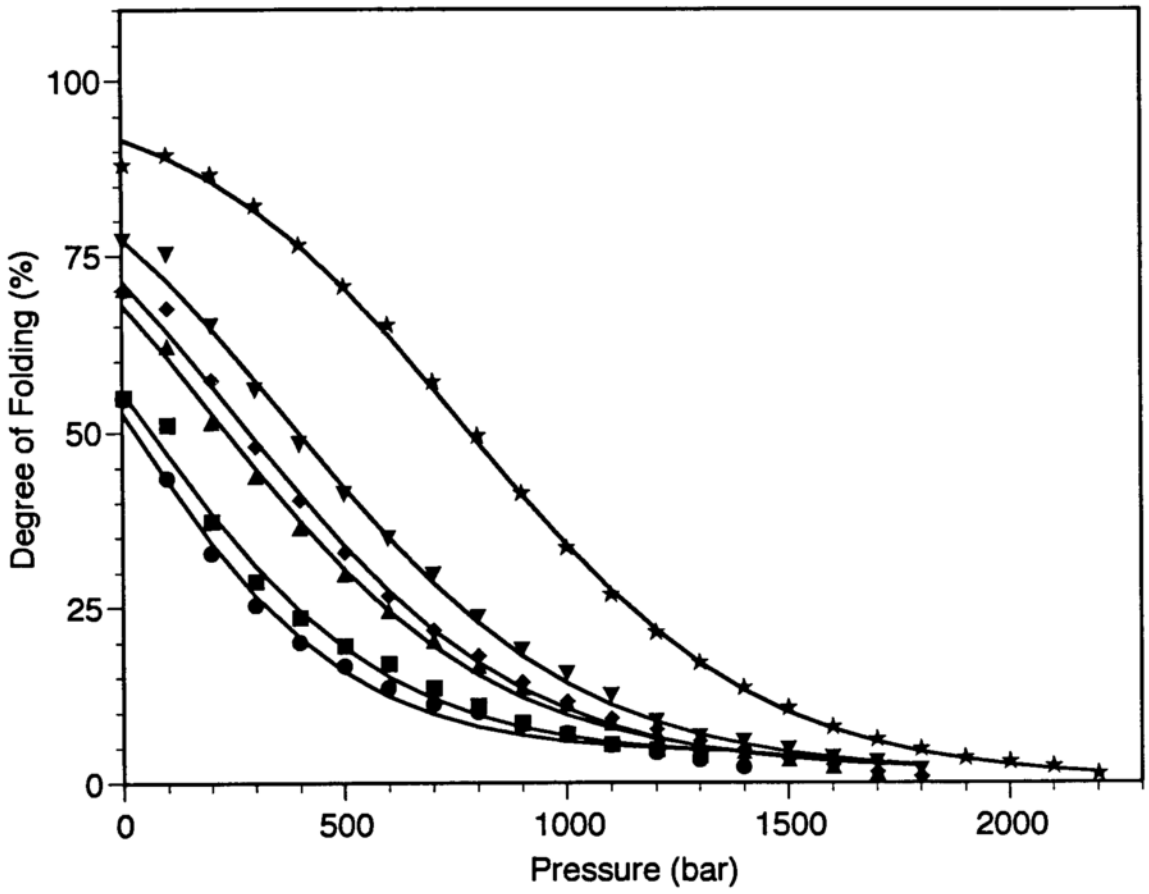

Figure II-5. Unfolding profiles for A69T + A90S as a function of pressure and millimole fraction xylose at pH 7.0 and 21°C. The symbols are the data from a representative set of experiments and the solid lines represent the unlinked curve analysis fits to the data (global curve analysis fits to the data are shown in Figure 5-3). (■) 0 mole fraction xylose, (●) 3.0 millimole fraction xylose, (▲) 6.2 millimole fraction xylose, (◆) 9.4 millimole fraction xylose, (▼) 12.7 millimole fraction xylose, (★) 19.6 millimole fraction xylose.

a

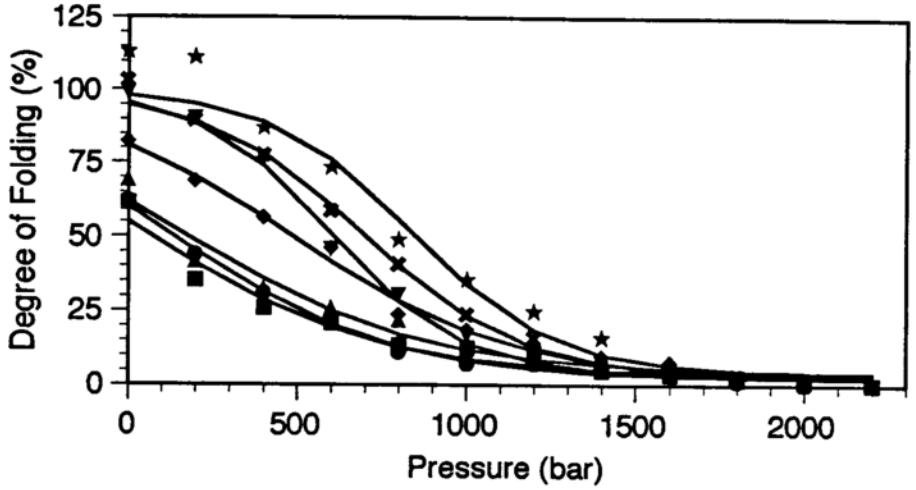

b

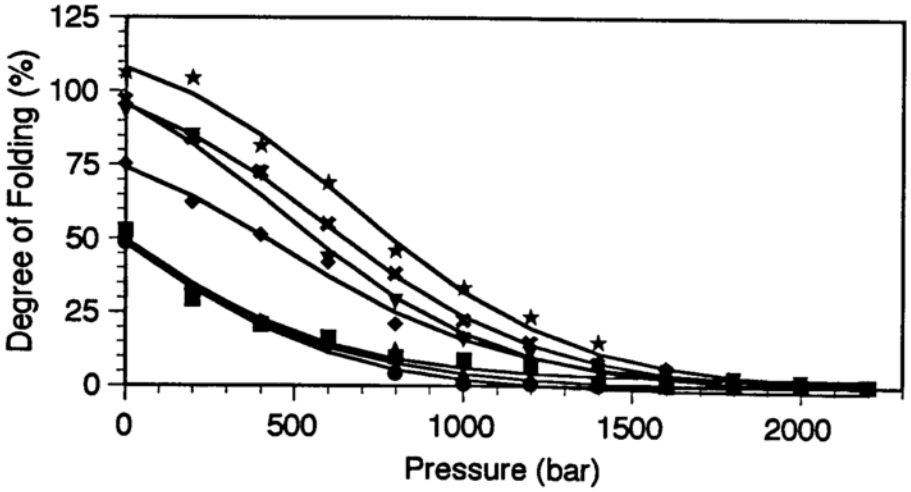

Figure II-6. Unfolding profiles for A69T + A90S as a function of pressure and millimole fraction xylose at pH 7.0 and 21°C. The symbols are the data from a representative set of experiments and the solid lines represent the (a) unlinked curve analysis and (b) global curve analysis fits to the data. (■) 0 mole fraction xylose, (●) 3.0 millimole fraction xylose, (▲) 6.2 millimole fraction xylose, (◆) 9.4 millimole fraction xylose, (▼) 12.7 millimole fraction xylose, (✖) 16.1 millimole fraction xylose (★) 19.6 millimole fraction xylose.

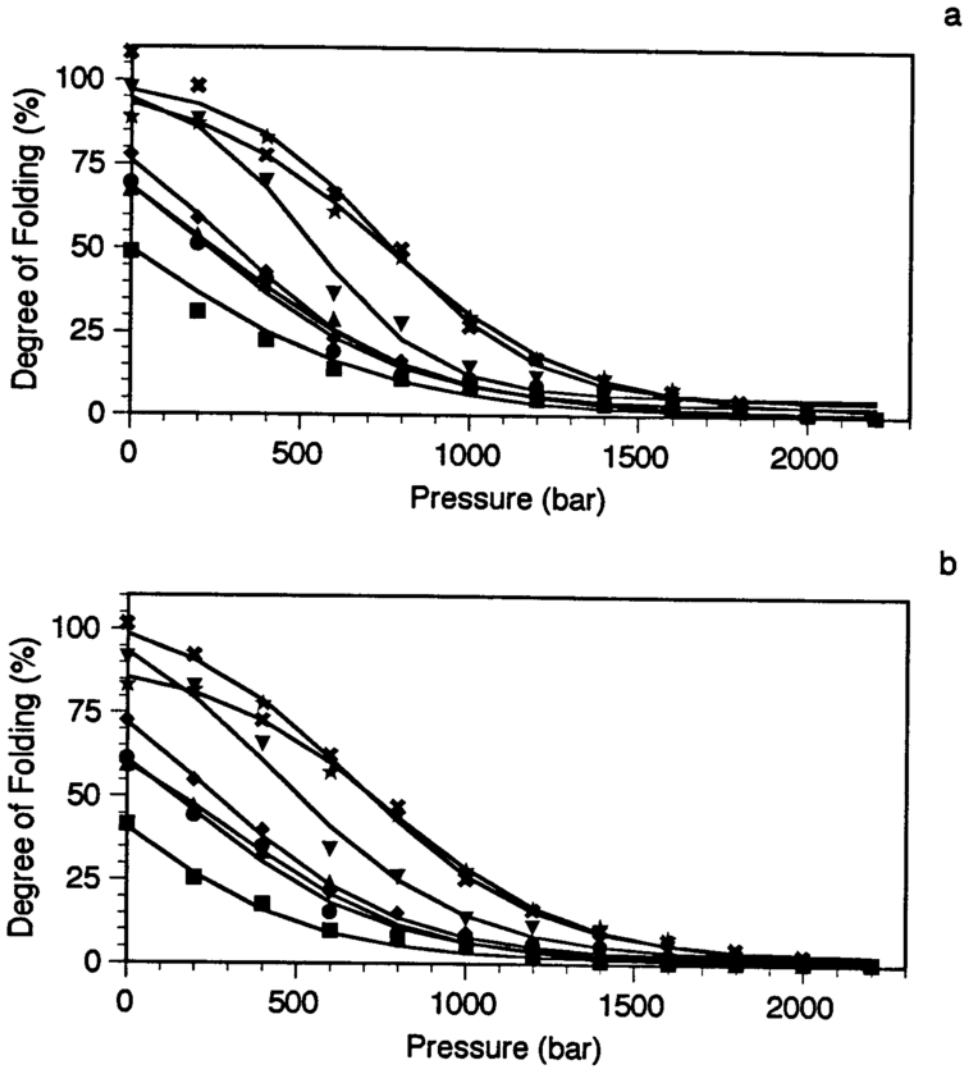

Figure II-7. Unfolding profiles for A69T + A90S as a function of pressure and millimole fraction xylose at pH 7.0 and 21°C. The symbols are the data from a representative set of experiments and the solid lines represent the (a) unlinked curve analysis and (b) global curve analysis fits to the data. (■) 0 mole fraction xylose, (●) 3.0 millimole fraction xylose, (▲) 6.2 millimole fraction xylose, (◆) 9.4 millimole fraction xylose, (▼) 12.7 millimole fraction xylose, (✖) 16.1 millimole fraction xylose (★) 19.6 millimole fraction xylose.

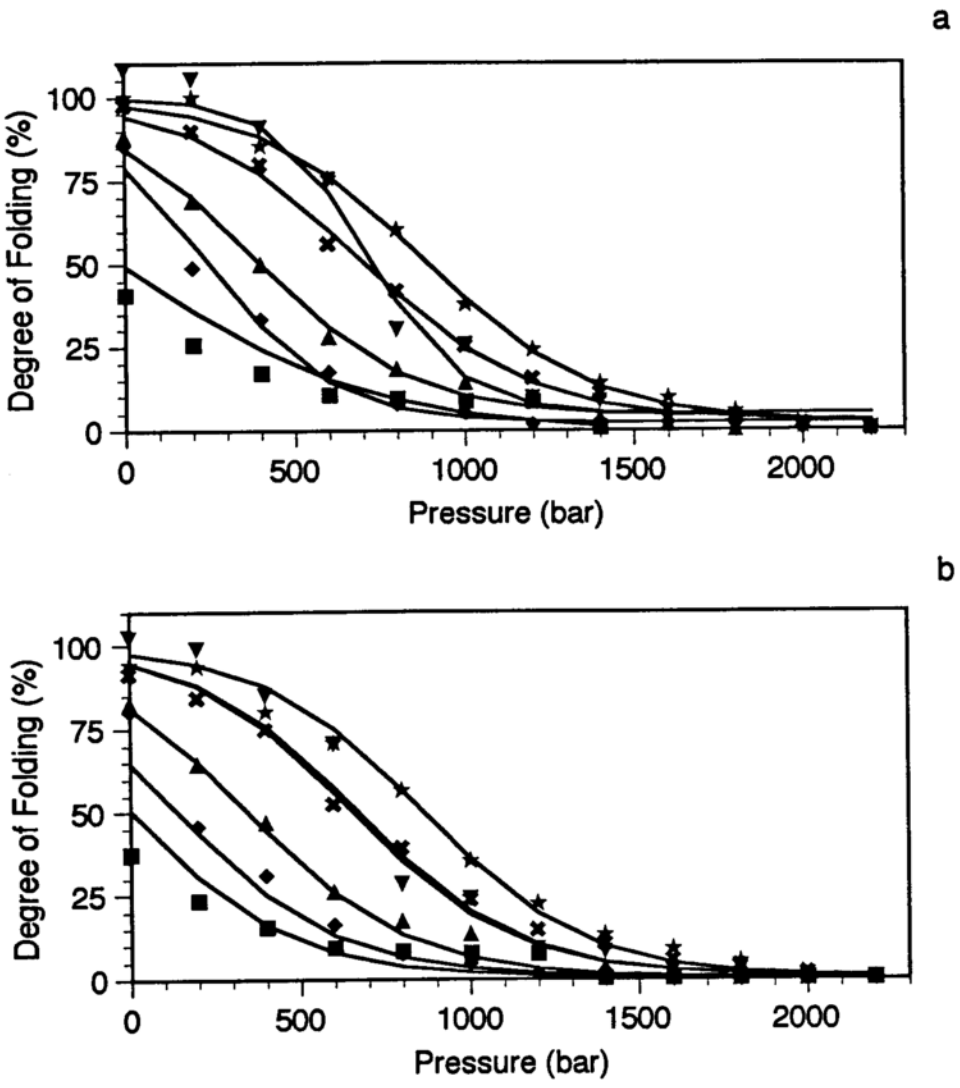

Figure II-8. Unfolding profiles for A69T + A90S as a function of pressure and millimole fraction xylose at pH 7.0 and 21°C. The symbols are the data from a representative set of experiments and the solid lines represent the (a) unlinked curve analysis and (b) global curve analysis fits to the data. (■) 0 mole fraction xylose, (▲) 6.2 millimole fraction xylose, (◆) 9.4 millimole fraction xylose, (▼) 12.7 millimole fraction xylose, (✖) 16.1 millimole fraction xylose (★) 19.6 millimole fraction xylose.

a

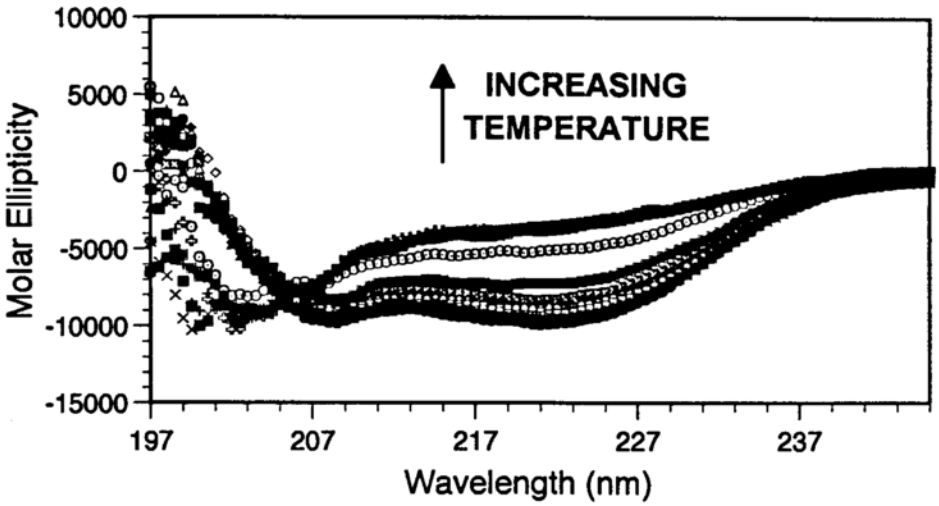

b

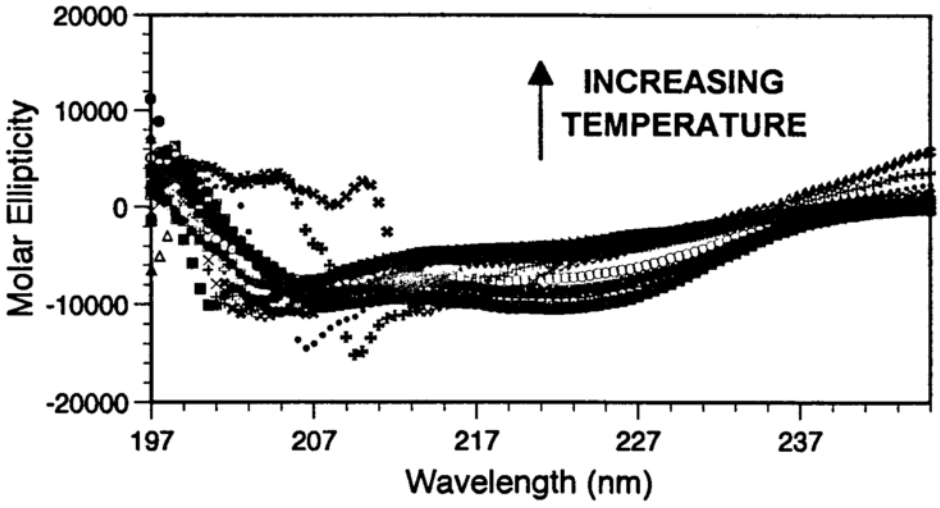

Figure II-9. CD spectra for WT nuclease as a function of temperature at pH 5.5 (a) without xylose and (b) with 19.6 millimole fraction xylose.

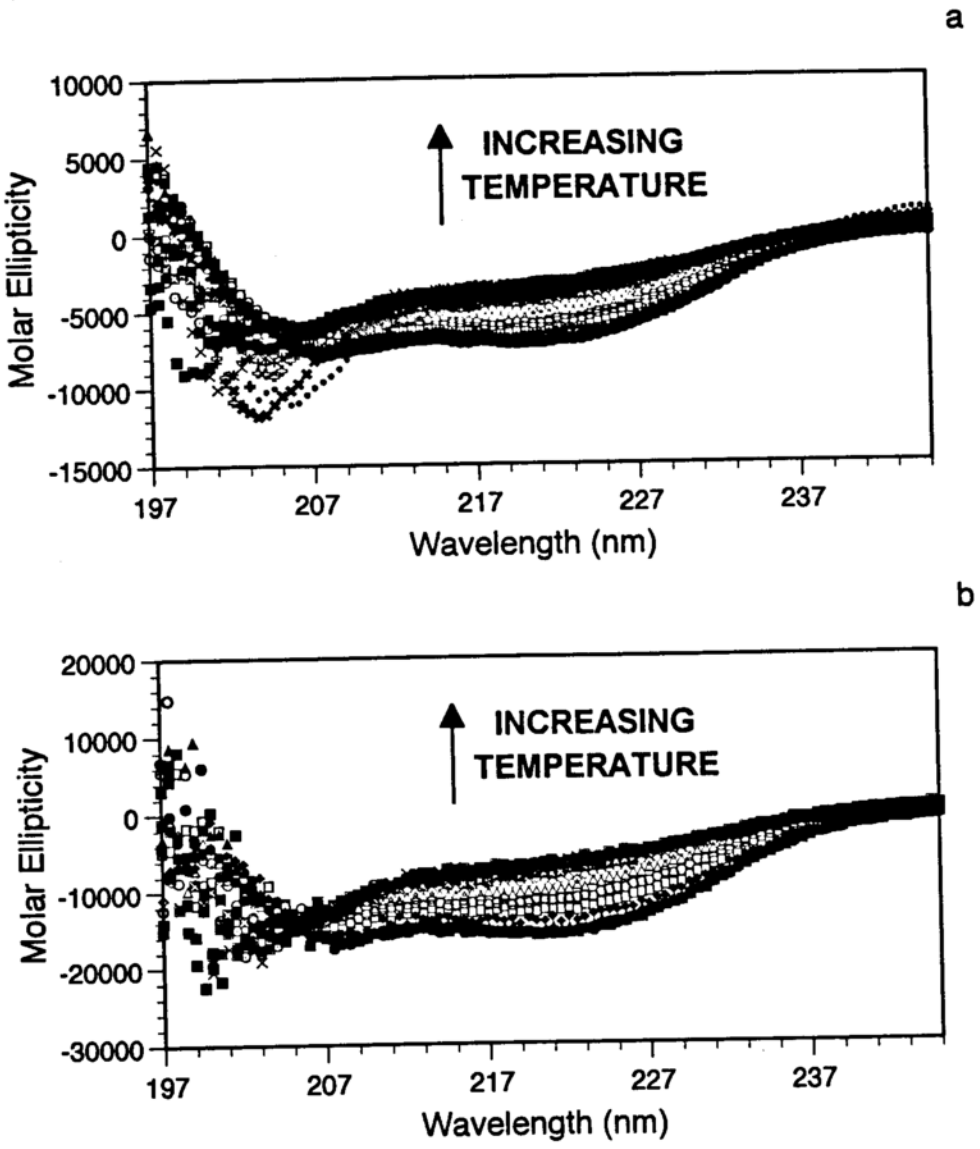

Figure II-10. CD spectra for H121P as a function of temperature at pH 7.0 (a) without xylose and (b) with 19.6 millimole fraction xylose.

a

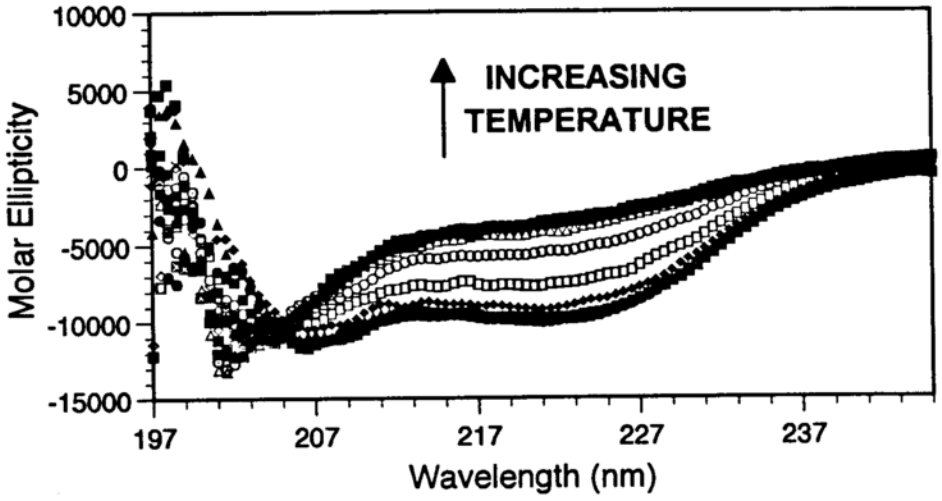

b

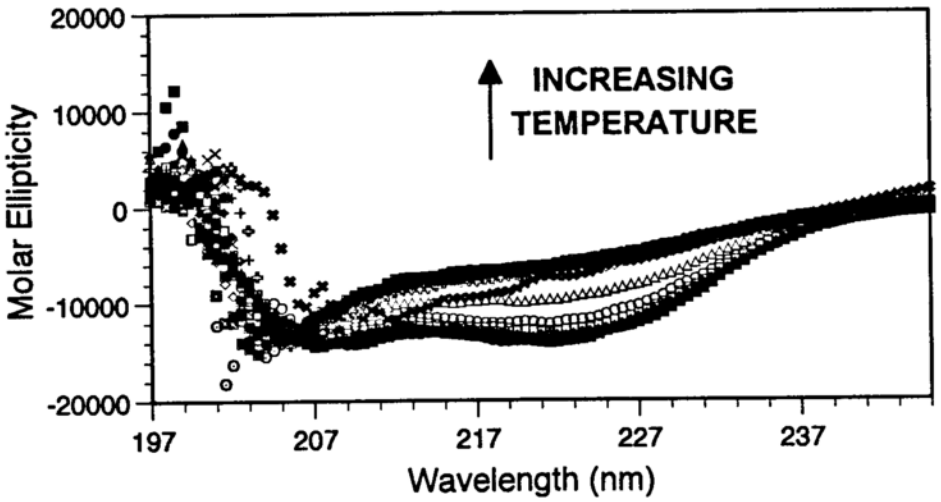

Figure II-11. CD spectra for A69T + A90S as a function of temperature at pH 7.0 (a) without xylose and (b) with 19.6 millimole fraction xylose.

APPENDIX III: ADDITIONAL DATA FROM CHAPTER 6

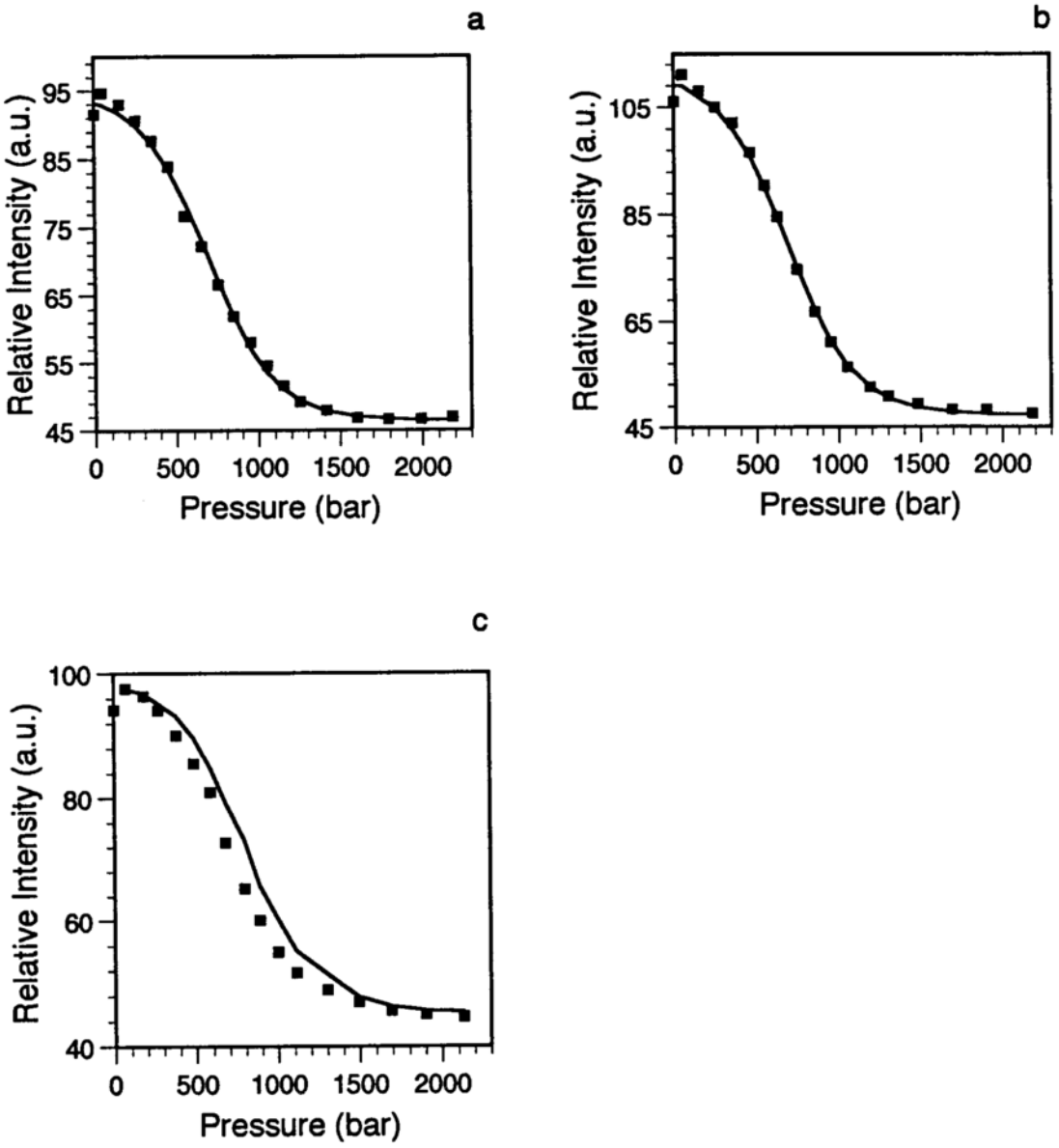

Figure III-1. Representative experiments for the unfolding of V66G at pH 7.0 and 21°C with 19.1 millimole xylose. The solid lines represent global curve analysis fits to the data.

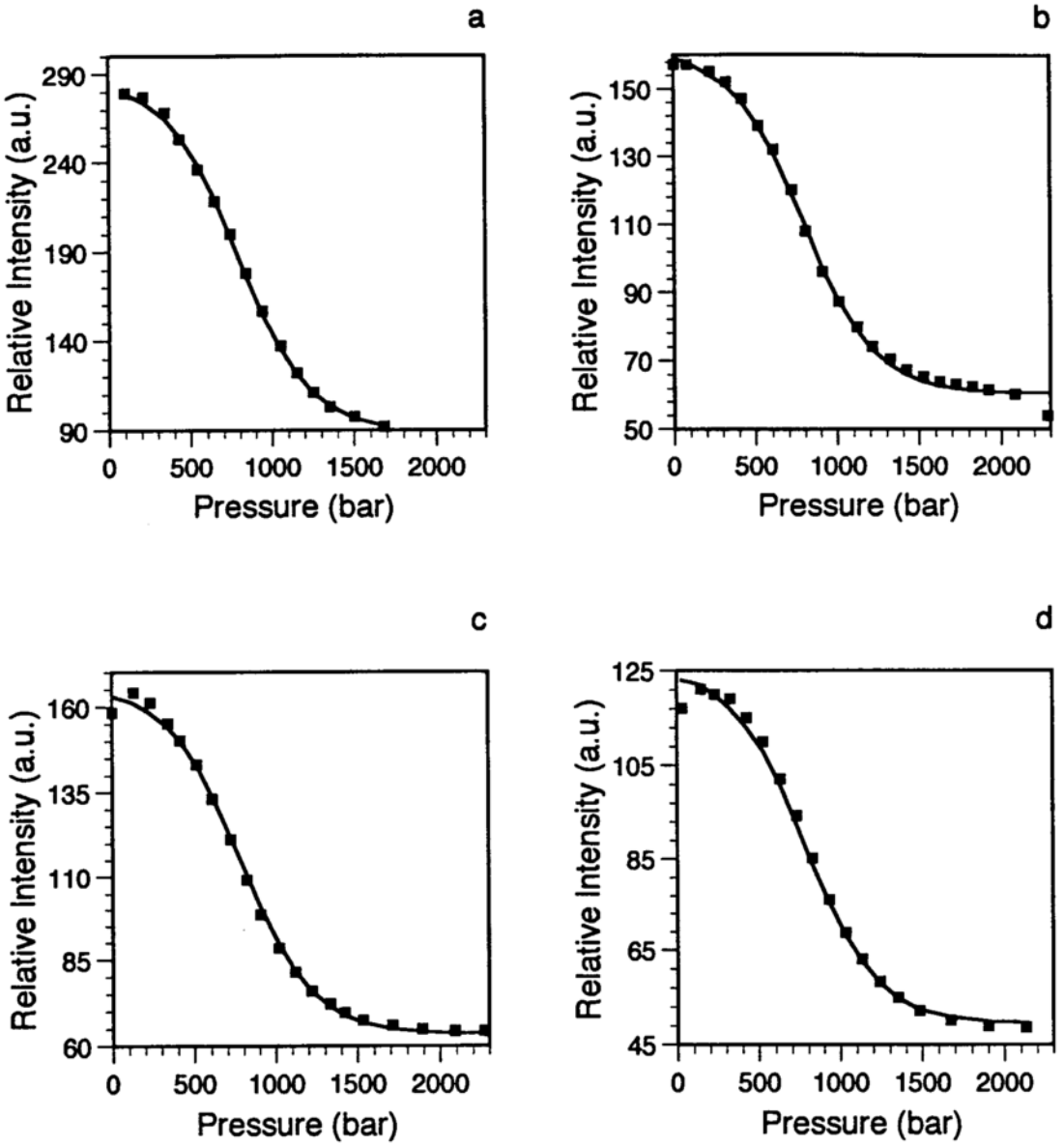

Figure III-2. Representative experiments for the unfolding of V66A at pH 7.0 and 21°C. The solid lines represent global curve analysis fits to the data.

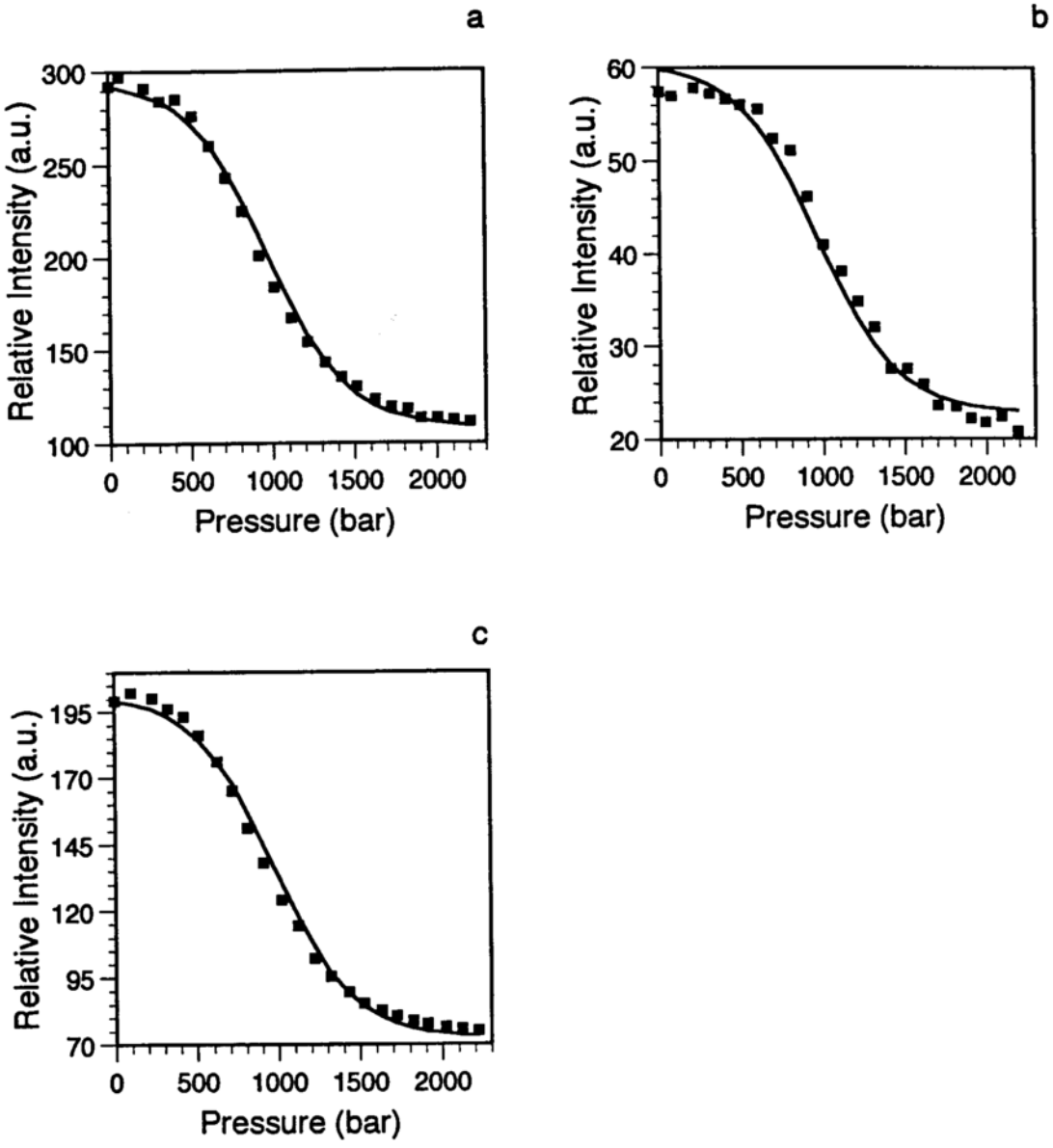

Figure III-3. Representative experiments for the unfolding of V66L at pH 5.5 and 21°C with 0.5 M guanidine. The solid lines represent global curve analysis fits to the data.